TU Delft

Delft University of Technology

Weyl Points In Superconducting Nanostructures

Chen, Y.

DOI
10.4233/uuid:be3935cb-1e7a-401d-a5a8-cd484648fff1

Publication date
2021

Document Version
Final published version

Citation (APA)
Chen, Y. (2021). *Weyl Points In Superconducting Nanostructures*. [Dissertation (TU Delft), Delft University of Technology]. https://doi.org/10.4233/uuid:be3935cb-1e7a-401d-a5a8-cd484648fff1

Important note
To cite this publication, please use the final published version (if applicable).
Please check the document version above.

Copyright
Other than for strictly personal use, it is not permitted to download, forward or distribute the text or part of it, without the consent of the author(s) and/or copyright holder(s), unless the work is under an open content license such as Creative Commons.

Takedown policy
Please contact us and provide details if you believe this document breaches copyrights.
We will remove access to the work immediately and investigate your claim.

This work is downloaded from Delft University of Technology.
For technical reasons the number of authors shown on this cover page is limited to a maximum of 10.

Weyl Points In Superconducting Nanostructures

Yuguang Chen

WEYL POINTS IN SUPERCONDUCTING NANOSTRUCTURES

WEYL POINTS IN SUPERCONDUCTING NANOSTRUCTURES

Proefschrift

ter verkrijging van de graad van doctor
aan de Technische Universiteit Delft,
op gezag van de Rector Magnificus Prof.dr.ir. T.H.J.J. van der Hagen,
voorzitter van het College voor Promoties,
in het openbaar te verdedigen op donderdag 20 mei 2021 om 15:00 uur

door

Yuguang CHEN

Master of Science in Physics,
University of Minnesota, Verenigde Staten van Amerika,
geboren te Baotou, China.

Dit proefschrift is goedgekeurd door de promotoren

Samenstelling promotiecommissie:

Rector Magnificus,	voorzitter
Prof.dr. Y.V. Nazarov,	Technische Universiteit Delft, promotor
Prof.dr. Y.M. Blanter,	Technische Universiteit Delft, promotor
Onafhankelijke leden:	
Prof.dr. M.G. Vavilov,	University of Wisconsin Madison, USA
Prof.dr. J.S. Meyer,	Université Grenoble Alpes, France
Prof.dr.ir. H.T.C. Stoof,	Universiteit Utrecht
Prof.dr. J. Aarts,	Universiteit Leiden
Prof.dr.ir. L.M.K. Vandersypen,	Technische Universiteit Delft
Prof.dr. A.F. Otte	Technische Universiteit Delft, reservelid

Printed by:

Front & Back: We originated from matters in the universe, crawl and toddle as infants, and will be lost in the infinitely meandering maze of thoughts, like that composed of the Peano curve.

Copyright © 2021 by Y. Chen

Casimir PhD Series, Delft-Leiden 2021-12

ISBN 978-90-8593-478-3

An electronic version of this dissertation is available at
http://repository.tudelft.nl/.

CONTENTS

SUMMARY

Topological band theory has contributed to some of the most astonishing developments in solid-state physics. The unique attributes that arise from topological effects are at the focus of modern experimental and theoretical research. Weyl point, a topological defect at the Fermi surface, enables topological transitions and transport phenomena. Its existence is considerably restricted in natural materials due to the tuning and dimension constraint.

Recently, The Weyl points have been predicted to accommodate within superconducting nanostructures in the spectrum of Andreev bound states. Theoretically, one can easily manipulate the dimensionality and the tuning process through elementary approaches with specially designed structures. This opens up a new window for explorations in a higher dimension, high-order topological effects, Majorana states, and other complications even though it may be still experimentally challenging.

One realization of such structures is the multi-terminal Josephson junction. The parameters are the superconducting phase differences of the terminals and the Weyl points reside at low energies within the superconducting gap. Chapter 2 of this thesis investigates the topological effect in the quantized transconductance of such a structure considering the presence of the continuous spectrum that is intrinsic to superconductors. This research is based on scattering formalism and relates the Landauer conductance to the continuous spectrum as a background field in the regular topological charge picture.

Chapter 3 is based on a very generic superconducting nanostructure setup so long as it hosts Weyl points in it. The research proposes a unit that tunnel-couples such a setup with a quantum dot. The distinct feature of the spectrum, especially the distinction between its spin-singlet and spin-doublet due to spin-orbit coupling, leads to an exploration of the state manipulation. Eventually, through adiabatic and diabatic approaches, one can feasibly realize a full unitary transformation of the spectrum. Because of this, the unit could easily find its promising application in entangled qubits.

Chapter 4 also relies on the generic low-energy Weyl point setup in the superconducting nanostructure, but instead, it is weakly tunnel-coupled to regular metallic leads. We know that spintronics explores the intrinsic spin degree of freedom. It is usually realized on magnetic materials. In the setup of this research, the energy spectrum contains a natural spin-orbit that creates a minimalistic magnetic state in the vicinity of the Weyl point. The spin structure of the spectrum allows fine-controls over the spin and switch between magnetic/non-magnetic state. Hence this chapter's research focuses on the possible spintronics features based on master equations.

Chapter 5 furthers the research of chapter 4. It considers a universal energy scale sets up by the tunnel coupling strength. In the language of the Green's function, this chapter studies the topological effect through the response function. This set up is a suitable example of low energy Weyl points situated in the presence of a low-energy continuous spectrum brought by electrons in the leads. We have seen in Chapter 1 how the contin-

uous spectrum above the gap modifies the topology leading to a non-quantized contribution to the transconductance. The peculiarity of coupling Weyl points to a low energy continuous spectrum is that the dissipation gives rise to a redefinition of the Berry curvature, which manifests as a continuous density of topological charge instead of a point-like one. This unusual characteristic can be captured by the tunnel current and thus can assist the detection of Weyl points experimentally.

SAMENVATTING

Topologische bandtheorie heeft bijgedragen aan enkele van de meest verbazingwekkende ontwikkelingen in de vaste-stoffysica. De unieke eigenschappen die voortkomen uit topologische effecten staan centraal in modern experimenteel en theoretisch onderzoek. Weyl point, een topologisch defect aan het Fermi-oppervlak, maakt topologische overgangen en transportverschijnselen mogelijk. Het bestaan ervan is aanzienlijk beperkt in natuurlijke materialen vanwege de afstemming en afmetingbeperkingen.

Onlangs is voorspeld dat de Weyl-punten passen binnen supergeleidende nanostructuren in het spectrum van aan Andreev gebonden staten. Theoretisch kan men de dimensionaliteit en het afstemmingsproces gemakkelijk manipuleren door middel van elementaire benaderingen met speciaal ontworpen structuren. Dit opent een nieuw venster voor verkenningen in een hogere dimensie, topologische effecten van hoge orde, Majorana-toestanden en andere complicaties, hoewel het nog steeds experimenteel uitdagend kan zijn.

Een realisatie van dergelijke structuren is de meerterminal Josephson-kruising. De parameters zijn de supergeleidende faseverschillen van de terminals en de Weyl-punten bevinden zich op lage energieën binnen de supergeleidende opening. Hoofdstuk 2 van dit proefschrift onderzoekt het topologische effect in de gekwantiseerde transconductantie van een dergelijke structuur, rekening houdend met de aanwezigheid van het continue spectrum dat intrinsiek is aan supergeleiders. Dit onderzoek is gebaseerd op het verstrooiingsformalisme en relateert de Landauer-geleiding aan het continue spectrum als achtergrondveld in het reguliere topologische ladingsbeeld.

Hoofdstuk 3 is gebaseerd op een zeer generieke supergeleidende nanostructuuropstelling, zolang er maar Weyl-punten in zitten. Het onderzoek stelt een eenheid voor die een dergelijke opstelling via een tunnel koppelt aan een kwantumpunt. Het onderscheidende kenmerk van het spectrum, vooral het onderscheid tussen zijn spin-singlet en spin-doublet als gevolg van spin-orbit-koppeling, leidt tot een verkenning van de toestandsmanipulatie. Uiteindelijk kan men door middel van adiabatische en diabatische benaderingen een volledige unitaire transformatie van het spectrum realiseren. Hierdoor zou de eenheid gemakkelijk zijn veelbelovende toepassing kunnen vinden in verstrengelde qubits.

Hoofdstuk 4 vertrouwt ook op de generieke lage-energie Weyl-puntopstelling in de supergeleidende nanostructuur, maar in plaats daarvan is het zwak tunnelgekoppeld aan gewone metalen draden. We weten dat spintronica de intrinsieke vrijheidsgraad van spin verkent. Het wordt meestal gerealiseerd op magnetische materialen. Bij de opzet van dit onderzoek bevat het energiespectrum een natuurlijke spinbaan die een minimalistische magnetische toestand cre´eert in de buurt van het Weylpunt. De spinstructuur van het spectrum maakt fijnregeling van de spin mogelijk en schakelt tussen magnetische / niet-magnetische toestand. Daarom richt het onderzoek van dit hoofdstuk zich op de mogelijke spintronica-eigenschappen op basis van mastervergelijkingen.

Hoofdstuk 5 bevordert het onderzoek van hoofdstuk 4. Het beschouwt een universele energieschaal die wordt gevormd door de tunnelkoppelingssterkte. In de taal van de Green's functie bestudeert dit hoofdstuk het topologische effect via de responsfunctie. Deze opstelling is een geschikt voorbeeld van Weyl-punten met lage energie die zich bevinden in de aanwezigheid van een continu spectrum met lage energie dat door elektronen in de leads wordt gebracht. We hebben in Hoofdstuk 1 gezien hoe het continue spectrum boven de gap de topologie wijzigt, wat leidt tot een niet-gekwantiseerde bijdrage aan de transconductantie. De bijzonderheid van het koppelen van Weyl-punten aan een continu spectrum met lage energie is dat de dissipatie aanleiding geeft tot een herdefinitie van de Berry-kromming, die zich manifesteert als een continue dichtheid van topologische lading in plaats van een puntachtige lading. Deze ongebruikelijke eigenschap kan worden opgevangen door de tunnelstroom en kan zo experimenteel helpen bij het detecteren van Weyl-punten.

1

INTRODUCTION

1.1. PREFACE

Before I stepped into the actual postgraduate physics research, I was heavily influenced by my father and his colleagues, who are mathematicians, in the ideology. I was obsessed with the axiomatic structure that bears the foundation of modern mathematics and was willing to dive into the mathematical discipline that can rigorously describe quantum mechanics axiomatically. Historically, the relative concern in mathematical physics was first cited as Hilbert's sixth problem presented in the year 1900 [1]. Later, after the discovery of quantum mechanics, the basic framework for the quantum mechanics' mathematical formalism, the Dirac-von Neumann axioms, was founded in terms of operators on a Hilbert space introduced by Paul Dirac and von Neumann in the '30s of the last century [2, 3]. The evolution continued and in the 1950s and 1960s [4, 5], various "axiomatizations" of quantum field theory were established. It turns out that the whole series of work that followed becomes too mathematical for me to find practical. I realized this, especially after my graduate study in the physics department. The rich context seems a remote concern for many physicists to chase the shadow because essentially the beauty of mathematical physics has the quest that leads to the discoveries of experiments.

In the 1980s, the integer quantum Hall effect (IQHE) [6] and the geometric phase (Berry phase) were discovered [7]. The paradigm developed by Lev Landau suddenly faced a huge challenge. Differential geometry and topology were consequently introduced to the condensed matter physics, bridging the rich context in abstract mathematics with experimental physics. The motivation of generalizing the 2d IQHE in the viewpoint of topology, alongside the motivation to describe non-trivial systems using topological field theory, and as well as the motivation to a brand-new classification of states of matters quickly attracted talented generations in the field and became a pillar in the physics community. This new branch of physics flourishes ever since for decades with multiple Nobel Prizes awarded and is still producing fruitful predictions ahead.

Quantum physics has evolved so rapidly during the past few decades. It eventually is not only guidance to a conceptual framework or philosophical inspiration, but also

can be realized among technological applications. Physicists started to apply quantum mechanics to computer science and information theory by designing micro-fabricated quantum devices. Techniques such as lithography, cryogenics, and microwave control allow the designs and studies of quantum devices to the pinnacle of quantum mechanical limit. Our abilities have thus extended to the manipulation and control over single photons, single atoms, nuclear spins, individual electrons, and mesoscopic superconducting devices. Single systems are typically suitable with few specific tasks, such as transmitting quantum information, long-time storage of quantum memories, nanosecond-time-scaled quantum state processing, etc. On top of that, hybrid systems combining different individual subsystems of quantum devices can achieve complementary functionalities from each component and also obtain new functionalities that are seemingly forbidden in single systems. This most active interdisciplinary field of research stimulates many masterminds to test the boundary of both the theory and technology.

My past four years of research is nowhere near what I dreamed of when I was still a newbie physics student. I am fortunate enough to eventually work on the theoretical interplay of topology and quantum transport, neither too abstract to lose ground to an experimental science of the actual world, nor too concrete to be inaccessible to the epitome of intellect. Hereby I will give an introduction to display the core concepts involved in this thesis. It includes mainly four parts: superconductivity, some concepts of quantum transport, some unfamiliar theoretical methods applied in the research, and topology from the perspective of the band structure.

1.2. SUPERCONDUCTIVITY

Since the discovery of superconductivity in 1911 in the Leiden laboratory of Kamerlingh Onnes, it has been studied intensively for its fundamental interest and for promising applications. Superconducting materials exhibit unusual behaviors including zero resistivity, persistent current, perfect diamagnetism (Meissner effect) and possess an energy gap in the spectrum, etc.

Upon decades of studies, different varieties of superconductors were discovered and studied. They can be classified in accordance with several criteria depending on, e.g., the critical field, the causing mechanism, and the critical temperature. In the context of this thesis, we focus only on the ramification of the conventional superconductors that can be described microscopically as the result of Cooper pair condensation, or in BCS (Bardeen-Cooper-Schrieffer) framework.

We start with the reduced BCS mean-field Hamiltonian, and for generality, in the case of an inhomogeneous superconductor [8, 9]. Without translational symmetry, momentum is no longer a good quantum number, therefore we write the Hamiltonian with space variables:

$$H_{\mathrm{BCS}} = \int d\mathbf{r} \sum_{\sigma} \left\{ \psi_{\sigma}^{\dagger}(\mathbf{r}) \hat{H}(\mathbf{r}) \psi_{\sigma}(\mathbf{r}) + \frac{1}{2} \left(\Delta(\mathbf{r}) \psi_{\sigma}^{\dagger}(\mathbf{r}) \psi_{-\sigma}^{\dagger}(\mathbf{r}) + \Delta^{*}(\mathbf{r}) \psi_{-\sigma}(\mathbf{r}) \psi_{\sigma}(\mathbf{r}) \right) \right\}, \tag{1.1}$$

where $\sigma = \pm 1$ signifies spin, the grand canonical Hamiltonian $\hat{H}(\mathbf{r})$(measured from the Fermi energy) as the particle number is not preserved (doesn't commute with the number operator) has an eigenstate of $\xi(\mathbf{r})$, and the antisymmetric(fermionic) $\Delta(\mathbf{r})$ is the pairing potential that defines the gap in the superconductor.

To diagonalize H_{BCS} and find a good quantum number for the excitation state considering the fermionic statistics, we introduce the fermionic operator using the generalized Bogoliubov-Valatin transformation:

$$\psi_\sigma(\mathbf{r}) = \sum_n \left(u_n(\mathbf{r})\gamma_{n,\sigma} - \sigma v^*(\mathbf{r})\gamma^\dagger_{n,-\sigma} \right) \tag{1.2}$$

where the quasiparticle creation/annihilation operator $\gamma^\dagger_{n\sigma}, \gamma_{n\sigma}$ at state n and spin σ satisfies the commutation relations:

$$\begin{aligned} \{\gamma_{n\sigma}, \gamma^\dagger_{n'\sigma'}\} &= \delta_{nn'}\delta_{\sigma\sigma'} \\ \{\gamma_{n\sigma}, \gamma_{n'\sigma'}\} &= 0 \end{aligned} \tag{1.3}$$

Consequently, with the language of quasiparticles, we have a well-defined ground state $|g\rangle$, an excited state $|ex\rangle$, as well as spin states $|\sigma\rangle$:

$$\gamma_\sigma|g\rangle = 0; \quad \gamma^\dagger_\uparrow\gamma^\dagger_\downarrow|g\rangle = |ex\rangle; \quad \gamma^\dagger_\sigma|g\rangle = |\sigma\rangle \tag{1.4}$$

In the basis of an associated Nambu bispinor $\bar{\gamma}_{n\sigma} \equiv (\gamma_{n,\sigma}, \sigma\gamma^\dagger_{n,-\sigma})^T$, the BCS Hamiltonian can be rewritten as

$$H_{\mathrm{BCS}} = \frac{1}{2}\sum_{n\sigma} \bar{\gamma}^\dagger_{n\sigma}\hat{H}_{\mathrm{BdG}}\bar{\gamma}_{n\sigma} = \frac{1}{2}\sum_{n\sigma} E_n\gamma^\dagger_{n\sigma}\gamma_{n\sigma} \tag{1.5}$$

This is called the Bogoliubov-de Gennes (BdG) equations. They can be written in a matrix form:

$$\begin{pmatrix} \hat{H}(\mathbf{r}) & \Delta(\mathbf{r}) \\ \Delta^*(\mathbf{r}) & -\hat{H}^T(\mathbf{r}) \end{pmatrix} \begin{pmatrix} u_n(\mathbf{r}) \\ v_n(\mathbf{r}) \end{pmatrix} = E_n \begin{pmatrix} u_n(\mathbf{r}) \\ v_n(\mathbf{r}) \end{pmatrix} \tag{1.6}$$

Here, $(u_n(\mathbf{r}), v_n(\mathbf{r}))$ is the eigenstate n of the quasiparticle with positive energy. $(-v^*_n(\mathbf{r}), u^*_n(\mathbf{r}))$ is that with negative energy.

The gap energy $|\Delta(\mathbf{r})|$ characterizes the energy scale involved in the superconductor. The superconducting correlation length $\lambda \sim \hbar v_F/\Delta$ could roughly be understood as the Cooper pair size [10]. The length is of the order of 1 μm for type-I superconductors. As such, a normal metal brought into contact with a superconductor can feel the electron correlations, so that the metallic electron near the interface would also be superconducting. This is known as the proximity effect.

In the following context, we will express the results related to superconductivities in the BdG formalism in terms of quasiparticle states.

1.3. CONCEPTS OF QUANTUM TRANSPORT

SCATTERING FORMALISM

Nanostructures made with all fabrication methods are very complicated in detail and have versatile designs. There are also disorders and random defects. Seemingly the task to describe a nanostructure is deemed technically impossible.

1

Fortunately, a macroscopic approach with a small set of free parameters can describe the quantum transport process, so long as the electron scattering process within the nanostructure generates zero energy loss. This approach is call the scattering formalism [10]. This condition is satisfied at sufficiently low external energy. In between the thermo-equilibrated reservoirs (terminals) is the scattering region, where all the featured physics occurs. A scatter matrix $\hat{S}$ linear relates the plane waves' amplitudes at energy E coming through or reflected from the scattering region by a series of reflection and transmission amplitudes, i.e.,

$$b_{\alpha n} = \sum_{\beta,m} S_{\alpha n,\beta m} a_{\beta m} \tag{1.7}$$

where a, b label the amplitudes of incoming and outgoing plane waves, α, β label different terminals, and m, n label transport channels (quantized modes of electric transverse motion). All the designs and concrete configurations are encoded in the transmission eigenvalues distributions.

The scattering matrix satisfies symmetry conditions. Firstly, imposed by the conservation of total number of electrons (total probability summing to 1) in general, it is unitary:

$$\hat{S}^\dagger \hat{S} = 1 \tag{1.8}$$

Further, if time-reversal symmetry holds (not necessarily so), the scattering matrix is symmetric:

$$\hat{S}^T = \hat{S} \tag{1.9}$$

In particular, the energy dependent scattering matrix for electrons and holes satisfies

$$\hat{S}_h(E) = \hat{S}_e^*(-E) \tag{1.10}$$

LANDAUER FORMULAR

The current flows in a terminal α has two contributions: one originates from the terminal itself, described by a distribution function $f_\alpha(E)$ at energy E; one comes from the open channels transmitted through the scattering region from other terminals, described by a distribution function $f_\beta(E)$ at energy E and has a probability of $|S_{\alpha n,\beta m}|^2$. The current in terminal α is thus:

$$\begin{aligned} I_\alpha &= 2_s e \sum_n \left[\int_{-\infty}^{0} \frac{dE}{2\pi\hbar} f_\alpha(E) + \int_0^\infty \frac{dE}{2\pi\hbar} \sum_{\beta m} |S_{\alpha n,\beta m}|^2 f_\beta(E) \right] \\ &= 2_s e \int_0^\infty \frac{dE}{2\pi\hbar} \sum_{\beta mn} \left[|S_{\alpha n,\beta m}|^2 - \delta_{\alpha\beta}\delta_{nm} \right] f_\beta(E) \\ &= -\frac{G_Q}{e} \int_0^\infty \frac{dE}{2\pi\hbar} \sum_\beta \mathrm{Tr}\left[\delta_{\alpha\beta} - \hat{S}_{\alpha\beta}^\dagger \hat{S}_{\alpha\beta} \right] f_\beta(E), \end{aligned} \tag{1.11}$$

where 2_s takes care both spins, the trace takes over all the transport channels, and the conductance quanta $G_Q = 2e^2/h$. Due to the unitarity of the scattering matrix $\hat{S}$, the

current of all terminals sums up to zero. This is the Kirchhoff's current law based on the conservation of charges.

In the linear regime, consider the scattering matrix depends on much larger energy compared to the applied voltage V_β at one terminal β, the current induced in a terminal α is $I_\alpha = G_{\alpha\beta}V_\beta$, with the conductance

$$G_{\alpha\beta} = -G_Q \mathrm{Tr}\Big[\delta_{\alpha\beta} - \hat{S}^\dagger_{\alpha\beta}\hat{S}_{\alpha\beta}\Big], \tag{1.12}$$

where the scattering matrix is evaluated at the Fermi energy. This equation 1.12 is the Landauer formula in the scattering formalism [10].

ANDREEV BOUND STATE

Electrons impinging at the interface between a normal metal and a superconductor could either be reflected as electrons or holes. This peculiar process is called the Andreev reflection [11].

On the superconductor side, the gap energy is position-dependent and are elements of complex numbers. For convenient purposes, we assume the pairing potential has a modulus Δ and complex phase φ. Excitation states coupling electrons and holes have the corresponding energy counting from the Fermi surface

$$E = \sqrt{\xi^2 + \Delta^2}, \quad \xi = \hbar v_F(k - k_F). \tag{1.13}$$

If the excitation energy is above the gap energy $E > \Delta$, quasiparticles can propagate freely. If the excitation energy is within the gap $E < \Delta$, there are no propagating modes but only an evanescent solution falling off away from the interface.

On the normal metal side, hole states are decoupled from the electron states and the amplitude acquires an Andreev reflection factor r_A:

$$r_A(E) = e^{i\chi} = e^{-i\varphi}\Big(\frac{E}{\Delta} - i\frac{\sqrt{\Delta^2 - E^2}}{\Delta}\Big), \quad \chi = -\arccos\left(\frac{E}{\Delta}\right) - \varphi, \tag{1.14}$$

or in short, the reflected hole acquires an additional phase shift. The reflectivity $|r_A|^2 = 1$ when $E < \Delta$. This means when the energy is within the gap, the electron would always turn into a hole upon reflection. Similarly, the electron reflected from a hole acquires a phase shift

$$\bar{r}_A(E) = e^{i\bar{\chi}}, \quad \bar{\chi} = -\arccos\left(\frac{E}{\Delta}\right) + \varphi. \tag{1.15}$$

An interesting situation arises when a normal region is sandwiched by superconductors on two sides. The electrons in the gap are Andreev reflected back as holes at one interface. The holes are then reflected back as electrons on the other interface. We expect this confined motion of particles to form a discrete set of resonant states, in analogy to the finite square potential well. These resonant states are called the Andreev bound state (ABS) [12]. We can describe ABS using the scattering formalism.

A wave incident on the normal region can be represented by a vector of coefficient c_N^{in} that contains the amplitudes of incoming and outgoing electrons and holes. The reflected and transmitted wave have vector of coefficient c_N^{out}. The scattering matrix $S_N(E)$

of the normal region relates these two vectors, $c_N^{\text{out}} = S_N(E)c_N^{\text{in}}$. $S_N(E)$ decouples electrons and holes in the normal region thus has the block diagonal form in Nambu space. Each block satisfies unitarity conditions 1.8 and overall satisfies electron-hole symmetry 1.10:

$$S_N(E) = \begin{pmatrix} s_0(E) & \\ & s_0^*(-E) \end{pmatrix} \tag{1.16}$$

At the interface, specifically within the superconducting gap, define another scattering matrix $S_A(E)$ to count for the Andreev reflection $c_N^{\text{in}} = S_A(E)c_N^{\text{out}}$:

$$S_A(E) = \begin{pmatrix} & r_A(E)\mathbb{1} \\ \bar{r}_A(E)\mathbb{1} & \end{pmatrix} \tag{1.17}$$

where $\mathbb{1}$ is the unit matrix.

The bound state condition $c_N^{\text{in}} = S_A(E)S_N(E)c_N^{\text{in}}$ implies

$$\det\Big(\mathbb{1} - S_A(E)S_N(E)\Big) = \det\Big(\mathbb{1} - \bar{r}_A(E))\, s_0(E)\, r_A(E)\, s_0^*(-E)\Big) = 0, \tag{1.18}$$

which reduces to an eigenvalue problem to determine the ABS discrete energy spectrum of channel n:

$$E_n = \Delta\sqrt{1 - T_n \sin^2(\delta\varphi/2)}, \tag{1.19}$$

where T_n is the transmission eigenvalues corresponding to the scattering matrix $s_0(E)$ and $\delta\varphi$ is the phase difference across the junction. The minimum energy $\Delta\sqrt{1-T_n}$ is achieved at phase difference $\delta\varphi = \pi$. For the situation of a single-phase difference, zero energy only occurs when the scattering process is transparent $T_n = 1$.

The ground-state energy is the sum of single-particle excitations at negative energy. The phase variation of the ground-state energy gives rise to a persistent current – a supercurrent (Josephson current):

$$I(\delta\varphi) = -\frac{2e}{\hbar}\sum_n \frac{\partial E_n}{\partial(\delta\varphi)} = \frac{e\Delta}{2\hbar}\sum_n \frac{T_n \sin\delta\varphi}{\sqrt{1 - T_n\sin^2(\delta\varphi/2)}} \tag{1.20}$$

1.4. THEORETICAL METHODS

The derivations of some of the chapters in this thesis rely on several techniques to treat condensed matter systems. Despite playing important roles in the description of the dynamical behavior of the system, these techniques are not quite commonly known to non-experts. It is hence convenient to introduce them at the fundamental level.

MATSUBARA TECHNIQUE

In dealing with equilibrium systems at finite temperature, many texts employ the Matsubara technique, named after Takeo Matsubara [13]. This method lifts the conundrum that the perturbation theory of the many-body system breaks down at zero-temperature

[14]. It is based on the imaginary time quantum mechanics, which treats the finite temperature $T > 0$ perturbation theory by an analytical continuation of the real-time t to the imaginary time $-i\tau$ [15]. The method treats the equilibrium density matrix $e^{-\beta\hat{H}}$ as the evolution operator. The expectation value of an observable $\hat{\mathcal{O}}(\tau)$ is evaluated through the trace of the form $\langle\hat{\mathcal{O}}\rangle = \mathrm{T}\{\hat{\mathcal{O}}(\tau)e^{-\beta\hat{H}}\}$. It has the advantage that finite temperature perturbation theory can be expressed as integrals of imaginary-time quantities over the interval $-\beta \le \tau \le \beta$ (inverse temperature $\beta = 1/T$). Consequently, in the Fourier representation, the Green's function is defined on the Matsubara frequencies that are discretized on the imaginary axis of the complex energy plane. It is such that all contributions to the Green's function are mathematically well-defined.

To be precise, one decomposes the imaginary-time quantities $\tilde{g}(i\omega)$ into a Fourier series with period β and discrete imaginary frequencies that take forms depending on the bosonic/fermionic mode. Specifically, in the application to Green's function [16]:

$$g(\tau) = \frac{1}{\beta}\sum_{n=-\infty}^{\infty}\tilde{g}(i\omega_n)e^{-i\omega_n\tau} \tag{1.21}$$
$$\omega_n = \frac{2n\pi}{\beta}, \qquad \text{bosonic}$$
$$\omega_n = \frac{(2n+1)\pi}{\beta}, \qquad \text{fermionic}$$

In the zero-temperature limit $\beta \to \infty$, the summation 1.21 is equivalent to the integration over the imaginary frequency such that it becomes an evaluation of a contour integral,

$$\frac{1}{\beta}\sum_{i\omega} = \int_{-i\infty}^{i\infty}\frac{\mathrm{d}(i\omega)}{2\pi} \tag{1.22}$$

The imaginary-time ordered Green's function $g(\tau) = \langle -T_\tau\psi(\tau)\psi^*(0)\rangle$ defined on the imaginary time interval $(0,\beta)$ in the form of 1.21 satisfies the periodic boundary condition:

$$g(\tau+\beta) = g(\tau), \qquad \text{bosonic}$$
$$g(\tau+\beta) = -g(\tau), \qquad \text{fermionic}$$

In the presence of superconductivity, the wave function obeys the BdG equation 1.6. One can extend the Green's function $G_N(\tau)$ to the field operators $\Psi(\tau)$ of Nambu form

$$G(\tau) = -\langle T_\tau\Psi(\tau)\Psi^\dagger(0)\rangle, \quad \Psi(\tau) = \begin{pmatrix}\psi(\tau)\\ \psi^\dagger(\tau)\end{pmatrix}, \tag{1.23}$$

such that the equation of motion (Heisenberg equation) reads

$$\frac{\partial}{\partial\tau}\psi = [\hat{H},\psi], \quad \frac{\partial}{\partial\tau}\Psi = -\hat{H}_{\mathrm{BdG}}\Psi \tag{1.24}$$

and the Green's function satisfies

$$(i\omega_n - \hat{H}_{\mathrm{BdG}})\hat{G}(\tau) = \hat{\mathbb{1}} \tag{1.25}$$

1

ACTION FORMALISM

The scattering theory of electron transport can be incorporated into the formalism based on the semiclassical Green's function [17, 18]. In the circuit theory of quantum transport, this effort relates the more mathematical Green's function methods to a more heuristic and physical scattering language. In this language, the scatterer is characterized by an action, expressed as a determinant of a block of the scattering matrix. The generalization can extend to multi-terminal scatters and superconducting situation, eventually arriving at the block-determinant relation. For simplicity purposes, we slide over numerous derivations and only present some of the key results.

The establishment usually is based on the field theory and Keldysh Green's function. Keldysh technique is designed to describe out-of-equilibrium quantum systems and involves (anti-)time-ordered operators along the Keldysh contour. A Keldysh index ± denotes the forward or backward parts of the contour. It is common to use a "check" to denote the matrix structure with the Keldysh index.

For a perturbation to the Hamiltonian $\check{H} \to \check{H} + \check{h}(t)$, the variation of the action is

$$\delta S = \mathrm{Tr}[\check{h}\check{G}\tau_3] \tag{1.26}$$

where Pauli matrices $\hat{\tau}_{1,2,3}$ act on Keldysh indices, the "check" Green's function $\check{G}$ follows the conventional Keldysh Green's function definition [19], and the trace includes all the indices. In the context of a single level k of the reservoir, there is a $\check{\Sigma}$ acting as self-energy and typically can be written as $\check{\Sigma} = -i\sum_i (\Gamma_i/2)\check{g}_i$, Γ_i being the inverse escape time from the channel to the reservoir i and $\check{g}_i$ characterizing the reservoir with Eilenberger's normalization condition $\check{g}_i^2 = \mathbb{1}$ [20], then the Green's function of the state k is in the form of

$$\check{G}_k = \frac{1}{\epsilon - \epsilon_k - \check{\Sigma}}, \tag{1.27}$$

and the action can be written like

$$S = \mathrm{Tr}[\ln \check{G}_k \tau_3] \tag{1.28}$$

When it comes to the scattering theory among many channels, that a scattering matrix $\check{S}$ relates the incoming and outgoing wave function amplitude as in 1.7, the action is expressed in terms of the determinant of a block of the scattering matrix. Recall that in the Keldysh structure, the scattering matrix diagonal in Keldysh indices:

$$\check{S} = \begin{pmatrix} \hat{S}_+ & \\ & \hat{S}_- \end{pmatrix} \tag{1.29}$$

Here in addition to the terminal and channel indices as in 1.7, the time dependent $\hat{S}_\pm$ also is diagonal in time indices and corresponds to wave functions specified by $\check{H}_\pm$. It could be understood as that the "check" index refers to the sign of the velocity in corresponding channels. We can present this in a basis-invariant form as following:

$$L = \mathrm{Tr}\Big[\ln\Big(\frac{1-\check{g}}{2} + \frac{1+\check{g}}{2}\check{S}\frac{1+\check{g}}{2}\Big)\Big] = \ln\det\Big(\frac{1-\check{g}}{2} + \frac{1+\check{g}}{2}\check{S}\frac{1+\check{g}}{2}\Big) \tag{1.30}$$

So far, we haven't associated the action expression with superconductivity that contains a Nambu structure. The derivation of this is far from trivial. Nevertheless, the result is as per 1.30, apart from that there should be an additional 1/2 prefactor that comes with the trace over Nambu structure of all matrices and compensates the artificial fermionic states doubling. Additionally, under the spin-independent situation, a 2_s spin doubling factor cancels with this 1/2 factor of spin-independent scattering to retain the exact form as in 1.30.

1.5. TOPOLOGY

INTRODUCTION

Topology is a huge subject in mathematics concerned with the properties of certain defined structures. This structure can be a topological space, a group, a ring, etc. Often, the topological space is visualized by geometric objects that preserve many natural invariants upon continuous deformation, such as stretching and twisting but not tearing or puncturing. That's why it is sometimes referred to as rubber-sheet geometry.

In 1931, Dirac wrote a paper showing the natural occurrence of discrete magnetic charges, known as the Dirac monopole [21]. Although the related math work was done in parallel, it was until more than 40 years later did people realize the math structure behind it is that of fibre bundles [22]. Fibre bundles is a math language that helps to distinguish local and global geometry. The distinctive feature that characterizes the fibre bundle is the topological invariant.

Closely related with the Dirac monopole is the magnetic Aharonov-Bohm effect, or more generally the Berry phase. The concept of Berry phase quantifies the global phase evolution of a quantum state transported along a closed path in the parametric space. This is also the flux through an area enclosing a Dirac monopole. Having this analogy of electromagnetic vector potential of a charge moving in the background field of a monopole, relevant concepts of Berry connection, curvature, and Chern number can also be introduced.

Implementation of the fibre bundle in the band theory results in the topological band theory. It can be used to understand the Quantum Hall effect, which is the pedestal to the understandings of topological effect [23]. Further extension is generalized to classify phases of matter according to symmetries and dimensions [24–28]. This includes the topological insulators, topological semi-metals, topological superconductors, and many other systems.

The following subsections will only cover some basic concepts in the topological band theory for a better understanding of the subject.

TOPOLOGICAL BAND STRUCTURE

Consider a single-particle tight-binding Hamiltonian that has translational invariance [29, 30]. The parametric eigenvectors $|u_n(\mathbf{k})\rangle$ of the Bloch Hamiltonian

$$\mathscr{H}(\mathbf{k})|u_n(\mathbf{k})\rangle = E_n(\mathbf{k})|u_n(\mathbf{k})\rangle \tag{1.31}$$

that satisfies the normalization condition

$$\langle u_n(\mathbf{k})|u_{n'}(\mathbf{k})\rangle = \delta_{n,n'} \tag{1.32}$$

and commonly through a "periodic gauge choice" so that the eigenvectors

$$|u_{n'}(\mathbf{k}+\mathbf{G})\rangle = e^{-i\mathbf{G}\cdot\mathbf{r}}|u_{n'}(\mathbf{k})\rangle \tag{1.33}$$

with $\mathbf{r}$ being the position operator.

For a variation of the parameter $\mathbf{k}' = \mathbf{k} + d\mathbf{k}$, the deviation from the unit overlap 1.32 at first order in $d\mathbf{k}$,

$$\langle u_n(\mathbf{k})|u_n(\mathbf{k}+d\mathbf{k})\rangle \approx 1 + \langle u_n(\mathbf{k})|d\mathbf{k}\cdot\nabla_{\mathbf{k}}|u_n(\mathbf{k})\rangle = 1 - i\,d\mathbf{k}\cdot\mathbf{A}_n(\mathbf{k}) \tag{1.34}$$

defines the Berry connection

$$\mathbf{A}_n(\mathbf{k}) = i\langle u_n(\mathbf{k})|\nabla_{\mathbf{k}}|u_n(\mathbf{k})\rangle \tag{1.35}$$

The curl of this Berry connection gives Berry curvature $F^n_{ij}(\mathbf{k})$:

$$\begin{aligned}\mathbf{F}_n(\mathbf{k}) &= \mathrm{curl}\,\mathbf{A}_n(\mathbf{k}) = \epsilon_{ijk}F^n_{jk}(\mathbf{k})\\ F^n_{ij}(\mathbf{k}) &= i\langle\partial_i u_n(\mathbf{k})|\partial_j u_n(\mathbf{k})\rangle + \text{H.c.}\end{aligned} \tag{1.36}$$

In fact, this Berry curvature in the n-th band represents all the virtual transition to other bands. This can be seen by rewriting 1.36 as

$$F^n_{ij}(\mathbf{k}) = i\sum_{n\neq n'}\frac{\langle u_n(\mathbf{k})|\partial_i H(\mathbf{k})|u_{n'}(\mathbf{k})\rangle\langle u_{n'}(\mathbf{k})|\partial_j H(\mathbf{k})|u_n(\mathbf{k})\rangle}{(E_{n'}-E_n)^2} + \text{H.c} \tag{1.37}$$

The Berry curvature expressed in 1.37 manifests that it is valid and well-defined in the presence of multi bands with gaps. It also presents gauge invariance in contrast to the Berry connection from 1.35. The Berry curvature also possesses symmetries. For example, the periodicity, in contrast to the eigenvector, imposes:

$$F^n_{ij}(\mathbf{k}+\mathbf{G}) = F^n_{ij}(\mathbf{k}) \tag{1.38}$$

as well as the time-reversal symmetry and the inversion symmetry:

$$\begin{aligned}\text{TR:}\quad & F^n_{ij}(-\mathbf{k}) = -F^n_{ij}(\mathbf{k})\\ \text{I:}\quad & F^n_{ij}(-\mathbf{k}) = F^n_{ij}(\mathbf{k})\end{aligned} \tag{1.39}$$

Two other quantities can be immediate consequences of the Berry curvature. One is a gauge-invariant geometric phase acquired through a close orbit $\mathscr{C}$ in the parametric $\mathbf{k}$ space in the n-th band, or the Berry phase:

$$\Gamma_n(\mathscr{C}) = \oint_{\mathscr{C}} d\mathbf{k}\cdot\mathbf{A}_n(\mathbf{k}) = \int_S d^2k F^n_{xy}(\mathbf{k})\,[2\pi] \tag{1.40}$$

where $\partial S = \mathscr{C}$ and the Berry phase is defined modulo 2π.

Another quantity is the quantized integral of the Berry curvature over the Brillouin zone T^2 in space dimension two:

$$C_n = \frac{1}{2\pi}\int_{T^2} d^2k F^n_{xy}(\mathbf{k}) \in \mathbb{Z} \tag{1.41}$$

yields an integer, which is known as the Chern number. If both symmetries given in 1.39 are present, there is only a zero Chern number can be obtained.

CURRENT AND CONDUCTANCE

For a superconducting system, consider a BdG Hamiltonian $\mathscr{H}(t)$ with time-dependent parameter $\mathbf{k}(\mathbf{t})$. To calculate the averaged current electric current, we introduce the basis of instantaneous wave function for a particular spin σ in a given band n as in 1.31. The current operator is defined as

$$\mathbf{j} = \frac{2e}{\hbar}\frac{\partial \mathscr{H}}{\partial \mathbf{k}}, \tag{1.42}$$

$2e$ corresponds to the charge of the superconducting Cooper pairs, such as the electric current of spin σ in the band n up to first order in parametric velocity is [31, 32]

$$\begin{aligned}\mathbf{j}_{n,\sigma}(t) &= 2e\Big[\frac{1}{\hbar}\frac{\partial E_{n,\sigma}(t)}{\partial \mathbf{k}} + \big(i\langle\partial_{\mathbf{k}} u_{n,\sigma}(\mathbf{k})|\partial_t u_{n,\sigma}(\mathbf{k})\rangle + \text{H.c.}\big)\Big] \\ &= 2e\Big[\frac{1}{\hbar}\frac{\partial E_{n,\sigma}(t)}{\partial \mathbf{k}} - \dot{\mathbf{k}}(t)\times\mathbf{F}_n(\mathbf{k})\Big]\end{aligned} \tag{1.43}$$

The many-body expected value of the averaged supercurrent is obtained by integrating over the superconducting state. The first term (group velocity) corresponds to the adiabatic supercurrent and vanishes upon integration. The seconds term (anomalous velocity [33]) is quantized upon integration if $\dot{\mathbf{k}}$ is parametric independent, say linear with respect to some external applied vector field $\dot{\mathbf{k}} = \frac{e}{\hbar}\mathbf{E}$, as

$$\mathbf{j} = -2e\sum_{n,\sigma}(n_{n,\sigma} - \frac{1}{2})\dot{\mathbf{k}}\times\int_{T^2}\frac{d^2k}{2\pi}\mathbf{F}_n(\mathbf{k}) = -\frac{2e^2}{\hbar}\sum_{n,\sigma}(n_{n,\sigma} - \frac{1}{2})C_n\mathbf{E}\times\mathbf{e}_z \tag{1.44}$$

where n_n is the occupation number of the superconducting state n. The quantized conductance conductance is given by

$$\sigma_{xy} = -\frac{2e^2}{\hbar}\sum_{n,\sigma}(n_{n,\sigma} - \frac{1}{2})C_n^{xy} \tag{1.45}$$

We see that the contribution to the conductance is zero only when the many-body state is occupied by a single quasiparticle.

WEYL POINT

In the 3-dimensional space, a contact point between two bands can be modeled using a 2×2 Bloch Hamiltonian with Pauli matrices $\hat{\sigma} = (\sigma_x, \sigma_y, \sigma_z)$

$$\mathscr{H}(\mathbf{k}) = \mathbf{d}(\mathbf{k})\cdot\hat{\sigma} \tag{1.46}$$

The three coefficients are each analytical functions of three variables $\mathbf{k}$. The contact point $\mathbf{k}_c$ corresponds to $\mathbf{d}(\mathbf{k}_c) = 0$. As there are three linear equations and three unknown variables, there generally exists a solution in the parametric space of $\mathbf{k}$ [34]. Such an accidental degeneracy is not required by symmetries but is still topological robust. In the vicinity of the contact point of a small deviation $\mathbf{q} = \mathbf{k} - \mathbf{k}_c$, the Bloch Hamiltonian is

$$\mathscr{H}(\mathbf{k}_c + \mathbf{q}) = \mathscr{H}_W(\mathbf{q}) = \sum_{i,j} M_{ij} q_i \sigma_j, \tag{1.47}$$

where M_{ij} is a tensor that linearizes the affine projection.

This point in the parametric space can be considered as a topological defect, which can be characterized by a topological invariant (wrapping number). This invariant is also a Chern number and characterizes the total charge of the monopoles the parametric space encloses. It reads [35]

$$N = \frac{1}{2\pi}\int_{S^2} d\mathbf{S}\cdot\mathbf{F}_n(\mathbf{k}) \tag{1.48}$$

In the case of the present context, this number (or chirality) is given by

$$N = \operatorname{sign}\det(M_{ij}) \tag{1.49}$$

A Weyl Hamiltonian describes hypothetical chiral fermions and can be thought of as half of a Dirac fermion in the 3D space, in the sense that the Hamiltonian is 2×2 Pauli matrices instead of 4×4 Dirac matrices [36]. The chirality in this sense implies masslessness and has a linear dispersion relation. In order to annihilate the Weyl point, one needs to merge two Weyl points of opposite chirality ($N=\pm 1$) [37]. Each Weyl point occurs in pairs and corresponds to a single source of Berry flux or Berry charge [38].

In superconducting nanostructures, the energy spectrum resides in the space of independent superconducting phases, which play the role of band structure quasimomenta [39]. The spectrum is periodic such that Weyl singularities can be accommodated given enough dimension of the parametric space for level crossings. When time-reversal symmetry is preserved, as in 1.39, a Weyl point at $\mathbf{k}$ with chirality N guarantees another one at $-\mathbf{k}$ with the same chirality N. In order for the total chirality in the Brillouin zone to vanish, a minimum of four Weyl points is needed in that case.

1.6. THIS THESIS BRIEF

CHAPTER 2: TOPOLOGICAL PROPERTIES OF MULTI-TERMINAL SUPERCONDUCTING NANOSTRUCTURES: EFFECT OF A CONTINUOUS SPECTRUM

Multi-terminal superconducting nanostructures may possess topological properties that involve Berry curvatures in the parametric space of the superconducting phases of the terminals, and associated Chern numbers that are manifested in quantized transconductances of the nanostructure. This chapter investigates how the continuous spectrum that is intrinsically present in superconductors, affects these properties. Within scattering formalism, we derive the action and the response function that permits a redefinition of Berry curvature for continuous spectrum.

We found that the redefined Berry curvature may have a non-topological phase-independent contribution that adds a non-quantized part to the transconductances. This contribution vanishes for a time-reversible scattering matrix. We found compact expressions for the redefined Berry curvature for the cases of the weak energy dependence of the scattering matrix and investigated the vicinity of Weyl singularities in the spectrum.

CHAPTER 3: SPIN-WEYL QUANTUM UNIT: THEORETICAL PROPOSAL

Superconducting qubits are important for the practical implementation of quantum computers. In this chapter, we propose a novel type of the superconducting qubit: the spin-

Weyl quantum unit, a four-state hybrid quantum system that combines states of a spin and an Andreev superconducting qubit. We demonstrate how the unit can be manipulated to achieve an arbitrary unitary transformation in the space of four states by controlling the superconducting phase only, and a convenient readout.

CHAP 4: SPINTRONICS WITH A WEYL POINT IN SUPERCONDUCTING HETEROSTRUCTURES

We investigate transport in a superconducting setup housing a Weyl point in the spectrum of Andreev bound states. A minimum magnet state is realized in the vicinity of the point. We have shown that this minimum magnetic setup is suitable for realization of all common goals of spintronics: detection of a magnetic state, conversion of electric currents into spin currents, potentially reaching the absolute limit of one spin per charge transferred, detection of spin accumulation in the leads. The peculiarity and possible advantage of the setup is the ability to switch between magnetic and non-magnetic state by tiny changes of the control parameters: superconducting phase differences. We employ this property to demonstrate the feasibility of less common spintronic effects: spin on demand and alternative spin current.

CHAP 5: WEYL POINT IMMERSED IN A CONTINUOUS SPECTRUM: AN EXAMPLE FROM SUPERCONDUCTING NANOSTRUCTURES

A Weyl point in a superconducting nanostructure is a generic minimum model of a topological singularity at low energies. We connect the nanostructure to normal leads thereby immersing the topological singularity in the continuous spectrum of the electron states in the leads. This sets another simple and generic model useful to comprehend the modification of low-energy singularity in the presence of a continuous spectrum. The tunnel coupling to the leads gives rise to a new low energy scale Γ at which all topological features are smoothed. We investigate superconducting and normal currents in the nanostructure at this scale. We show how the tunnel currents can be used for the detection of the Weyl point. Importantly, we find that the topological charge is not concentrated in a point but rather is spread over the parameter space in the vicinity of the point. We introduce and compute the resulting topological charge density. We also reveal that the pumping to the normal leads helps to detect and investigate the topological effects in the vicinity of the point.

REFERENCES

[1] D. Hilbert, *Mathematical problems,* Bull. Amer. Math. Soc. **8**, 437 (1902).

[2] J. Von Neumann, *Mathematical foundations of quantum mechanics*, print version, paperback ed. (Princeton University Press, 1955).

[3] P. Dirac, *The Principles of Quantum Mechanics*, fourth edition (revised) ed. (Oxford at the Clarendon Press, 1958).

[4] D. Buchholz, *Current trends in axiomatic quantum field theory,* Lect. Notes Phys. **558**, 43 (2000), arXiv:hep-th/9811233 .

[5] S. J. Summers, *A perspective on constructive quantum field theory,* (2016), arXiv:1203.3991 [math-ph] .

[6] K. v. Klitzing, G. Dorda, and M. Pepper, *New method for high-accuracy determination of the fine-structure constant based on quantized hall resistance,* Phys. Rev. Lett. **45**, 494 (1980).

[7] F. R. S. M. V. Berry, *Quantal phase factors accompanying adiabatic changes,* Proceedings of the Royal Society of London A: Mathematical, Physical and Engineering Sciences **392**, 45 (1984).

[8] M. Tinkham, *Introduction to Superconductivity*, 2nd ed. (Dover Publications, 2004).

[9] Y. V. Nazarov and J. Danon, *Advanced Quantum Mechanics: A Practical Guide* (Cambridge University Press, 2013).

[10] Y. Nazarov and Y. Blanter, *Quantum Transport* (Cambridge University Press, 2009).

[11] A. Andreev, *The thermal conductivity of the intermediate state in superconductors,* Sov. Phys. JETP **19**, 1228 (1964).

[12] C. W. J. Beenakker, *Universal limit of critical-current fluctuations in mesoscopic josephson junctions,* Phys. Rev. Lett. **67** (1991), 10.1103/PhysRevLett.67.3836.

[13] A. Fetter and J. Walecka, *Quantum Theory of Many-Particle System*, Vol. 25 (Dover Publications, 2003).

[14] W. Kohn and J. M. Luttinger, *Ground-state energy of a many-fermion system,* Phys. Rev. **118**, 41 (1960).

[15] T. Matsubara, *A New Approach to Quantum-Statistical Mechanics,* Progress of Theoretical Physics **14**, 351 (1955), https://academic.oup.com/ptp/article-pdf/14/4/351/5286981/14-4-351.pdf .

[16] W. Huaiyu, *Green's Function in Condensed Matter Physics* (Science Press, 2012).

[17] Y. V. Nazarov, *Block-determinant formalism for an action of a multi-terminal scatterer,* Physica E: Low-dimensional Systems and Nanostructures **74**, 561 (2015).

[18] I. Snyman and Y. V. Nazarov, *Keldysh action of a multiterminal time-dependent scatterer,* Physical Review B **77** (2008), 10.1103/physrevb.77.165118.

[19] E. LIFSHITZ and L. PITAEVSKI, *Chapter x - the diagram technique for non- equilibrium systems,* in *Physical Kinetics*, edited by E. LIFSHITZ and L. PITAEVSKI (Butterworth-Heinemann, Oxford, 1981) pp. 391–412.

[20] T. Kita, *Gor'kov, eilenberger, and ginzburg–landau equations,* in *Statistical Mechanics of Superconductivity* (Springer Japan, Tokyo, 2015) pp. 201–227.

[21] P. A. M. Dirac, *Quantised singularities in the electromagnetic field,,* Proc. Roy. Soc. Lond. A **133**, 60 (1931).

[22] T. T. Wu and C. N. Yang, *Concept of nonintegrable phase factors and global formulation of gauge fields,* Phys. Rev. D **12**, 3845 (1975).

[23] F. D. M. Haldane, *Model for a quantum hall effect without landau levels: Condensed-matter realization of the "parity anomaly",* Phys. Rev. Lett. **61**, 2015 (1988).

[24] A. P. Schnyder, S. Ryu, A. Furusaki, and A. W. W. Ludwig, *Classification of topological insulators and superconductors in three spatial dimensions,* Phys. Rev. B **78**, 195125 (2008).

[25] X.-L. Qi, T. L. Hughes, and S.-C. Zhang, *Topological field theory of time-reversal invariant insulators,* Phys. Rev. B **78**, 195424 (2008).

[26] A. Kitaev, *Periodic table for topological insulators and superconductors,* AIP Conference Proceedings **1134**, 22 (2009).

[27] X. Chen, Z.-C. Gu, Z.-X. Liu, and X.-G. Wen, *Symmetry-protected topological orders in interacting bosonic systems,* Science **338**, 1604 (2012), https://science.sciencemag.org/content/338/6114/1604.full.pdf .

[28] Z.-C. Gu and X.-G. Wen, *Symmetry-protected topological orders for interacting fermions: Fermionic topological nonlinear σ models and a special group supercohomology theory,* Phys. Rev. B **90**, 115141 (2014).

[29] B. A. BERNEVIG and T. L. Hughes, *Topological Insulators and Topological Superconductors*, stu - student edition ed. (Princeton University Press, 2013).

[30] J. Cayssol and J. N. Fuchs, *Topological and geometrical aspects of band theory,* (2020), arXiv:2012.11941 [cond-mat.mes-hall] .

[31] D. Xiao, M.-C. Chang, and Q. Niu, *Berry phase effects on electronic properties,* Rev. Mod. Phys. **82**, 1959 (2010).

[32] G. Sundaram and Q. Niu, *Wave-packet dynamics in slowly perturbed crystals: Gradient corrections and berry-phase effects,* Phys. Rev. B **59**, 14915 (1999).

[33] R. Karplus and J. M. Luttinger, *Hall effect in ferromagnetics,* Phys. Rev. **95**, 1154 (1954).

[34] J. von Neumann and E. Wigner, *Über merkwürdige diskrete Eigenwerte. (German) [On unusual discrete eigenvalues],* j-PHYSIKAL-Z **30**, 465 (1929).

[35] G. Volovik, *The Universe in a Helium Droplet,* International series of monographs on physics (Oxford University Press, 2009).

[36] P. B. Pal, *Dirac, majorana, and weyl fermions,* American Journal of Physics **79**, 485 (2011), https://doi.org/10.1119/1.3549729 .

[37] G. E. Volovik, *Quantum phase transitions from topology in momentum space,* in *Quantum Analogues: From Phase Transitions to Black Holes and Cosmology*, edited by W. G. Unruh and R. Schützhold (Springer Berlin Heidelberg, Berlin, Heidelberg, 2007) pp. 31–73.

[38] H. Nielsen and M. Ninomiya, *The adler-bell-jackiw anomaly and weyl fermions in a crystal,* Physics Letters B **130**, 389 (1983).

[39] R.-P. Riwar, M. Houzet, J. S. Meyer, and Y. V. Nazarov, *Multi-terminal josephson junctions as topological matter,* Nature Communications **7**, 11167 EP (2016).

2

TOPOLOGICAL PROPERTIES OF MULTI-TERMINAL SUPERCONDUCTING NANOSTRUCTURES: EFFECT OF A CONTINUOUS SPECTRUM

This work was done jointly with E.V. Repin, it has also been included to his Ph. D. thesis. This chapter has been published as E. V. Repin, **Y. Chen**, and Y. V. Nazarov, *Topological properties of multi-terminal superconducting nanostructures: effect of a continuous spectrum*, Phys. Rev. B **99**, 165414 (2019). The numerical data has been reposited to http://doi.org/10.5281/zenodo.4376665

2.1. INTRODUCTION

The study of topological materials has been on the front edge of the modern research in condensed matter physics for the past decade [1–5]. These materials are appealing from fundamental point of view and for possible applications (TI-based Photodetector[6, 7], spintronics[8], field-effect transistor[9], catalyst[10] and quantum computing[11, 12]). The basis for applications is the topological protection of quantum states, which makes the states robust against small perturbations and leads to many unusual phenomena, e.g. topologically protected edge states[13–15]. The topological superconductors[16–19] and Chern insulators[20–23] are the classes of topological materials that are relevant for the present paper. In the case of the Chern insulator the topological characteristic is an integer Chern number[24, 25] computed with the Green's function of electrons occupying the bands in a Brillouin zone of a material - WZW form[26–29]. The first Chern number reduces to the sum of first Chern numbers of the filled bands. For each band, the first Chern number is defined as an integral of the Berry curvature over the Brillouin zone[30, 31]. The Berry curvature is commonly defined[32] as $B_{\alpha\beta} = 2\mathrm{Im}\langle\partial_\alpha k|\partial_\beta k\rangle$ with $|k\rangle$ being the wavefunction in this band and α, β being the parameters: in this case two components of a wavevector. If the Chern number of a crystal is not zero, the edge states necessarily appear at the interface between the crystal and the vacuum (since the Chern number of the vacuum is zero). The dimensionality of topological materials in real space is restricted by three from above, which significantly limits possible topological phases.

However, there is a way to circumvent this fundamental limitation. Recently, the multi-terminal superconducting nanostructures with conventional superconductors were proposed to realize the topological solids in higher dimensions[33]. Such nanostructures host discrete spectrum of so called Andreev bound states[34–36]. The energies and wavefunctions of these states depend periodically on the phases of superconducting terminals. This sets an analogy with a bandstructure that depends periodically on the wavevectors. The dimensionality of this bandstructure is the number of terminals minus one. Also, as it was noted[33], the multi-terminal superconducting nanostructures cannot be classified as the high-dimensional topological superconductors from the standard periodic table of topological phases[37]. The authors of [33] have considered in detail 4-terminal superconducting nanostructures and proved the existence of Weyl singularities[38, 39] in the spectrum. The Weyl singularity is manifested as level crossing of Andreev bound states at a certain point in 3-dimensional phase space. Each Weyl singularity can be regarded as a point-like source of Berry curvature. Owing to this, a nonzero two-dimensional Chern number can be realized and is manifested as a quantized transconductance of the nanostructure. This transconductance is the response of the current in one of the terminals on the voltage applied to the other terminal in the limit of small voltage, this signifies an adiabatic regime.

The peculiarity of the system under consideration is the presence of a continuous spectrum next to the discrete one. These states are the extended states in the terminals with energies above the superconducting gap. Were a spectrum discrete, the adiabaticity condition would imply the level spacing being much larger than the driving frequency. The level-spacing is zero for a continuous spectrum, so this complicates the adiabaticity conditions. This has been pointed out already in Ref.[33] but was not investigated in detail. We note the generality of the situation: a generic gapped system might have

a continuous spectrum above the certain threshold, and the adiabaticity condition required for the manifestations of topology needs to be revisited in this situation.

The aim of the present chapter is to investigate this question in detail for a generic model of a superconducting nanostructure. We have studied the linear response of currents on the changes of superconducting phases in the terminals. We model a multi-terminal superconducting nanostructure within the scattering approach[40]. In this approach the terminals of the nanostructure are described with semiclassical Green's functions and the scatterer coupled to the terminals is described by a unitary (in real time) S-matrix. Although it is not crucial, we made use of Matsubara formalism which conveniently allows us to concentrate on the ground state of the system and the limit of zero temperature is formally achieved by considering continuous Matsubara frequencies. So we do the calculations in imaginary time formalism[41]. At the first step, we obtain the general effective action describing the nanostructure in terms of the S-matrix and time-dependent semiclassical Green's functions of the terminals. At the second step, we expand the action to the second power in time-dependent phases of the terminals. At the third step, we concentrate on the limit of small voltage and driving frequency, to obtain the response function relevant for topological properties.

We can use the properly anti-symmetrized response function as a generalized definition of the Berry curvature that is suitable for the systems with and without a continuous spectrum. The main result of the present article is that so-defined Berry curvature is contributed to by a continuous spectrum as well as discrete one even in the case of energy-independent S-matrix. We derive an explicit formula for it. This solves the paradox mentioned in [33]: the Berry curvature associated with discrete Andreev bands is discontinuous when the highest Andreev bound state merges with the continuum, which indicates that the integral of the Berry curvature defined only for discrete spectrum will not reduce to an integer. The redefined Berry curvature that we find is continuous. It gives rise to integer Chern numbers if the S-matrix is time-reversible. If it does not we reveal a specific additional non-topological contribution that does not depend on the superconducting phases. We note the the importance of the energy scales much larger than superconducting gap $|\Delta|$ in this context. This is why we also discuss in detail the case of an energy-dependent S-matrix the energy scale of variation of which may be in any relation with superconducting gap. We find that the non-topological contribution depends on the regularization of the S-matirx at large energies. In particular, it vanishes if the S-matrix is regularized as $S_{\pm\infty} = 1$, this corresponds to no conduction between the terminals.

The chapter is organized as follows. In Sec. 2.2 we introduce the details of a model of a multi-terminal superconducting nanostructure and review the main aspects of a scattering matrix approach formalism in this case. The derivation and discussion of the response function are given in Sec. 2.4. In Sec. 2.6 we discuss the specific behaviour near the Weyl singularities, in the absence and presence of a weak spin-orbit coupling. In Sec. 2.5 we apply the general formulae to the case of a scattering matrix that varies only slightly on the scale of the superconducting gap $|\Delta|$. In Sec. 2.7 we address the energy-dependent S-matrices at arbitrary energy scale for a specific model of an energy dependence. We conclude the paper with the discussion of our results (Sec. 2.8). The technical details of the derivations are presented in Appendices.

2.2. MULTI-TERMINAL SUPERCONDUCTING NANOSTRUCTURE

Generally a multi-terminal superconducting nanostructure (Fig. 3.1) is a small conducting structure that connects n superconducting leads. The leads are macroscopic and are characterized by the phases of the superconducting order parameter. Each lead labeled by $\alpha \in \{0, 1, \cdots, n-1\}$ has its own superconducting phase ϕ_α and one of the leads' phase can be set to zero value $\phi_0 = 0$, according to the overall gauge invariance. The nanostructure design and these phases determine the superconducting currents I_α in each lead, that are the most relevant quantities to observe experimentally.

We aim to describe a general situation without specifying the nanostructure design. To this end, we opt to describe the system within the scattering approach pioneered by Beenakker [42]. The superconducting leads are treated as terminals: they are regarded as reservoirs which contain macroscopic amount of electrons and are in thermal equilibrium. A common assumption that we also make in this chapter is that all terminals are made from the same material and thus have the same modulus of the superconducting order parameter $|\Delta|$. At sufficiently low temperatures and applied voltages one can disregard possible inelastic processes in the nanostructure and concentrate on elastic scattering only. Following the basics of the scattering approach[40], we assume N_α spin-degenerate transport channels in terminal α. The conducting structure connecting the terminals is a scattering region and is completely characterized by a scattering matrix S which generally depends on energy ε and is a unitary matrix at any ε. In Matsubara formalism we use imaginary energy ϵ and the matrix S satisfies the condition $S_\epsilon S^\dagger_{-\epsilon} = 1$. All the details of the nanostructure design are incorporated into the scattering matrix.

The electrons and holes in the superconducting transport channels involved in the scattering process may be described as plane waves that scatter in the region of the nanostructure and then return to the corresponding terminals. Amplitudes of incoming and outgoing waves are linearly related by the S-matrix. The numbers of transport channels in the terminal α denoted as N_α determines the dimension of the scattering matrix: $\dim S = M \times M$, where $M = 2_S \sum_\alpha N_\alpha$ and 2_s counts for the spin. The electrons and holes experience Andreev reflection in the superconducting terminals: the electrons are converted into holes and turn back, the same happens to holes. The Andreev reflection is complete at the energies smaller than the superconducting gap Δ. Therefore, electron-hole waves may be confined in the nanostructure giving rise to discrete energy levels called Andreev bound states (ABS). The amplitudes and phases of these confined states are determined by the scattering matrix and Andreev reflection phases that involve the superconducting phases of the corresponding terminals. One can find the energies of the ABS ε through Beenakker's determinant equation[36]:

$$\det(e^{2i\chi} - S_\varepsilon e^{i\phi}\sigma_y (S^T_{-\varepsilon})^{-1}\sigma_y e^{-i\phi}) = 0, \quad \chi = \arccos(\frac{\varepsilon}{\Delta}) \tag{2.1}$$

where S_ε is the S-matrix at the real energy ε, $\sigma_y = \begin{pmatrix} 0 & -i \\ i & 0 \end{pmatrix}$ is a Pauli matrix acting in the spin space and $e^{i\phi}$ is the diagonal matrix in channel space ascribing the stationary superconducting phases of the terminals to the corresponding channels, $e^{i\phi} \to \delta_{ab} e^{i\phi_\alpha}$ where a, b label the channels and α is the terminal corresponding to the channel a. The

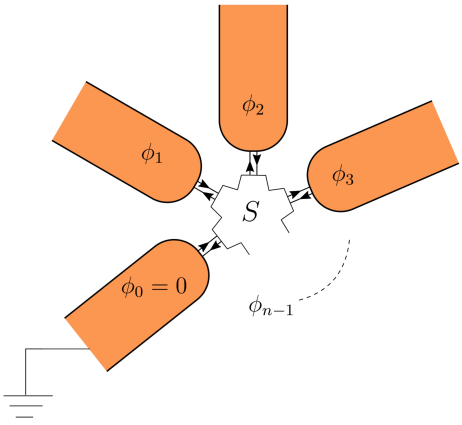

Figure 2.1: A multi-terminal superconducting nanostructure. Superconducting terminals are characterized by the corresponding superconducting phases. Electrons and holes coming from a terminal are scattered at the scattering region and can go to any other terminals. At least 4 terminals with 3 independent phases are required for a nanostructure to simulate a 3-dimensional bandstructure with topological properties.

ABS energies and the corresponding eigenvectors in the space of the channels depend parametrically on $n-1$ independent phases $\phi_\alpha \in [0, 2\pi]$ and thus can be viewed as a bandstructure defined in a "Brilluoin zone" of phases. It was noted[33] that (without spin-orbit interaction) three independent parameters are needed to tune the $n-1$ dimensional band structure of energy levels of ABS to reach the Weyl singularity at zero energy. It was also noted[33] that only one parameter is required to satisfy the condition for the highest ABS to touch the continuum above the gap ($\varepsilon = |\Delta|$). The ABS merges the continuum in this case and this implies that one cannot change this level adiabatically even for arbitrarily slow change of the parameters. When the incommensurate small voltages are applied to two terminals to sweep the phases[33], the system passes the points where the highest level merges with the continuum. This makes it questionable to apply the adiabaticity reasoning in this case. This makes it necessary to consider the contribution of the continuous spectrum to the response function of the currents in the limit of slow change of the parameters.

2.3. ACTION

The most general way to describe the nanostructure under consideration is to use an action method. This method has been pioneered in the context of a simple Josephson junction in [41]. In this method one deals with an action of the nanostructure that depends on the time-dependent superconducting phases $\phi_\alpha(\tau)$. The transport properties of the nanostructure as well as quantum fluctuations of the phases in case the nanostructure is embedded in the external circuit [41], can be derived from this action.

One of the advances of this Article is the derivation of such action for multi-terminal nanostructure and arbitrary S-matrix in Matsubara formalism. The details of the deriva-

tion are given in 2.9. Here we give the answer:

$$2L = -\mathrm{Tr}\log[\Pi_+ + \Pi_- \hat{S}_\epsilon], \quad \Pi_\pm = \frac{1 \pm g}{2} \tag{2.2}$$

where $\Pi_\pm$ and $\hat{S}_\epsilon$ are matrices in a space that is a direct product of the space of channels, the imaginary-time space, spin and Nambu space. The matrix $\hat{S}_\epsilon$ is diagonal in the corresponding energy representation, therefore it depends on the difference of the imaginary time indices only. Its Nambu structure is given by

$$\hat{S}_\epsilon = \begin{pmatrix} S_\epsilon & 0 \\ 0 & S^T_{-\epsilon} \end{pmatrix} \tag{2.3}$$

where S_ϵ is the electron energy-dependent S-matrix (see App. 2.9). The matrix g is composed of the matrices diagonal in energy and diagonal in time in the following way:

$$g = U^\dagger \tau_z U, \quad U^\dagger = \begin{pmatrix} e^{\frac{i\phi(\tau)}{2}} & 0 \\ 0 & e^{\frac{-i\phi(\tau)}{2}} \end{pmatrix} \begin{pmatrix} A_{-\epsilon} & A_\epsilon \\ A_\epsilon & A_{-\epsilon} \end{pmatrix} \tag{2.4}$$

where

$$A_\epsilon = \sqrt{\frac{E+\epsilon}{2E}}, \quad E = \sqrt{\epsilon^2 + |\Delta|^2}, \tag{2.5}$$

where τ_z is the 3rd Pauli matrix acting in Nambu space and the Nambu structure has been made explicit in $U^\dagger$. This form assumes that $|\Delta|$ is the same in all the terminals. If it is not so, the matrix A_ϵ also acquires the dependence on the channel index. It is worth noting that $g^2 = 1$ so that $\Pi_\pm$ are projectors. The matrix g can be associated with the semiclassical Green's function in a terminal[40, 43]: $e^{i\phi(\tau)}$ is the diagonal matrix in channel space ascribing the time-dependent superconducting phases of the terminals to the corresponding channels, $e^{i\phi(\tau)} \to \delta_{ab} e^{i\phi_\alpha(\tau)}$ where a, b label the channels and α is the terminal corresponding to the channel a. We note the gauge invariance of the action: due to the invariance of the trace under unitary transformations, the superconducting phases can be ascribed to the terminal Green's functions g as well as to the scattering matrix. Let us assume that the matrix S_ϵ does not depend on spin. Then the trace over spin is trivial. It is convenient to apply the unitary transformation $U^\dagger$ as in (2.4) to all the matrices in (2.2). This transforms the matrix g to τ_z. Then the projectors take a simple form $\Pi_\pm \to \frac{1\pm\sigma_z}{2}$ and the matrix in (2.2) reduces to the lower block-triangular form in Nambu space. The determinant is then equal to the determinant of the lower right block of the transformed matrix $\bar{S}_\epsilon$. Then the action takes the form

$$\begin{aligned} -2L = 2_S \mathrm{Tr}\log[A_\epsilon e^{\frac{-i\phi(\tau)}{2}} S_\epsilon e^{\frac{i\phi(\tau)}{2}} A_\epsilon + \\ + A_{-\epsilon} e^{\frac{i\phi(\tau)}{2}} S^T_{-\epsilon} e^{\frac{-i\phi(\tau)}{2}} A_{-\epsilon}] \end{aligned} \tag{2.6}$$

the S-matrix in Matsubara formalism is subject to the unitarity constraint,

$$S^\dagger_{-\epsilon} S_\epsilon = 1 \tag{2.7}$$

In what follows we ascribe the stationary phase to the S matrix. We also concentrate on the zero-temperature limit $k_B T \ll |\Delta|$, so the summations over discrete frequencies are replaced with integrations $\int \frac{d\epsilon}{2\pi}$.

2.3.1. STATIONARY PHASES

In the stationary case $\phi(\tau) = \phi + \delta\phi(\tau)$ with constant ϕ and $\delta\phi(\tau) \equiv 0$ the value of the action gives the stationary phase-dependent ground state energy of the nanostructure $E_g = \lim_{k_B T \to 0} TL_0$:

$$E_g = -\frac{2_S}{2}\int \frac{d\epsilon}{2\pi}\mathrm{Tr}\log Q_\epsilon \tag{2.8}$$

$$Q_\epsilon = A_\epsilon^2 S_\epsilon + A_{-\epsilon}^2 S_{-\epsilon}^T \tag{2.9}$$

where Trace is now over the channel space and the Trace over spin space is taken explicitly as a factor of 2_S unless specifically addressed. The operator Q_ϵ introduced here has the properties of the inverse of the Green's function although it is not related to an operator average: its determinant as function of complex ϵ vanishes, $\det Q_\epsilon = 0$, at imaginary values $\epsilon = \pm i\varepsilon_k$ corresponding to the ABS energies (compare with (2.1)). In addition to these singularities the operator Q_ϵ has two cuts in the plane of complex ϵ corresponding to the presence of a continuous spectrum in the terminals above the gap $|\Delta|$. We choose the cuts as shown in Fig. 2.2. The expression (2.8) can be simplified in the case when the S-matrix does not depend on energy

$$E_g = -\tfrac{2_S}{2}\int \tfrac{d\epsilon}{2\pi}\mathrm{Tr}\log\left(\tfrac{E+\epsilon}{2E} + \tfrac{E-\epsilon}{2E}SS^*\right) + \tfrac{2_S}{2}\int \tfrac{d\epsilon}{2\pi}\log\det(S^T) \tag{2.10}$$

the second (divergent) contribution here does not depend on the superconducting phases so we omit it. To compute the integral it is convenient to choose the basis in which the unitary matrix $\Lambda = SS^*$ is diagonal. This is a unitary matrix, so the eigenvalues are unimodular complex numbers. The phases of the eigenvalues are related to the energies of ABS: $\Lambda_k = e^{2i\chi_k}$, $\chi_k = \arccos[\epsilon_k/|\Delta|]$, $\chi \in [-\pi/2;\pi/2]$. The eigenvalue $\Lambda_k = 1$ is doubly degenerate and corresponds to the values $\epsilon_k = \pm|\Delta|$. The eigenvalues come in complex conjugated pairs $\Lambda_k^* = \Lambda_{-k}$, where $(-k)$ corresponds to the Nambu-counterpart of the $k-$th eigenvector. So only the eigenvalues $\mathrm{Im}\Lambda_k > 0$ correspond to the quasiparticle states with positive energies. We will label them with positive indices k. In what follows we define a "bar" operation that links these pairs $|\bar{k}\rangle = S|k^\star\rangle = |-k\rangle$ where $|k\rangle$ is some eigenvector of Λ. We note, however, that this operation is not a convolution, since $|\bar{\bar{k}}\rangle = \Lambda_k|k\rangle$.

In this basis we can rewrite the integral as

$$E_g = -\frac{2_S}{2}\sum_{k>0}\int \frac{d\epsilon}{2\pi}\log[\frac{(E+\epsilon)^2 + (E-\epsilon)^2 + 2\cos 2\chi_k}{4(\epsilon^2 + |\Delta|^2)}] \tag{2.11}$$

Evaluation of the integral brings to the known result

$$E_g = -\frac{2_S}{2}\sum_{\epsilon_k>0}\epsilon_k \tag{2.12}$$

where ϵ_k are the stationary phase-dependent ABS energies, as discussed above. The derivative of the ground state energy with respect to a stationary phase in terminal α gives the stationary current in the corresponding terminal,

$$I_\alpha = 2e\frac{\partial E_g}{\partial \phi_\alpha^{(0)}}. \tag{2.13}$$

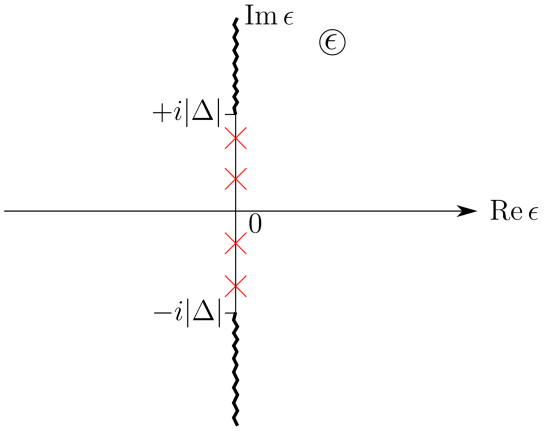

Figure 2.2: Singularities of the matrix Q_ϵ in the complex plane of energy ϵ. The symmetric cuts $[\pm i|\Delta|, \pm\infty]$ manifest the states of continuous spectrum. The isolated zeroes of the determinant of the matrix are situated at the imaginary axis within the interval $[-i|\Delta|, +i|\Delta|]$ (red crosses in the Figure). Their positions correspond to the ABS energies.

We expect this relation to hold in the adiabatic limit. In the following Section, we will access the time-dependent currents concentrating on the next order correction in the limit of small frequencies.

2.4. RESPONSE FUNCTION OF THE CURRENTS

To compute the response function of the currents we assume small nonstationary phase addition to the stationary phases ϕ, $\phi(\tau) = \phi + \delta\phi(\tau)$, $\delta\phi(\tau) \ll 2\pi$ and expand the action to the second order in $\delta\phi(\tau)$ (first order vanishes automatically since $\delta\phi(\tau)$ is nonstationary $\int_0^\beta d\tau\delta\phi(\tau) = 0$). We give the details in Append. 2.10. The total contribution to the action reads

$$\delta L = \sum_{\alpha,\beta} \int \frac{d\omega}{2\pi} \frac{\delta\phi_\omega^\alpha \delta\phi_{-\omega}^\beta}{2} R_\omega^{\alpha\beta}, \tag{2.14}$$

$\delta\phi_\omega$ being the Fourier transform of $\delta\phi(\tau)$. The frequency-dependent response function of the current $R_\omega^{\alpha\beta}$ is given by

$$\begin{aligned} R_\omega^{\alpha\beta} = & \\ & -2_S \int \frac{d\epsilon}{2\pi} \mathrm{Tr}\Big\{ Q_\epsilon^{-1} A_\epsilon^2 [\frac{P_\alpha}{2}(S_{\epsilon-\omega} - S_\epsilon)\frac{P_\beta}{2} + \\ & + \frac{P_\beta}{2}(S_{\epsilon+\omega} - S_\epsilon)\frac{P_\alpha}{2}] + \qquad (2.15) \\ & + \frac{1}{2} Q_\epsilon^{-1} \frac{\partial^2 Q_\epsilon}{\partial\alpha\partial\beta} - \qquad (2.16) \\ & - \frac{1}{2} Q_{\epsilon+\omega}^{-1} (A_{-(\epsilon+\omega)} (\frac{iP_\alpha}{2} S_{-\epsilon}^T - S_{-(\epsilon+\omega)}^T \frac{iP_\alpha}{2}) A_{-\epsilon} - \end{aligned}$$

$$
\begin{aligned}
&- A_{\epsilon+\omega}\left(\frac{iP_\alpha}{2}S_\epsilon - S_{\epsilon+\omega}\frac{iP_\alpha}{2}\right)A_\omega)\times \\
&\times Q_\epsilon^{-1}(A_{-\epsilon}\left(\frac{iP_\beta}{2}S^T_{-(\epsilon+\omega)} - S^T_{-\epsilon}\frac{iP_\beta}{2}\right)A_{-(\epsilon+\omega)} - \\
&- A_\epsilon\left(\frac{iP_\beta}{2}S_{\epsilon+\omega} - S_\epsilon\frac{iP_\beta}{2}\right)A_{\epsilon+\omega)}\Big\}
\end{aligned}
\tag{2.17}
$$

here the stationary phases are ascribed to the S-matrix. We use a shorthand notation $\partial/\partial_\alpha = \partial/\partial_{\phi_\alpha}$ and define a set of matrices that project channel space onto the space of the channels in the terminal α, $(P^\alpha)^{ab} = \delta^{ab}$ if a is a channel in terminal α and $(P^\alpha)^{ab} = 0$ otherwise. The term in (2.15) vanishes at zero frequency and in the case of the energy-independent S-matrix. The second term (2.16) does not depend on frequency ω. In the limit of zero frequency the second and the third terms (2.17) reproduce the stationary response function of the currents

$$
\lim_{\omega\to 0} R^{\alpha\beta}_\omega = -\frac{2_S}{2}\frac{\partial^2}{\partial\alpha\partial\beta}\int\frac{d\epsilon}{2\pi}\mathrm{Tr}\log Q_\epsilon = \frac{\partial^2 E_g}{\partial\alpha\partial\beta}
\tag{2.18}
$$

Let us consider the limit of small $\omega \ll |\Delta|$ and concentrate on the first order correction to the adiabatic limit

$$
R^{\alpha\beta}_\omega = \frac{\partial^2 E_g}{\partial\alpha\partial\beta} + \omega B_{\alpha\beta} + O(\omega^2)
\tag{2.19}
$$

We note that the response function is analytic in the vicinity of $\omega = 0$. This is guaranteed by the gap in the density of states, which is given by the energy of the lowest ABS. Away from the zero-energy Weyl singularity it can be estimated as $|\Delta|/N$ with N being the total number of ABS in the nanostructure. The vicinity of a Weyl singularity has to be treated more carefully as we discuss in Sec. 2.6. Let us note that for any system with a discrete spectrum the quantity $B_{\alpha\beta}$ can be related to the *Berry curvature*[30–32]. For any state in the discrete spectrum the Berry curvature corresponding to this state is given by $B^{(i)}_{\alpha\beta} = 2\mathrm{Im}\langle\partial_\alpha i|\partial_\beta i\rangle$ with i labeling discrete states and $|i\rangle$ being the wavefunction of the corresponding state. In our case we are interested in the total Berry curvature of the superconducting ground state defined as $B_{\alpha\beta} = -\frac{1}{2}\sum_i B^{(i)}_{\alpha\beta}$ where i labels the (spin-degenerate) wavefunctions of the BdG equation with positive eigenvalues[33]. However, the adiabaticity condition which justifies the expansion in Eq. (2.19) for the case of discrete spectrum requires the frequency to be much smaller than the smallest energy spacing between the levels.

In our system, the continuous spectrum above the superconducting gap is present. In principle, any continuous spectrum can be approximated with a discrete spectrum with a vanishing level spacing $\overline{\delta} \to 0$. By doing this we can utilize the previous expression for the response function $B_{\alpha\beta}$ since it is valid for the discrete spectrum. However, the adiabaticity condition which is necessary for this expression to be valid would reduce to $\omega \ll \overline{\delta} \to 0$. This condition contains an artificially introduced $\overline{\delta}$ and is by construction very restrictive in ω. On the other hand, the expansion in Eq. (2.19) is valid under a physically meaningful and less restrictive condition $\omega \ll |\Delta|/N$. Taken all that into account, we conclude that the response function $B_{\alpha\beta}$ defined in Eq. (2.19) does not have to reduce to the expression for a total Berry curvature of a superconducting ground state

of a system discussed above. The topological properties of this quantity also have to be investigated separately.

One may conjecture that the resulting response function in Eq. (2.19) reduces to the sum of the Berry curvatures of the discrete ABS spectrum, so that it is not contributed to by the continuous spectrum. This conjecture relies on the analogy between the expressions for the total Berry curvature and the superconducting ground state energy. In the case when the S-matrix is energy-independent, only the discrete states contribute to the ground state energy. Thus motivated, in the following we investigate the response function $B_{\alpha\beta}$ defined by means of Eq. (2.19) in detail. We find that there is a contribution from the continuous spectrum to this quantity as well as from the discrete one. We also find that in general the integral of $B_{\alpha\beta}$ over the phases ϕ_α, ϕ_β that would normally define an integer Chern number, is not integer. Therefore, $B_{\alpha\beta}$ contains a non-topological contribution. This non-topological part is contributed by the continuous as well as the discrete part of the spectrum.

The tensor $B_{\alpha\beta}$ defined in Eq. (2.19) is antisymmetric (since $R_{\omega}^{\alpha\beta} = R_{-\omega}^{\beta\alpha}$). The concrete expression for $B_{\alpha\beta}$ reads:

$$B_{\alpha\beta} = -\frac{2_S}{2}\int \frac{\mathrm{d}\epsilon}{2\pi}\left(\frac{1}{2}\mathrm{Tr}\left[Q_\epsilon^{-1}\frac{\partial Q_\epsilon}{\partial\epsilon}Q_\epsilon^{-1}\frac{\partial Q_\epsilon}{\partial\alpha}Q_\epsilon^{-1}\frac{\partial Q_\epsilon}{\partial\beta}\right] + \\ + \frac{\partial}{\partial\beta}\mathrm{Tr}\left[Q_\epsilon^{-1}A^2(\epsilon)\{\frac{\partial S_\epsilon}{\partial\epsilon}, \frac{iP_\alpha}{2}\}\right]\right) - (\alpha \leftrightarrow \beta) \tag{2.20}$$

The first term here resembles the usual WZW form[29] for a Chern number. Usually, the form contains the matrix Green's functions[29], in our case the form utilizes the matrix Q_ϵ defined by Eq. (2.9). We note however that in distinction from common applications of WZW forms here one cannot regard Q_ϵ as a smooth function of parameters $\phi_\alpha, \phi_\beta, \epsilon$ defined on a compact manifold without a boundary. This is because in general this matrix has different limits at positive and negative infinite energies $S_{-\infty}$ for $\epsilon \to -\infty$ and $S_{-\infty}^T$ for $\epsilon \to +\infty$ that also depend on the phases. Due to this reason the integral of the first term over a compact surface without a boundary in a space of phases does not have to reduce to an integer $\cdot(2\pi)^{-1}$. The second term in Eq. (2.20) has a form of a total derivative with respect to a phase of a periodic and smooth function, so the integral of this one over a compact surface will give zero.

In order to obtain the value of this integral let us consider first the variation of this value upon the small smooth variation of the matrix $Q_\epsilon \to Q_\epsilon + \delta Q_\epsilon$ that comes from the small variation of the S-matrix δS_ϵ, so $\delta Q_\epsilon = A_\epsilon^2 \delta S_\epsilon + A_{-\epsilon}^2 \delta S_{-\epsilon}^T$. The value of the integral of the second contribution in Eq. (2.20) does not contribute to the integral over a compact submanifold in phase space, so we needn't consider its variation. It is known [44] that the variation of the first contribution to $B_{\alpha\beta}$ reduces to the total derivatives with total antisymmetric tensor $e^{\alpha\beta}$:

$$\delta\{\int \frac{d\epsilon}{2\pi}\mathrm{Tr}\left[Q_\epsilon^{-1}\frac{\partial Q_\epsilon}{\partial\epsilon}Q_\epsilon^{-1}\frac{\partial Q_\epsilon}{\partial\alpha}Q_\epsilon^{-1}\frac{\partial Q_\epsilon}{\partial\beta}e^{\alpha\beta}\right]\} = \\ = \int \frac{d\epsilon}{2\pi}\partial_\epsilon \mathrm{Tr}\left[Q_\epsilon^{-1}\delta Q_\epsilon Q_\epsilon^{-1}\frac{\partial Q_\epsilon}{\partial\alpha}Q_\epsilon^{-1}\frac{\partial Q_\epsilon}{\partial\beta}\right]e^{\alpha\beta} + \tag{2.21}$$

$$+\int \frac{d\epsilon}{2\pi}\partial_\alpha \mathrm{Tr}\left[Q_\epsilon^{-1}\delta Q_\epsilon Q_\epsilon^{-1}(\frac{\partial Q_\epsilon}{\partial\beta}Q_\epsilon^{-1}\frac{\partial Q_\epsilon}{\partial\epsilon}-\frac{\partial Q_\epsilon}{\partial\epsilon}Q_\epsilon^{-1}\frac{\partial Q_\epsilon}{\partial\beta})\right]e^{\alpha\beta} \tag{2.22}$$

The value of the integral of (2.22) over a compact submanifold in phase space vanishes if the submanifold does not pass Weyl singularities corresponding to $\det Q_\epsilon^{-1}\to\infty$, because it has a form of a total derivative of a smooth function. Evaluation of the integral in (2.21) yields the following contribution to the variation of $B_{\alpha\beta}$

$$\frac{1}{2\pi}\delta\{\mathrm{Tr}[S_{-\infty}\frac{P_\alpha}{2}S_{+\infty}^\dagger\frac{P_\beta}{2}]\}e^{\alpha\beta} \tag{2.23}$$

We note that this contribution is generally nonzero and does not depend on phases.

Let us turn to the evaluation of the topological charge that is proven to be very useful in the field [28]. The value of the topological charge is defined in a usual way with the divergence of the topological field $\vec{E}$ and total antisymmetric tensor $e^{\gamma\alpha\beta}$

$$2\pi q=\mathrm{div}\vec{E},\quad E^\gamma\equiv\frac{1}{2}e^{\gamma\alpha\beta}B_{\alpha\beta} \tag{2.24}$$

To compute the topological charge we need to consider a special variation of the S-matrix that just corresponds to the stationary phase derivative $\delta S_\epsilon=[S_\epsilon,\frac{iP_\gamma}{2}]\delta\phi_\gamma$. Since the expression under the trace in (2.23) does not depend on phases, the topological charge vanishes at any point where the field $\vec{E}$ is well-defined, or alternatively $\det Q_\epsilon^{-1}$ is finite. The Weyl singularities give rise to the point-like integer charges being the sources of the field $\vec{E}$. We consider this in detail in Sec. 2.6. This situation is in complete analogy with that of the standard Berry curvature of a discrete spectrum where Weyl singularities correspond to band crossings. However, we have computed the topological charge for the particular phase-dependence of the S-matrix on phases ($e^{-\frac{i\phi}{2}}Se^{-\frac{i\phi}{2}}$). We have not considered the topological charge in the space of 2 phases ϕ_α,ϕ_β and some other parameter characterizing the scattering matrix, this charge could be nonzero and have a continuous distribution. The investigation of the general parametric dependence of the S-matrix is beyond the scope of the present article.

We separate the field $\vec{E}$ into three parts: a part produced by the point-like charges, divergenceless field that is zero in average, and a constant part $\vec{\bar{E}}$. The value of the integral

$$2\pi C^{12}=\int_0^{2\pi}\int_0^{2\pi}d\phi_1 d\phi_2\frac{B_{\alpha\beta}e^{\alpha\beta}}{2}=\int(d\vec{s},\vec{E}) \tag{2.25}$$

is given by the flux of the topological field through the corresponding surface. This flux reduces to the integer for the first contribution to $\vec{E}$, vanishes for the second divergenceless contribution and may result in some value for the constant part of the field. We stress that the last contribution being present is the main distinction from the common case. The value of this constant field is then given by the integration of the variation (2.23):

$$\bar{E}^\gamma=\frac{1}{2\pi}\{\mathrm{Tr}[S_{-\infty}\frac{P_\alpha}{2}S_{+\infty}^\dagger\frac{P_\beta}{2}]\}e^{\gamma\alpha\beta} \tag{2.26}$$

This constant field can contribute to the flux through any plane in the phase space:

$$C=n+2\pi(\vec{\bar{E}},\vec{n}) \tag{2.27}$$

where $\vec{n}$ is the normal vector to this plane. As it has been shown in Ref. [33] the value of C^{12} is directly related to the observable transconductance between the leads α and β. Therefore, in contrast to the conclusions of Ref. [33] the value of transconductance does not always quantize although the change of transconductance with a phase can be quantized.

So, in principle a nonzero non-topological contribution to (2.27) can be present. This contribution is nonzero if the S-matrix is not regularized at infinite energy such that $[S_{-\infty}, P_\alpha] = 0$. If the S-matrix is regularized in this way, then the Q_ϵ matrix is defined on a compact space of parameters $(\epsilon, \alpha, \beta)$, so the first contribution to Eq. (2.20) would reduce to an integer n (with proper normalization). If it is not regularized this way, then this boundary term leads to the presence of a non-topological contribution to the response function, that comes due to the presence of a continuous spectrum and, formally, from the fact that the matrix Q_ϵ is not defined on a compact space, as discussed above. In the limit of energy-independent S-matrix, this contribution reduces to the antisymmetric part of the Landauer conductance[40, 45]. In this case, if the bare S-matrix (without the stationary phases of terminals ascribed) is non-symmetric (which means the breaking the time-reversibility condition) we obtain a nonzero value of (2.26). If the S-matrix is time-reversible, the non-topological contribution is zero and the integer quantization of transconductance is restored.

2.5. WEAK ENERGY DEPENDENCE OF THE $S-$MATRIX

In the description of the realistic nanostructure a reasonable approximation is to consider the S-matrix to be constant on the scale of $|\Delta|$. It corresponds to the case of a short nanostructure (smaller than the superconducting coherence length). So a logical approximation would be to describe the nanostructure with a constant S-matrix at all energies. The response function $B_{\alpha\beta}$ is given by an integral over energy in Eq. (2.20). Would this integral accumulate in the region $\epsilon \sim |\Delta|$, then the approximation of a constant S-matrix at all energies would be accurate. However, there can be a significant contribution from the energy scales $\epsilon \gg |\Delta|$ to the integral yielding $B_{\alpha\beta}$. In this case the energy dependence of the S-matrix at the large energies becomes important. To investigate this we consider the contributions from the small scales $\epsilon \gtrsim |\Delta|$ and from the large scales $\epsilon \gg |\Delta|$ in the Subsections 2.5.1 and 2.5.2 respectively.

2.5.1. ENERGY-INDEPENDENT $S-$MATRIX:

In this Subsection we analyze the small-scale ($\epsilon \sim |\Delta|$) contribution to (2.20). For this we approximate the S-matrix to be constant at all energies and extend the integration limits to infinity. The second term in (2.20) vanishes since $\frac{\partial S_\epsilon}{\partial \epsilon} = 0$. The integral in the first term in (2.20) converges on the scale $\epsilon \gtrsim |\Delta|$. This statement only necessarily holds if the S-matrix is energy-independent. Otherwise, the contribution from the larger scales can be present and we investigate it in 2.5.2. Similarly to (2.11), the result of integration under consideration can be expressed in terms of the eigenvalues and eigenvectors of the unitary matrix $\Lambda = SS^*$. We use the same notations $|k\rangle$ and $|\bar{k}\rangle$ for the eigenvectors related to the complex conjugated eigenvalues pair Λ_k and Λ_k^* correspondingly as described after Eq.(2.10). We remind that the phase of the eigenvalue $\Lambda_k = e^{2i\chi_k}$ with $k > 0$ is related

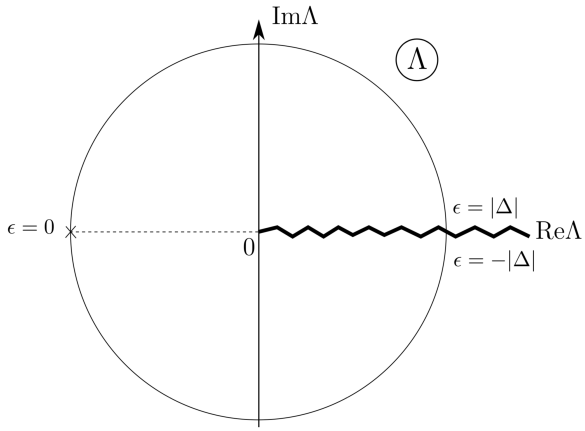

Figure 2.3: The choice of the branch cut of the logarithm in Eq. (2.28) in the plane of complex Λ.

to the energy of ABS as $\chi_k = \arccos[\epsilon_k/|\Delta|]$. We also remind that $\Lambda_k = 1$ is degenerate and corresponds to the energy of one of the ABS $\epsilon_k = |\Delta|$. Upon crossing this point in phase space, this ABS state exchanges the wave function with its Nambu counterpart with the eigenvalue $\epsilon_{k'} = -|\Delta|$. Due to this we call such points gap touching singularities.

Evaluating the integral yields

$$4\pi B_{\alpha\beta} = -2\sum_k \big(\log\Lambda_k - \log(1+i0sgn(k))\big)\langle\partial_\alpha k|\partial_\beta k\rangle - \\ -\sum_{k,j}(1-\frac{\Lambda_k}{\Lambda_j})\langle\bar{j}|\partial_\alpha\bar{k}\rangle\langle j|\partial_\beta k\rangle - (\alpha\leftrightarrow\beta) \tag{2.28}$$

where k, j label the eigenvalues of Λ, and the summation goes over indices with both signs. If the number of channels is odd, there is an eigenvector of Λ corresponding precisely to the eigenvalue $\Lambda_k = 1$. Then the index $k = 0$ corresponds to this state. If the number of channels is even, the indices in Eq.(2.28) do not take the zero value. In the following we consider the number of channels to be even. The logarithm here has a branch cut along the real axis as $[0, +\infty]$ (see Fig. 2.3) to avoid the gap touching singularity ambiguity $\Lambda_k = 1$. Let us consider the behaviour of $B_{\alpha\beta}$ in the vicinity of the gap touching singularity. Since the wave function corresponding to $\Lambda_k \to 1 + i0$ is discontinuous upon crossing this singularity, it is not obvious that $B_{\alpha\beta}$ is continuous. However, one can observe that the first term is a sum of Berry curvatures of individual levels multiplied by the eigenvalue-dependent prefactors $\log\Lambda_k$. This prefactors vanish for the discontinuous wavefunctions at the gap touching degeneracy and guarantee the continuity of the first term. Also, one can show that the second term in Eq.(2.28) is continuous. Consequently, $B_{\alpha\beta}$ is continuous at this point (see Fig. 2.4). The only possibility for $B_{\alpha\beta}$ to be ill-defined at some points in phase space is the zero-energy Weyl singularity where $\det Q_\epsilon^{-1}$ diverges (see Sec.2.6).

The response function $B_{\alpha\beta}$ is expressed in terms of eigenvalues and eigenvectors of the matrix Λ. So is the ABS contribution to the ground state Berry curvature, which was

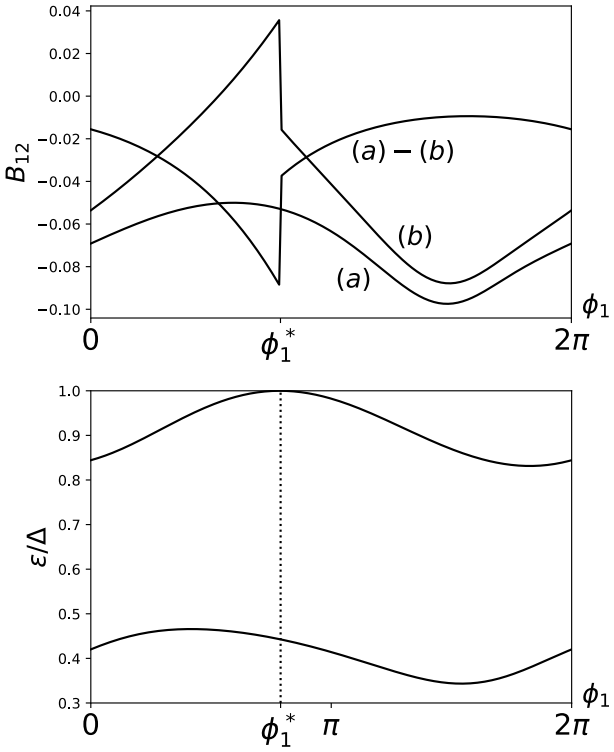

Figure 2.4: Example plots of B_{12}. To produce the plots, we chose one channel per terminal and took a random non-symmetric 4×4 scattering matrix describing the structure. We fix $\phi_2 = 1.20\pi, \phi_3 = 0.48\pi$ and change ϕ_1. (Upper panel) (a) the value of B_{12} as given (2.28). It is clearly a continuous function of ϕ_1. (b) The contribution of the discrete ABS to B_{12}. The contribution experiences a jump at a point where the highest ABS merges with the continuum. (a)-(b) is thus the contribution from the continuous spectrum. (See also Fig. 2.6)
(Lower panel) The ABS energies versus ϕ_1. The point where the highest level touches the gap egde by coincides with the point of discontinuity of the discrete spectrum contribution

conjectured as a result for $B_{\alpha\beta}$ (see Sec. 2.4). It was shown[33] that this ABS contribution is given by $B^{\mathrm{ABS}}_{\alpha\beta} = -\frac{2_S}{2}\sum_{k>0} B^{(k)}_{\alpha\beta}$, $B^{(k)}_{\alpha\beta} = 2\mathrm{Im}\langle\partial_\alpha k|\partial_\beta k\rangle$. Since one of the wavefunctions contributing to this sum is discontinuous at the gap touching singularity, we conclude that $B^{\mathrm{ABS}}_{\alpha\beta}$ is discontinuous contrary to $B_{\alpha\beta}$. One can understand the difference between $B_{\alpha\beta}$ and $B^{\mathrm{ABS}}_{\alpha\beta}$ by considering the computation of the integral in the first term in Eq. (2.20) by means of complex analysis (in the plane of complex ϵ). By shifting the integration contour to the upper half-plane, one can see that the integral is contributed to by the poles, corresponding to ABS and the cut above the gap (see Fig. 2.2). The contribution from the poles results in B_{ABS}, but the contribution from the cut, $B^{\mathrm{cut}}_{\alpha\beta} = B_{\alpha\beta} - B^{\mathrm{ABS}}_{\alpha\beta} \neq 0$, is equally important (see Fig. 2.4 and Fig. 2.6).

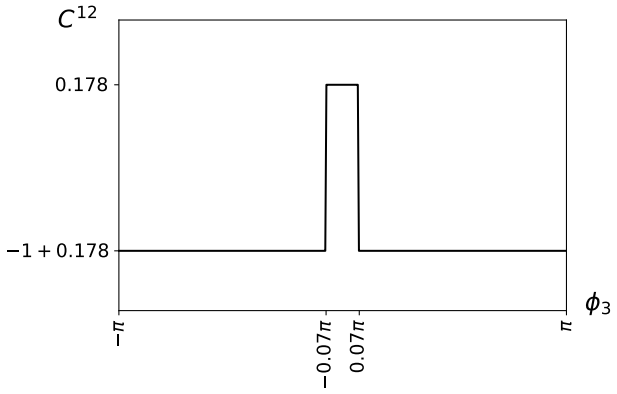

Figure 2.5: An example plot of the "Chern number" C_{12} defined as the integral of B_{12} over $\phi_{1,2}$ (see (2.27)). To produce the plot, we have chosen a randon 4×4 scattering matrix that is not invariant with respect to time reversal. We have found two Weyl singularities of opposite charge at $\phi_3=\pm0.07\pi$. We plot C^{12} versus ϕ_3 to demonstrate the integer jumps at the positions of Weyl singularities along with a non-integer, non-universal offset.

For the integrated $B_{\alpha\beta}$ we obtain in accordance with Eq. (2.27)

$$\int_0^{2\pi}\int_0^{2\pi} d\phi_1 d\phi_2 \frac{e^{\alpha\beta}B_{\alpha\beta}}{2} = 2\pi(n+\frac{1}{4}\mathrm{Tr}(S^\dagger P_\beta S P_\alpha)e^{\alpha\beta}) \tag{2.29}$$

so the value of transconductance is not necessarily quantized in the approximation of the energy-independent S-matrix.

2.5.2. CONTRIBUTION FROM THE LARGE SCALES

In the previous Section we have shown that the non-topological contribution to the transconductance comes from the boundary terms at $\epsilon=\pm\infty$ (see Eq.(2.21)). This means that, contrary to intuition, there is an essential contribution to $B_{\alpha\beta}$ coming from the energy scales much larger than the energy gap. In order to investigate the large energy contribution we assume the regularization of the S-matrix at large energies. So, in this Subsection we consider $B_{\alpha\beta}$ for a particular energy-dependence of the S-matrix. It is chosen such that the S-matrix is regularized at infinity such that it varies slowly on the scale of a superconducting gap $|\Delta|$ and $S_{\pm\infty}=1$. This S-matrix corresponds to a complete isolation of the terminals at the largest energies. With this regularization, the matrix Q_ϵ is defined on a compact parameter space (α,β,ϵ) and the first contribution in (2.20) must reduce to an integer. Due to the scale separation, there are two contributions to $B_{\alpha\beta}$. One comes from the scales $\epsilon\sim|\Delta|$ and is given by the same result (2.28). Another one comes from the scales $\epsilon\gg|\Delta|$.

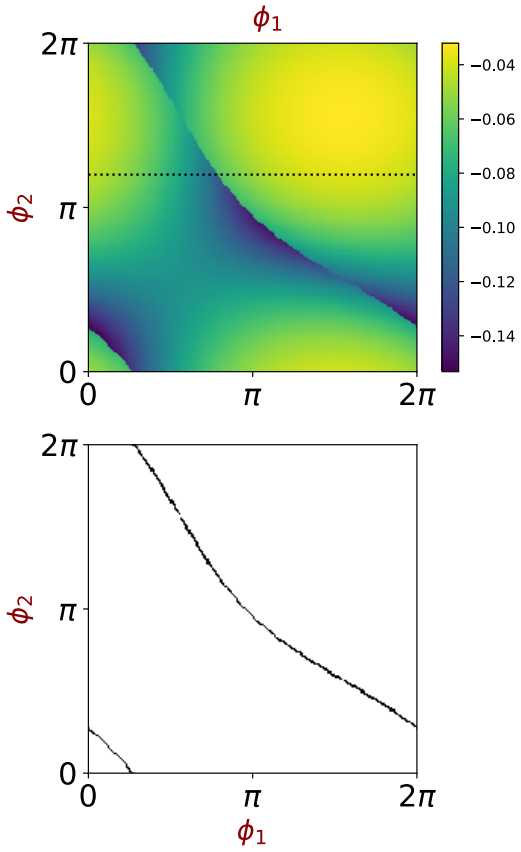

Figure 2.6: Example plots versus ϕ_1, ϕ_2. A random non-symmetric scattering matrix has been chosen to produce the plots, that varies slowly at the scale of $|\Delta|$, while $S_\infty = 1$. Upper panel: A density plot of the continuous spectrum contribution to B_{12} (Eq. (2.20))versus ϕ_1, ϕ_2 at $\phi_3 = 0.48\pi$. There is a discontinuity at the lines of the gap edge touching. Lower panel: the lines of the gap touching.

For negative energies, the large scale contribution with asymptotic accuracy equals

$$
\begin{aligned}
&-\frac{1}{2}e^{\alpha\beta}\int_{-\infty}^{0}\frac{d\epsilon}{2\pi}\mathrm{Tr}[\frac{\partial S_{-\epsilon}^{\dagger}}{\partial\epsilon}S_\epsilon\frac{\partial S_{-\epsilon}^{\dagger}}{\partial\alpha}\frac{\partial S_\epsilon}{\partial\beta}] = \\
&=-\frac{1}{2}e^{\alpha\beta}\int_{-\infty}^{0}\frac{d\epsilon}{2\pi}\partial_\epsilon\mathrm{Tr}[S_{-\epsilon}^{\dagger}\frac{iP_\alpha}{2}S_\epsilon\frac{iP_\beta}{2}] = \\
&=-\frac{1}{4\pi}e^{\alpha\beta}\mathrm{Tr}[S^{\dagger}\frac{iP_\alpha}{2}S\frac{iP_\beta}{2}]+\frac{1}{4\pi}e^{\alpha\beta}\mathrm{Tr}[S_{+\infty}^{\dagger}\frac{iP_\alpha}{2}S_{-\infty}\frac{iP_\beta}{2}]
\end{aligned}
\tag{2.30}
$$

with the notation $S = S_{\epsilon=0}$.

For positive ones:

$$
-\frac{1}{2}e^{\alpha\beta}\int_{0}^{+\infty}\frac{d\epsilon}{2\pi}\mathrm{Tr}[\frac{\partial S_\epsilon^{\star}}{\partial\epsilon}S_{-\epsilon}^{T}\frac{\partial S_\epsilon^{\star}}{\partial\alpha}\frac{\partial S_{-\epsilon}^{T}}{\partial\beta}] =
$$

$$= -\frac{1}{2}e^{\alpha\beta}\int_0^{+\infty}\frac{d\epsilon}{2\pi}\partial_\epsilon \mathrm{Tr}[S_\epsilon^\star \frac{iP_\alpha}{2}S_{-\epsilon}^T\frac{iP_\beta}{2}] =$$
$$= -\frac{1}{4\pi}e^{\alpha\beta}\mathrm{Tr}[S^\dagger\frac{iP_\alpha}{2}S\frac{iP_\beta}{2}] + \frac{1}{4\pi}e^{\alpha\beta}\mathrm{Tr}[S_{+\infty}^\dagger\frac{iP_\alpha}{2}S_{-\infty}\frac{iP_\beta}{2}]. \quad (2.31)$$

So, the both contributions give the following addition to the response function

$$\frac{1}{2\pi}e^{\alpha\beta}\mathrm{Tr}[S^\dagger\frac{P_\alpha}{2}S\frac{P_\beta}{2}] - \frac{1}{2\pi}e^{\alpha\beta}\mathrm{Tr}[S_{+\infty}^\dagger\frac{P_\alpha}{2}S_{-\infty}\frac{P_\beta}{2}] \quad (2.32)$$

Both terms here do not depend on phases. The first one is exactly equal to the constant part of the topological field defined previously with an opposite sign (computed for an energy-independent S-matrix case). So after integration over two phases, it cancels the non-topological contribution from small scales in (2.29). Since we assume a regularization $S_{\pm\infty} = 1$, the second term is zero ($\mathrm{Tr}[S_{+\infty}^\dagger\frac{P_\alpha}{2}S_{-\infty}\frac{P_\beta}{2}] = 0$), so the total mean value of the transconductance is quantized in correspondence with the theory of characteristic classes.

The second contribution to $B_{\alpha\beta}$ in Eq. (2.20) contains the energy-derivative of the S-matrix under the integral. Due to this the energy scale of its dependence drops out from the integral. So, one may expect that it contributes to the large scale contribution to $B_{\alpha\beta}$. However, with asymptotic accuracy it vanishes in the limit when the S-matrix varies slowly on the scale $|\Delta|$. Indeed, in the limit $|\epsilon| \gg |\Delta|$

$$Q_\epsilon^{-1} \simeq S_\epsilon^\star, \quad A_\epsilon^2 \simeq 0, \quad \epsilon > 0 \quad (2.33)$$
$$Q_\epsilon^{-1} \simeq S_{-\epsilon}^\dagger, \quad A_\epsilon^2 \simeq 1, \quad \epsilon < 0 \quad (2.34)$$

In this limit for $\epsilon < 0$, the integrand equals

$$\frac{\partial}{\partial\beta}\mathrm{Tr}[Q_\epsilon^{-1}A^2(\epsilon)\{\frac{\partial S_\epsilon}{\partial\epsilon}, \frac{iP_\alpha}{2}\}] \simeq$$
$$\simeq \partial_\beta\mathrm{Tr}[\frac{iP_\alpha}{2}(\frac{\partial S_\epsilon}{\partial\epsilon}S_{-\epsilon}^\dagger - \frac{\partial S_{-\epsilon}^\dagger}{\partial\epsilon}S_\epsilon)] = 0 \quad (2.35)$$

with asymptotic accuracy, since the expression under the trace does not depend on phases. For $\epsilon > 0$ the integrand vanishes since $A_\epsilon^2 \to 0$ for $\epsilon \gg |\Delta|$.

2.6. THE VICINITY OF A WEYL POINT

In this Section, we investigate the Berry curvature in the vicinity of a Weyl singularity, that occurs at some point $\vec{\phi}_0$ in the 3-dimensional phase space. Such Weyl points have been analyzed in [33] assuming spin symmetry, in [46] the analysis has been extended to cover weak spin-orbit interaction. Without spin-orbit coupling, the Weyl points are situated at zero energy and $\det Q_{\epsilon=0}^{-1}$ diverges near the point. A conical spectrum of ABS is found in the vicinity of the point [33]. A weak spin-orbit coupling splits the energy cones in spin and shifts the Weyl point to a finite energy [46]. Further, we discuss separately the cases of vanishing and weak spin-orbit coupling.

2.6.1. VANISHING SPIN-ORBIT COUPLING

When the spin-orbit (SO) coupling is absent, the Weyl singularities are located at some points in the phase space $\vec{\phi}_0$ and occur at zero energy $\epsilon_\pm = 0$. To consider the vicinity of the singularity, we assume a small phase deviation $\delta\hat{\phi} = \hat{\phi} - \hat{\phi}_0 \ll 1$ from the singularity point and assign it to each channel via the diagonal matrix $e^{\delta\hat{\phi}}$. In the vicinity, $B_{\alpha\beta}$ defined by Eq. (2.20) only has non-zero contributions from the first term of quasi-WZW term. The second term vanishes asymptotically when the energy approaches zero, as shown in Eq. 2.33. Conform to these approximations, we extend the domain of the integration over the phases to infinity since $B^{\alpha\beta}$ is concentrated near the singularity point.

To compute $B^{\alpha\beta}$, we approximate the Q matrix near the Weyl point with the expression that keeps the first orders in ϵ and of the variation: $Q = (\epsilon + \frac{1}{2}\delta\Lambda)S^T = MS^T$, S being the scattering matrix in the singularity point at $\epsilon = 0$. Conveniently, we can replace Q with M in Eq.(2.20). We find the variation $\delta\Lambda$ by expanding the S-matrix in $\delta\vec{\phi}$:

$$S \to S + \delta_\phi S = e^{-i\delta\hat{\phi}/2} S e^{i\delta\hat{\phi}/2} = S - [\frac{i\delta\hat{\phi}}{2}, S] \tag{2.36}$$

$$\Lambda = SS^* \to \Lambda + \delta_\phi\Lambda = \Lambda + iS\delta\hat{\phi}S^\dagger\Lambda - i\delta\hat{\phi}\Lambda \tag{2.37}$$

We can contract the dimension of M projecting it to two eigenvectors of Λ that achieve singular values at the Weyl point. Following [33], we separate the singular part of M and write in the basis of ABS eigenvectors $|+\rangle$ and $|-\rangle$ satisfying $S|\pm\rangle = \pm|\mp\rangle^*$, $\Lambda|\pm\rangle = -|\pm\rangle$:

$$M = \epsilon + \frac{1}{2}\delta\Lambda \equiv \epsilon + \frac{i}{2}\vec{h}\cdot\vec{\tau} \tag{2.38}$$

where $\vec{\tau}$ are the Pauli matrices in the space of these two eigenvectors, and the components of $\vec{h}$ are proportional to the components of $\vec{\phi}$: $h_x + ih_y = 2\langle -|\delta\hat{\phi}|+\rangle$, $h_z = \langle +|\delta\hat{\phi}|+\rangle - \langle -|\delta\hat{\phi}|-\rangle$.

The form of M is similar to the generic form of Green's function of a two-level system. We expect that the two poles of M^{-1} should be positioned symmetrically on the imaginary axis ϵ due to BdG particle-hole symmetry. Indeed, we find these poles at $\epsilon_\pm = \pm i\frac{|\vec{h}|}{2}$. Using the trace relations of Pauli matrices, we reduce in the leading order $B_{\alpha\beta}$ to the Berry curvature of the corresponding levels :

$$\begin{aligned} B^{\alpha\beta} &= -\frac{1}{4}\int \frac{d\epsilon}{2\pi}\mathrm{Tr}\left(M_\epsilon^{-1}\frac{\partial M_\epsilon}{\partial\epsilon}M_\epsilon^{-1}\frac{\partial M_\epsilon}{\partial\alpha}M_\epsilon^{-1}\frac{\partial M_\epsilon}{\partial\beta}\right) \\ &= \frac{1}{8}\int\frac{d\epsilon}{2\pi}\sum_{\substack{a,b,c\\=x,y,z}}\frac{1}{(\det M)^2}\Big(h_a\partial_\alpha h_b\partial_\beta h_c\epsilon_{abc} - \\ &- (\alpha\leftrightarrow\beta)\Big) = \frac{\vec{h}}{4|\vec{h}|^3}\cdot\partial_\alpha\vec{h}\times\partial_\beta\vec{h} - (\alpha\leftrightarrow\beta) \end{aligned} \tag{2.39}$$

We note that in this section all the matrices have the spin index. For an N dimensional space of superconducting phases, the singularities are concentrated in the $N-3$ dimensions and the relevant space is reduced to a 3-dimensional subspace $\{\delta\phi_1, \delta\phi_2, \delta\phi_3\}$. For certainty, we set the indices $\alpha, \beta = 1, 2$, and consider the curvature defined in the $\phi_1 - \phi_2$ plane at a fixed phase ϕ_3.

The ϕ_3 dependence of the integral of the curvature with respect to superconducting phases ϕ_1, ϕ_2 witnesses the change of first Chern number C^{12} when the integration plane passes the singularity point. Since we only concentrate on the vicinity of the Weyl singularity, the integral under the approximations made can only indicate the change of the Chern number, rather than its total value that can be determined by integration over the regions far from the singularity point. To compute the integrated $B_{\alpha\beta}$, we notice from Eq.(2.38) that the energy spectrum is linear in $\delta\phi$, and introduce a linear relation $h_i = \sum_\alpha \delta\phi_\alpha T_{\alpha i}$ with $T_{\alpha i} = \partial_\alpha h_i$ being a real invertible matrix. The integrated B_{12} is then obtained as:

$$C^{12} = \frac{1}{2\pi}\int B_{12}\mathrm{d}\phi_1\mathrm{d}\phi_2 = \frac{1}{2}\mathrm{sgn}(\delta\phi_3 \det T) \tag{2.40}$$

$\mathrm{sgn}(\delta\phi_3)$ determining the orientation of the $\delta\phi_3$ deviation.

This implies that whenever the integration plane passes the Weyl point, the first Chern number is changed by $\Delta C^{12} = \frac{1}{2}\mathrm{sgn}(\delta\phi_3 \det T) - \frac{1}{2}\mathrm{sgn}(-\delta\phi_3 \det T) = \pm 1$. This manifest the the integer values of the topological charge. The integrated $B_{\alpha\beta}$ in Eq.(2.40) specifies the flux of the Berry field penetrating the plane which is either above or below the singularity point. This flux, owing to symmetry, is a half of the total flux, this explains the half-integer values. Therefore, the main contribution to Eq.(2.28) in the vicinity the Weyl point is given by the Berry curvatures of the two levels that are close to zero energy, and can be presented as

$$2\pi B_{\alpha\beta} = 2\pi i[\langle\partial_\alpha +|\ \partial_\beta +\rangle - \langle\partial_\alpha -|\ \partial_\beta -\rangle] \tag{2.41}$$

2.6.2. WEAK SPIN-ORBIT COUPLING

Let us turn on a weak spin-orbit interaction and take it into account perturbatively giving a small spin-dependent change to the scattering matrix that preserves its unitarity, as is done in [46]. The first order variation thus reads

$$\begin{aligned} S \to & e^{-i\delta\phi/2} S e^{i\vec{\sigma}\cdot\vec{K}} e^{i\delta\phi/2} \\ = & S + \delta_\phi S + iS(\vec{\sigma}\cdot\vec{K}) \end{aligned} \tag{2.42}$$

$$\begin{aligned} \Lambda = & S\sigma_y S^*\sigma_y \to \Lambda + \delta_\phi\Lambda + \delta_K\Lambda \\ = & \Lambda + \delta_\phi\Lambda + iS(\vec{\sigma}\cdot\vec{K})S^\dagger\Lambda + i\Lambda(\vec{\sigma}\cdot\vec{K}^*) \end{aligned} \tag{2.43}$$

where the last equality sign implies the commutation relation $\sigma_y\sigma_i^*\sigma_y = -\sigma_i$. Here, $\vec{\sigma}$ are the Pauli matrices in spin space and $\vec{K}$ being the corresponding Hermitian matrix in the channel space characterizing the spin-orbit effects. Owing to the time reversibility, $\vec{K}(\vec{\phi}) = -\vec{K}(-\vec{\phi})$, yet in the vicinity of the singularity we may disregard its dependence on superconducting phases.

As in the previous Subsection, we project the matrix Q onto singular subspace that has now dimension of 4 to account for spin, and replace it with the matrix M. Writing the latter in the basis of eigenvectors $|\pm\rangle|\uparrow(\downarrow)\rangle$:

$$M = \epsilon + \frac{1}{2}\delta\Lambda = \epsilon + \frac{i}{2}(\vec{h}\cdot\vec{\tau} - \vec{\sigma}\cdot\vec{K}') \tag{2.44}$$

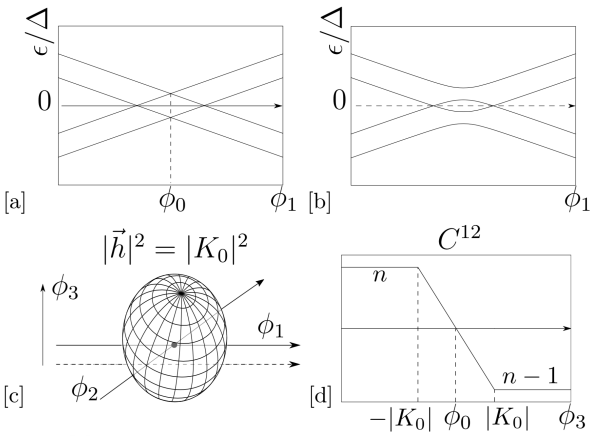

Figure 2.7: Spin-orbit splitting of Weyl singularity [a]: ABS energies versus ϕ_1 through the singularity for a choice $\phi_{2,3}$ corresponding to the singularity. The cone shifted upward(downward) specifies spin up (down). [b]: ABS energy with the same $\phi_{2,3}$ along the line ϕ_1 that misses the singularity. [c]: The ABS cross zero energy at the surface of the ellipsoid depicted. The ellipsoid encloses the singularity (central point). The ground state within the ellipsoid is of odd parity and the Berry curvature is zero. The central dot is the the Weyl singularity ϕ_0 enclosed in the ellipsoid. The ABS energies in [a,b] are plotted along the solid [a] and dashed [b]lines in the Figure. [d]: The "Chern number"C_{12} versus ϕ_3. The topological quantization is absent owing to the discontinuity of the ground state at the surface of the ellipsoid.

$\vec{K}' = \langle +|\vec{K}^*|+\rangle + \langle -|\vec{K}^*|-\rangle$. We can conveniently choose the spin quantization axis in the direction of $\vec{K}'$ replacing the operator $\vec{\sigma}\cdot\vec{K}'$ with its eigenvalues $\pm|K_0| = \pm\sqrt{|\vec{\sigma}\cdot\vec{K}'|}$ for spin up and down, respectively.

The spin-orbit coupling lifts the spin degeneracy of the ABS in the vicinity of a Weyl point. The poles at imaginary energies become $\epsilon_\uparrow = i(\pm\frac{|\vec{h}|}{2} + \frac{|K_0|}{2})$ for spin up and $\epsilon_\downarrow = i(\pm\frac{|\vec{h}|}{2} - \frac{|K_0|}{2})$ for spin down. Contrary to the spin-degenerate case, the singularities at $|\vec{h}| = 0$ are no longer at zero energy. Instead, they are shifted to $\pm i|K_0|$, see Fig. 2.7. The conical singularity of the spectrum remains and the topology is still protected, as we will explain below in detail.

The ABS energies cross zero energy when

$$|K_0| = |\vec{h}| = \sqrt{\sum \delta\phi_\alpha X_{\alpha\beta}\delta\phi_\beta} \tag{2.45}$$

is satisfied. (Here, we introduce a positively defined matrix $X_{\alpha\beta} = \sum_i T_{\alpha i}T_{i\beta}$. Eq.(2.45) defines an ellipsoidal surface in the 3D superconducting phase space that encloses the singularity at $\hat{\phi}_0$ where $|\vec{h}| = 0$. Outside the ellipsoid, two positive imaginary poles at $\epsilon_{+\uparrow(\downarrow)} = \frac{i}{2}(|\vec{h}| \pm |K_0|)$ hold a half of the residue of the spin degenerate pole ϵ_+ each. Two negative imaginary poles $\epsilon_{-\uparrow(\downarrow)}$ at $\epsilon_{-\uparrow(\downarrow)} = \frac{i}{2}(-|\vec{h}| \pm |K_0|)$ have the opposite residues. Inside the ellipsoid, poles of $\epsilon_{+\uparrow}$ and $\epsilon_{-\downarrow}$ exchange their values as well as wave functions, thus canceling the contributions from the other two poles. Thus, $B_{\alpha\beta}$ is zero inside the

ellipsoid and is the same as in the spin-degenerate case outside the ellipsoid,

$$B^{\alpha\beta} = \begin{cases} \frac{\vec{h}}{4|\vec{h}|^3} \cdot \partial_\alpha \vec{h} \times \partial_\beta \vec{h} - [\alpha \leftrightarrow \beta], & |K_0| < |\vec{h}| \\ 0, & |K_0| > |\vec{h}| \end{cases} \tag{2.46}$$

The result of integration of B^{12} over two superconducting phases ϕ_1,ϕ_2 at a fixed $\delta\phi_3$ thus reads

$$C^{12} = \frac{1}{2\pi} \int \mathrm{d}\phi_1 \mathrm{d}\phi_2 B^{12} \theta(|\vec{h}| \geq |K_0|^2) \tag{2.47}$$

One can understand this result geometrically by presenting Eq. (2.47) as an integral over the corresponding plane in $\vec{h}$ space,

$$\begin{aligned} C^{12} &= \frac{1}{2\pi} \int_{|\vec{h}^2| > |K_0|^2} \Big(\frac{\vec{h}}{2|\vec{h}|^3} \cdot \hat{n}^h_{12} \Big) \mathrm{d}^2 h_{12} \\ &= \frac{\mathrm{sgn}(\delta\phi_3 \det T)}{4\pi} \int_{|\vec{h}^2| > |K_0|^2} \frac{\mathrm{d}^2 h_{12}}{h^2} \\ &= \frac{\mathrm{sgn}(\delta\phi_3 \det T)}{2} \frac{\Omega_{12}}{2\pi} \end{aligned} \tag{2.48}$$

where $\hat{n}^h_{12}$ is the vector normal of the corresponding plane and Ω_{12} is eventually the solid angle at which a part of the $\phi_1 - \phi_2$ plane outside the ellipsoid is seen from the Weyl singularity (see Fig.2.7). Generally, this angle is expressed through elliptic integrals.

The integral can be simplified if we choose the coordinate system in 3D space of the phases in such a way that $T_{13} = T_{31} = T_{23} = T_{32} = 0$. With this, the integral can be evaluated as

$$\begin{aligned} C^{12} &= \frac{\mathrm{sgn}(\det T)\delta\phi_3}{2} \int_1^\infty \frac{(|K_0|^2 - T_{33}^2 \delta\phi_3^2) r \mathrm{d}r}{[(|K_0|^2 - T_{33}^2 \delta\phi_3^2) r^2 + T_{33} \delta\phi_3^2]^{\frac{3}{2}}} \\ &= \frac{1}{2} \mathrm{sgn}(\det T) \frac{\delta\phi_3}{|K_0|} \end{aligned} \tag{2.49}$$

We see that in the vicinity of a Weyl point the C^{12} is not a topologically protected quantity confined to the integer values: rather, it changes linearly in an interval of $\delta\phi_3$ defined by the strength of the spin-orbit coupling (Fig. 2.7)

To explain this, and eventually restore the topological protection of C_{12}, let us consider many-body states in the vicinity of the Weyl point. Their energies are given by the eigenvalues of the many-body Hamiltonian H_{MB}

$$H_{\mathrm{MB}} = E_\uparrow (\hat{n}_\uparrow - \frac{1}{2}) + E_\downarrow (\hat{n}_\downarrow - \frac{1}{2}) \tag{2.50}$$

where $E_{\uparrow(\downarrow)} = \frac{1}{2}(|\vec{h}| \pm |K_0|)$ are the energies of quasiparticle excitations with spin up(down), $\hat{n}_{\uparrow(\downarrow)}$ are the number operators of the quasiparticles with the corresponding spin. The energy spectrum E_{MB} for each of the four possible states is given in Fig. 2.8. As we see from the Figure, the ground state of the superconducting nanostructure corresponds to

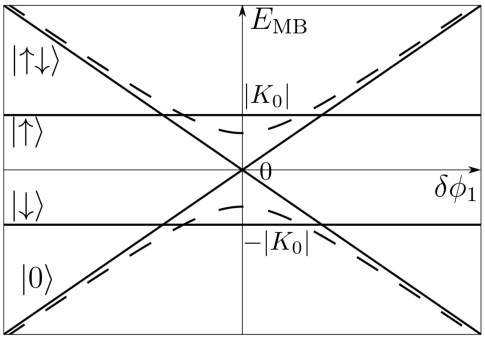

Figure 2.8: Many-body energy spectrum E_{MB} given by (2.50) corresponding to FIG. 2.7. The ground singlet state, single quasiparticle states of different spin and the excited singlet are labeled as $|0\rangle$, $|\downarrow(\uparrow)\rangle$ and $|\uparrow\downarrow\rangle$, respectively. The solid (dashed) lines correspond to the ABS plots FIG. 2.7 a (FIG. 2.7b). As the phase is varied, the ground state parity transition between $|0\rangle$ state and $|\downarrow\rangle$ state takes place at the point defined by (2.45).

$n_\uparrow = n_\downarrow = 0$ at $|\vec{h}| > |K_0|$ and to $n_\downarrow = 1, n_\uparrow = 0$ within the ellipsoid $|\vec{h}| < |K_0|$. These states differ in fermion parity, that is the conserving quantity for the superconducting Hamiltonian. This is why the parity transition that takes place at $|\vec{h}| = |K_0|$ is accompanied by the discontinuity of the wave functions, which violates the topological quantization of C^{12}. It is evident from Fig. 2.8 that the states of the odd fermion parity do not depend on phases in the vicinity of the Weyl point therefore corresponding to zero B^{12}.

The topological protection is restored if one considers the ground state at fixed parity. Then for the even ground state C^{12} is the same as for the spin-degenerate case and experiences an integer jump when the integration plane passes the singularity point. No change of topological charge occurs for the odd ground state and it remains topologically trivial.

2.7. ENERGY-DEPENDENT $S-$MATRIX

In this Section we consider the effect of the energy dependence of the S-matrix on B_{12} given by (2.20) for arbitrary relation between the energy scales of the scattering matrix and the gap $|\Delta|$.

We make use of the following model scattering matrix:

$$S_\epsilon = \frac{i\epsilon - \mu - \mathscr{E}(\hat{H} + i\hat{\Gamma}/2)}{i\epsilon - \mu - \mathscr{E}(\hat{H} - i\hat{\Gamma}/2)}, \quad [\hat{H}, \hat{\Gamma}] = 0 \tag{2.51}$$

where $\hat{\Gamma}, \hat{H}$ are Hermitian dimensionless matrices with eigenvalues of the order of one, $\mathscr{E}$ being some real energy scale. This expression can be regarded as a rather general polar decomposition of an energy-dependend scattering matrix. Since the matrices $\hat{\Gamma}, \hat{H}$ can be diagonalized simultaneously, the expession has poles at the complex energies

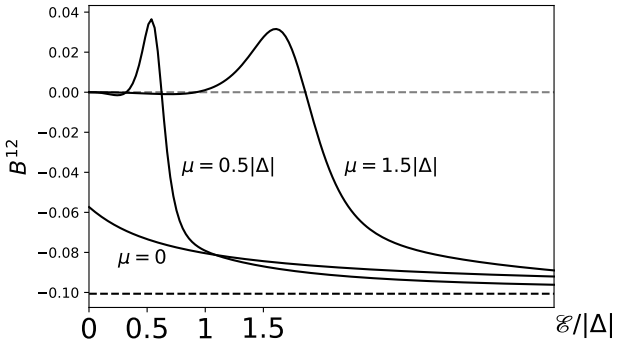

Figure 2.9: An example plot of B_{12} (Eq. 2.20) for a randomly chosen energy-dependent S versus the energy scale $\mathscr{E}$ for several choices of the energy scale μ at $\phi_1 = 0.22\pi, \phi_2 = -0.67\pi, \phi_3 = -\pi$. The dashed line gives the limiting value of B_{12} at $\mathscr{E} \gg |\Delta|$ where the energy dependence of the scattering matrix is weak.

$E = \mu + \mathscr{E}(H_n - i\Gamma_n/2)$ defined by the corresponding eigenvalues. The poles can be seen as the scattering resonances. The eigenvalues H_n set the energies of those resonances and the corresponding eigenvalues Γ_n give the inverse lifetimes of these resonances, Γ_n must be positive to assure the correct causal properties of the scatterimg. Real energy scale $\mathscr{E}$ then sets the typical spread of the poles in energy around their average position μ. We note that $S_\epsilon \to 1$ as $\epsilon \to \infty$, so the conditions of regularization described in a previous Section are fulfilled and the integral of B_{12} over a compact subspace in phase space that does not cross the Weyl singularities, reduces to an integer. We remind that the limit $S_\epsilon \to 1$ corresponds to isolated terminals. In distinction from the weak energy dependence case, the ABS energies defined by Eq. (2.1) can not be readily obtained and the resulting spectrum may be complicated with more ABS per transport channel. It is no more plausible to separate the contributions to $B_{\alpha\beta}$ coming from discrete and continuous spectrum. This, however, does not change the qualitative features of these contributions discussed above.

Let us consider and illustrate the dependence of B_{12} on these two energy scales. We choose random matrices $\hat{H}$, $\hat{\Gamma}$ that satisfy the conditions stated, and compute B_{12} from Eq. (2.20) at rather arbitrary settings of 3 phases. The integration over the imaginary energy in Eq. (2.20) permits the evaluation with no regard for the details of a complicated ABS spectrum. We plot the result versus the energy scale $\mathscr{E}$ at several settings of μ. (Fig. 2.9)

Let us consider $\mu \neq 0$ first. In this case, at $\mathscr{E} \to 0$ the transmission between the terminals is limited to a small circle of the radius $\simeq \mathscr{E}$ near μ. This suppresses the Andreev scattering that requires good transmission at opposite energies, and all quantities that depend on the phase differences including $B_{\alpha\beta}$. In Fig. 2.9, this is manifested as almost zero B_{12} at $\mathscr{E} < \mu$. The further increase of $\mathscr{E}$ restores the Andreev scattering bringing B_{12} to its typical values of $\sim (2\pi)^{-2}$. We note a non-monotonous dependence on $\mathscr{E}$ and explain it by the fact that different poles of the scattering matrix contribute to B_{12} with typically different signs, and the magnitude of the contribution depends on the position of the pole with respect to the energy scale $\simeq \Delta$. At $\mathscr{E} \gg \Delta$ the energy dependence of the

scattering matrix is weak at $\epsilon \simeq \Delta$ and B_{12} saturates at a value that does not depend on μ and is given by Eqs. (2.28) and (2.32) (dashed line in the Figure 2.9).

The case of $\mu = 0$ is special at small $\mathscr{E}$ since the concentration of transmission in a small circle of energies does not suppress the Andreev scattering. The ABS in this case are concentrated in this small energy circle (see [47]) and depend on all phases. This is why B_{12} does not drop to 0 but rather approaches a finite limit at $\mathscr{E} \to 0$. At $\mathscr{E} \gg \Delta$ B_{12} still saturates at the value corresponding to the weak energy dependence case.

2.8. SUMMARY AND CONCLUSIONS

In this Article, we address the topological properties of multi-terminal superconducting nanostructures. This involves Berry curvatures in the parametric space of the superconducting phases of the terminals and associated Chern numbers that manifest themselves in quantized transconductances [33].

The specifics of the superconducting nanostuctures is the presence of continuous spectrum along with the discrete one. The Berry curvature is readily defined for a discrete spectrum. Its generalization for a (partly) continuous spectrum is not straightforward, and is a problem of general interest. It has not been solved in Ref. [33].

We perform the calculation in imaginary time, and model the nanostructure with an energy-dependend scattering matrix. We have derived a general action of superconducting nanostructure with time-dependent phases, this is a separate advance. We expand the action near a point in the space of phases to compute the response function at finite frequency. We define the tensor quantity $B_{\alpha\beta}$ (Eq. (2.20)) as a first term in the expansion of the response function at small frequency. This quantity would have been Berry curvature if the spectrum were entirely discrete.

We analyze the topological properties of the computed quantity. Like for Berry curvature, the topological charge associated with divergence of $B_{\alpha\beta}$ is concentrated in the singular points of 3d phase space where ABS cross zero energy — Weyl points. Unlike Berry curvature, the quantity $B_{\alpha\beta}$ has a non-topological contribution that is constant over the space of phases (Eq. (2.26)). This in general adds a non-quantized part to "Chern" numbers defined as integrals of $B_{\alpha\beta}$ over two superconducting phases, and to the corresponding transconductances. This contribution is determined by the scattering matrix at $\epsilon \to \infty$. It vanishes if the scattering matrix without superconducting phases is time-reversible and if the scattering matrix approaches isolation limit $S_\epsilon = 1$ at large energies. For an energy-independent scattering matrix, the non-topological term is associated with the anti-symmetrized part of the conductance matrix of the structure in the normal state.

We consider in detail the case of weak energy dependence of the scattering matrix. We separate the contributions of the discrete and continuous spectrum, find them equally important and derive a compact relation for $B_{\alpha\beta}$ (Eq. (2.28)).

We analyze in detail the Berry curvature in the vicinity of Weyl points. We have found a violation of topological protection of "Chern" number in case of weak spin-orbit coupling. This, however, is rather trivially related to the transition between the ground states of different parity near the Weyl point and associated discontinuity of the wave functions. The topological protection is restored if one considers a ground state of a fixed parity.

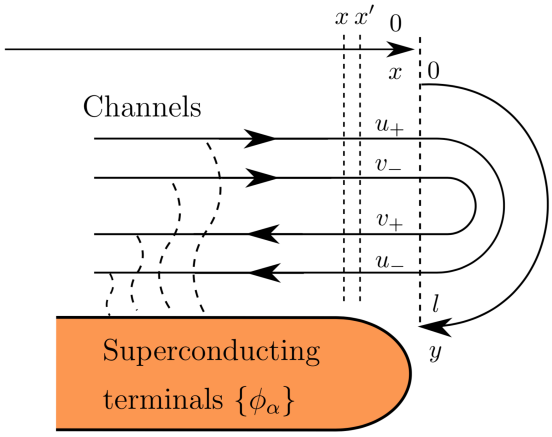

Figure 2.10: The concrete model for the derivation of the action. The electons are moving in $2N$ spin-degenerate channels connected to the corresponding superconducting terminals by tunneling (wavy dashed lines). In the picture, all the terminals in Eq.3.1 are combined into a single superterminal for convenience. Right of the vertical line, the tunnelling between the channels provides the scattering described by $N \times N$ matrix.

We also investigate the properties of $B_{\alpha\beta}$ for the scattering matrices that essentially depend on energy at the energy scale $\simeq \Delta$.

2.9. APPENDIX A: DERIVATION OF THE ACTION

In this Appendix, we derive the effective action for a multi-terminal superconducting junction within the scattering approach. We follow the lines of Ref.[48]. In contrast to Ref.[48] we proceed in Matsubara formalism. Let us start with the formulation of a concrete microscopic model. Since the scattering formalism is universal, there is a great degree of arbitrariness in the choice of the model: all models that are characterized by the same scattering matrix will result in the same action. Properties of the scatterer are to be completely described by an S-matrix, the details of the model that describes the system are not important. So we choose the model in a way we find it convenient (see Fig. 2.10). We consider a system of independent 1-dimensional channels with pairwise opposite velocities and a linear spectrum. They are defined in the interval $-\infty < x < 0$. The total number of channels is $2N$, number N includes the spin doubling. Two channels in a pair with opposite velocities are coupled to the same superconducting reservoir: this is required to assure the time-reversibility of the model at this level. The coupling is a tunnel one, and the coupling strength is characterized by the dwell time scale τ: at this time scale, an electron in a channel would tunnel to a reservoir. The tunneling results in an addition of self-energy to Green's functions in the channels, which is proportional to the tunneling rate $1/\tau$ and to a matrix Green's function g characterizing a reservoir (see its concrete definition below). The channels defined in such a way model the electron states coming from and going to the reservoirs that are scattered at the nanoscructure. In the scattering region with a coordinate $y \in [0, l]$, there are N spin-degenerate channels of

the same velocity direction. At the boundary $y = 0$ the electron amplitudes in the channels match those in the channels of positive velocity at $x = 0$ (incoming states), while at $y = l$ the amplitudes match those in the channels with the negative velocity(outgoing states). As we will show, the S-matrix relates the amplitudes at $y = l$ and $y = 0$.

To find the action for the nanostructure, we will compute its variation with respect to the variation of g. To this end, we require the values of the Green's functions in the channels $x, x' < 0$ in close points $x \approx x'$. We find the variation in three steps. At the first step, we express the Green's functions at any x in terms of the Green's functions at $x \approx 0$. At the second step, we consider the scattering region that provides a boundary condition. With this, we relate these Green's functions, and solve for them. This permits to find the variation and the action at the third step.

In the channels, we choose the basis in the following form

$$\begin{pmatrix} u_+ \\ v_- \\ u_- \\ v_+ \end{pmatrix} \tag{2.52}$$

where $u_\pm, v_\pm$ are N vectors in the space of the channels associated with the electron and hole amplitudes of the Bogolyubov wave function, and $\pm$ refers to the sign of the velocity in corresponding channels. In this basis, the equation for Green's function reads

$$\left(i\epsilon\tau_3 + i\nu\eta_3\tau_3\partial_x + \frac{i}{2\tau}g\right) G_{\mathrm{Ch}}(x, x') = \delta(x - x') \tag{2.53}$$

where ν is the velocity that we can set the same for all the channels, ϵ is the Matsubara frequency, τ_i are Pauli matrices in Nambu space, and $\eta_3 = \pm$ distinguishes channels with positive and negative velocities. The matrix g is block-diagonal in the channel space. For a given reservoir, it is given by

$$g = \frac{1}{\sqrt{\epsilon^2 + |\Delta|^2}}(\epsilon\tau_3 + i\sigma_2[\tau_1(\frac{\Delta - \Delta^*}{2}) + i\tau_2(\frac{\Delta + \Delta^\star}{2})]), \tag{2.54}$$

$g^2 = 1$, Δ being the superconducting order parameter in the corresponding reservoir.

We define a block structure

$$G_{\mathrm{Ch}} = \begin{pmatrix} G_1 & G_3 \\ G_4 & G_2 \end{pmatrix} \tag{2.55}$$

We are only interested in the diagonal blocks $G_{1;2}$ since the off-diagonal blocks will not contribute to the variation of the action. We integrate the equation assuming $\epsilon\tau \ll 1$ for $G(x, x')$ at $x < x'$ we obtain

$$G_1(x, x') = [(\frac{1 - g}{2} e^{\frac{(x-x')}{2\nu\tau}} + \frac{1 + g}{2} e^{-\frac{(x-x')}{2\nu\tau}})] G_1^-(x') \tag{2.56}$$

$$G_2(x, x') = [(\frac{1 + g}{2} e^{\frac{(x-x')}{2\nu\tau}} + \frac{1 - g}{2} e^{-\frac{(x-x')}{2\nu\tau}})] G_2^-(x') \tag{2.57}$$

where we use special notations for the Green's functions in the close points

$$G_1^-(x') = G_1(x' - 0, x'), \quad G_2^-(x') = G_2(x' - 0, x') \tag{2.58}$$

Since the solution for the Green's function should not grow $x \to -\infty$, these Green's functions should satisfy the following conditions

$$\Pi_+ G_1^- = 0, \quad \Pi_+ = \frac{1+g}{2}, \quad G_1^- = \lim_{x' \to -0} G_1^-(x') \tag{2.59}$$

$$\Pi_- G_2^- = 0, \quad \Pi_- = \frac{1-g}{2}, \quad G_2^- = \lim_{x' \to -0} G_2^-(x') \tag{2.60}$$

These matrices $G_{1;2}^-$ can be fixed if we consider the boundary conditions, that can be obtained by solving the equations for the Green's functions in the the scattering region $y \in [0; l]$. To derive these condition, let us introduce the amplitude vectors $\Psi(y) = G(y,x)$, $X(y) = G(x,y)$ that have Nambu structure $\begin{pmatrix} u(y) \\ v(y) \end{pmatrix}$ and satisfy the equations

$$\left(i\epsilon\tau_3 + iv\tau_3\partial_y - \begin{pmatrix} U(y) & 0 \\ 0 & U^T(y) \end{pmatrix} \right) \Psi(y) = 0 \tag{2.61}$$

$$\left(i\epsilon\tau_3 - iv\tau_3\partial_{y'} \right) X(y') - X(y') \begin{pmatrix} U(y') & 0 \\ 0 & U^T(y') \end{pmatrix} = 0 \tag{2.62}$$

where $U(y,\epsilon)$ is the $N \times N$ matrix potential acting on electrons inside the scattering region and mixing different channels. The solution of the Eq.(2.62) gives a linear relation on the amplitudes

$$X(y = l) = X(y = 0)\hat{S}_{-\epsilon}^{\dagger} \tag{2.63}$$

where we define the S-matrix for electrons and holes arranged in Nabmu structure

$$\hat{S}_\epsilon = \begin{pmatrix} S_e(\epsilon) & 0 \\ 0 & (S_h(\epsilon))^{-1} \end{pmatrix} \tag{2.64}$$

$$(S_h(\epsilon))^{-1} \equiv S_{-\epsilon}^T. \tag{2.65}$$

The electron scattering matrix is given by

$$S_e(\epsilon) = S_\epsilon = e^{-\frac{\epsilon l}{v}} \times T_y e^{-\frac{i}{v}\int_0^l dy U(y,\epsilon)} \tag{2.66}$$

where T_y implies the ordering of the $U(y)$ operators in the exponent according to the values of y in the increasing order. We do not need to specify the energy dependence fo the S-matrix except for the general condition $S_\epsilon S_{-\epsilon}^{\dagger} = 1$.

The relation on the amplitude (2.63) gives the relation between the diagonal and off-diagonal blocks of the Green's function (2.55) outside the scattering region but close to it $|x\epsilon/v| \ll 1, |x'\epsilon/v| \ll 1$

$$G_3(x,x) = G_1(x,x')\hat{S}_{-\epsilon}^{\dagger} = G_1^- \hat{S}_{-\epsilon}^{\dagger}, \quad (x < x') \tag{2.67}$$

The solution of Eq. (2.61)

$$\Psi(y = l) = \hat{S}_\epsilon \Psi(y = 0) \tag{2.68}$$

yields another relation between the blocks

$$G_2(x',x) = G_2^+ = \hat{S}_\epsilon G_3(x,x), \quad (x < x') \tag{2.69}$$

Combining Eq. (2.69) and (2.67) we obtain the required boundary condition that relates the diagonal sub-blocks

$$\hat{S}_\epsilon G_1^- \hat{S}_{-\epsilon}^\dagger = G_2^+ \tag{2.70}$$

Combining the equations (2.70), (2.59) and (2.60), and the condition

$$G_{\mathrm{Ch}}^+ - G_{\mathrm{Ch}}^- = -\frac{i}{\nu}\tau_3\eta_3 \tag{2.71}$$

that follows directly from (2.53) we solve the complete linear system of the equations to obtain the follwing for the diagonal blocks of the general Green's function (2.55)

$$G_1^- = \frac{i}{\nu}\frac{1}{\Pi_+ + \Pi_-\hat{S}_\epsilon}\Pi_-\hat{S}_\epsilon, \quad G_1^+ = \frac{-i}{\nu}\frac{1}{\Pi_+ + \Pi_-\hat{S}_\epsilon}\Pi_+ \tag{2.72}$$

$$G_2^- = \frac{-i}{\nu}\frac{1}{\Pi_- + \Pi_+\hat{S}_{-\epsilon}^\dagger}\Pi_+\hat{S}_{-\epsilon}^\dagger, \quad G_2^+ = \frac{i}{\nu}\frac{1}{\Pi_- + \Pi_+\hat{S}_{-\epsilon}^\dagger}\Pi_- \tag{2.73}$$

Next, we employ the formula that expresses the action variation in terms of Green's functions. We vary the reservoir Green's function g keeping normalization $g^2 = 1$, so that $\{g, \delta g\} = 0$, then the variation of the action L is

$$\delta L = \int dx \mathrm{Tr}[\delta\Sigma(x) G_{\mathrm{Ch}}(x,x)] \tag{2.74}$$

where $\delta\Sigma = \frac{-i}{2\tau}\delta g$ is the variation of self-energy of electrons in channels and $G_{\mathrm{Ch}}(x,x)$ is their Green's function at coinciding points. We note here that indeed only the diagonal blocks $G_{1;2}$ in Eq.(2.55) contribute since Σ is diagonal in this basis. The contribution from the channels corresponding to G_1 gives

$$2\delta L_{in} = +\int_{-\infty}^{0} dx \mathrm{Tr}[\delta\Sigma G_{\mathrm{Ch}}(x,x)] =$$

$$= \frac{-i}{2\tau}\int_{-\infty}^{0} dx \mathrm{Tr}[\delta g G_{\mathrm{Ch}}(x,x)] = \frac{-1}{2}\mathrm{Tr}[\delta g \frac{1}{\Pi_+ + \Pi_-\hat{S}_\epsilon}\Pi_+] \tag{2.75}$$

The futher calculations is convenient to do in the basis that diagonalizes g. In this basis,

$$\delta g = \begin{pmatrix} 0 & V \\ W & 0 \end{pmatrix}, \quad g = \begin{pmatrix} 1 & 0 \\ 0 & -1 \end{pmatrix}, \quad \hat{S} = \begin{pmatrix} S_1 & S_2 \\ S_3 & S_4 \end{pmatrix}$$

$$Y^{-1}(g + \delta g)Y = g, \quad Y(\hat{S} + \delta\hat{S})Y^{-1} = \hat{S} \tag{2.76}$$

we find

$$Y = \begin{pmatrix} 1 & \frac{-V}{2} \\ \frac{W}{2} & 1 \end{pmatrix}, \quad \delta S_4 = -S_3\frac{V}{2} - \frac{W}{2}S_2$$

$$2\delta L_{in} = \frac{1}{2}\mathrm{Tr}V S_4^{-1} S_3 \tag{2.77}$$

where all the realtions are valid up to the first order in variations. The contribution from the outgoing channels reads

$$2\delta L_{out} = \frac{1}{2}\mathrm{Tr}[\delta g \frac{1}{\Pi_- + \Pi_+ \hat{S}^\dagger_{-\epsilon}} \Pi_-] =$$

$$= \frac{1}{2}\mathrm{Tr}[\delta g S_\epsilon \frac{1}{\Pi_- S_\epsilon + \Pi_+} \Pi_-] = \frac{1}{2}\mathrm{Tr} W S_2 S_4^{-1} \tag{2.78}$$

Summing both contributions, we obtain

$$2\delta L = -\mathrm{Tr}[\delta S_4 S_4^{-1}] \tag{2.79}$$

Hence

$$2L = -\mathrm{Tr}\log S_4 = -\mathrm{Tr}\log[\Pi_+ + \Pi_- \hat{S}_\epsilon] \tag{2.80}$$

This so-called block-determinant result for the action is similar to the one obtained previously [48] within the Keldysh formalism.

2.10. APPENDIX B: DERIVATION OF THE RESPONSE FUNCTION

In this Appendix, we present the details of the derivation of the Eq.(2.17) and Eq.(2.20). We start with the action as given by Eq. (2.6). In order to derive the response function, we assume that the time-dependent deviation ($\delta\phi(\tau)$) from the stationary phase denoted as ϕ is small ($\delta\phi(\tau) \ll 2\pi$) so we can expand the action in Taylor series in $\delta\phi(\tau)$. We also note that in time representation the total phase operator is diagonal ($\phi_{\tau\tau'} = \delta_{\tau\tau'}\phi(\tau)$), which implies that the energy representation of ϕ reads

$$\phi_{nm} = \phi(\omega), \quad \omega = \epsilon_n - \epsilon_m \tag{2.81}$$

We consider here the general case of the energy-dependent scattering matrix. The action from Eq.(2.6) reads

$$-2L = \mathrm{Tr}\log[B + B^T], \quad B = A_\epsilon e^{\frac{-i\phi}{2}} S_\epsilon e^{\frac{i\phi}{2}} A_\epsilon \tag{2.82}$$

T implies the complete operator transposition that includes the reversing of the sign of energy. We remind the definition

$$A_\epsilon = \sqrt{\frac{E+\epsilon}{2E}}, \quad E = \sqrt{\epsilon^2 + |\Delta|^2}, \tag{2.83}$$

We ascribe the stationary part of the phases to an S-matrix $S_\epsilon \to S_\epsilon(\phi)$ and expand in small nonstationary deviation $\delta\phi(\tau)$.

$$B \simeq B_0 + B_1 + B_2 = B_0 + \frac{\partial B}{\partial \phi^\alpha_\omega}\delta\phi^\alpha_\omega + \frac{1}{2}\frac{\partial^2 B}{\partial\phi^\alpha_\omega \partial\phi^\beta_{-\omega}}\delta\phi^\alpha_\omega \delta\phi^\beta_{-\omega} \tag{2.84}$$

We introduce

$$Q_\epsilon = B_0 + B_0^T = A_\epsilon^2 S_\epsilon + A^2_{-\epsilon} S^T_{-\epsilon} \tag{2.85}$$

With this,

$$\delta \mathrm{Tr}\log[B+B^T] \simeq \mathrm{Tr}Q^{-1}(B_1+B_1^T+B_2+B_2^T)- \\ \frac{1}{2}\mathrm{Tr}Q^{-1}(B_1+B_1^T)Q^{-1}(B_1+B_1^T). \tag{2.86}$$

We remind the definition of the matrix, that projects on the channels connected to a given terminal α:

$$(P^\alpha)^{ab} = \delta^{ab}\begin{cases}1, & a=\alpha\\ 0, & a\neq\alpha\end{cases} \tag{2.87}$$

where a, b indices are in channels. With the help of this matrix the phase variation can be conveniently expressed as

$$(\delta\phi^\alpha)^{ab} = (P^\alpha)^{ab}\delta\phi^\alpha(\tau) \tag{2.88}$$

For simplicity of the notations, we denote the stationary phase derivatives $\partial_{\phi_\alpha} = \partial_\alpha$. With all this we consider the expansion of the S-matrix

$$e^{\frac{-i\delta\phi(\tau)}{2}} S_\epsilon e^{\frac{i\delta\phi(\tau)}{2}} \simeq S_\epsilon + [S_\epsilon, \frac{i\delta\phi(\tau)}{2}] + \frac{\delta\phi(\tau)}{2} S_\epsilon \frac{\delta\phi(\tau)}{2} - \\ - \frac{1}{2}\{(\frac{\delta\phi(\tau)}{2})^2, S_\epsilon\} \tag{2.89}$$

Let us we also note the identities for the derivatives with respect to the stationary phases:

$$\frac{\partial S}{\partial\alpha} = [S, \frac{iP_\alpha}{2}] \tag{2.90}$$

$$\frac{\partial^2 S}{\partial\alpha\partial\beta} = \frac{P_\alpha}{2}S\frac{P_\beta}{2} + \frac{P_\beta}{2}S\frac{P_\alpha}{2} - \delta_{\alpha\beta}\{\frac{P_\alpha}{4}, S\} \tag{2.91}$$

the first term in the expansion (2.86) vanishes since $\delta\phi_{\omega=0} = 0$. The second term is

$$\mathrm{Tr}Q^{-1}(B_2+B_2^T) = 2\mathrm{Tr}Q^{-1}B_2 = \\ \delta\phi_\omega^\alpha\delta\phi_{-\omega}^\beta \int \frac{d\epsilon}{2\pi}\mathrm{Tr}Q_\epsilon^{-1}A_\epsilon^2[-\delta_{\alpha\beta}\{\frac{P_\alpha}{4}, S_\epsilon\}+ \\ + \frac{P_\alpha}{2}S_{\epsilon-\omega}\frac{P_\beta}{2} + \frac{P_\beta}{2}S_{\epsilon+\omega}\frac{P_\alpha}{2}] = \\ = \frac{\delta\phi_\omega^\alpha\delta\phi_{-\omega}^\alpha}{2}\int\frac{d\epsilon}{2\pi}\mathrm{Tr}Q_\epsilon^{-1}[\frac{\partial^2 Q_\epsilon}{\partial\alpha\partial\beta}]+ \\ \delta\phi_\omega^\alpha\delta\phi_{-\omega}^\alpha\int\frac{d\epsilon}{2\pi}\mathrm{Tr}Q_\epsilon^{-1}A_\epsilon^2[\frac{P_\alpha}{2}(S_{\epsilon-\omega}-S_\epsilon)\frac{P_\beta}{2}+ \\ \frac{P_\beta}{2}(S_{\epsilon+\omega}-S_\epsilon)\frac{P_\alpha}{2}] \tag{2.92}$$

The first term here does not depend on frequency and does not vanish in the limit $\omega \to 0$. The second term up to linear order in ω can be rewritten as

$$2\omega\delta\phi^{\alpha}_{\omega}\delta\phi^{\alpha}_{-\omega}\int\frac{d\epsilon}{2\pi}\mathrm{Tr}[Q_{\epsilon}^{-1}A_{\epsilon}^{2}\frac{P_{\beta}}{2}\frac{\partial S_{\epsilon}}{\partial\epsilon}\frac{P_{\alpha}}{2}]= \\ \omega\delta\phi^{\alpha}_{\omega}\delta\phi^{\alpha}_{-\omega}\int\frac{d\epsilon}{2\pi}\mathrm{Tr}Q_{\epsilon}^{-1}A_{\epsilon}^{2}\partial_{\beta}\{\frac{\partial S_{\epsilon}}{\partial\epsilon},\frac{iP_{\alpha}}{2}\} \tag{2.93}$$

The second term in the expansion (2.86) reads

$$-\frac{1}{2}\mathrm{Tr}Q^{-1}(B_1+B_1^T)Q^{-1}(B_1+B_1^T)= \\ \frac{-\delta\phi^{\alpha}_{\omega}\delta\phi^{\beta}_{-\omega}}{2}\int\frac{d\epsilon}{2\pi}\mathrm{Tr}Q_1^{-1}(A_{-1}(\frac{iP_{\alpha}}{2}S^T_{-2}-S^T_{-1}\frac{iP_{\alpha}}{2})A_{-2}- \\ A_1(\frac{iP_{\alpha}}{2}S_2-S_1\frac{iP_{\alpha}}{2})A_2)Q_2^{-1}(A_{-2}(\frac{iP_{\beta}}{2}S^T_{-1}- \\ S^T_{-2}\frac{iP_{\beta}}{2})A_{-1}-A_2(\frac{iP_{\beta}}{2}S_1-S_2\frac{iP_{\beta}}{2})A_1) \tag{2.94}$$

where subscripts mean taking the function at the frequency $\epsilon_{1,2}$: $\epsilon_1=\epsilon_2+\omega$ and we denoted $\epsilon_2=\epsilon$. Summing it with (2.92) we get the general response function as in Eq. (2.17).

To perform the adiabatic expansion in the small parameter $\omega/|\Delta|$ here we keep ω as an independent parameter. We will use the identities

$$\frac{iP_{\alpha}}{2}S_2-S_1\frac{iP_{\alpha}}{2}=-\frac{\partial S_{cl}}{\partial\alpha}-\{S_q,\frac{iP_{\alpha}}{2}\} \tag{2.95}$$

where we introduced "classical" and "quantum" S-matrices as

$$S_{cl}=\frac{S_1+S_2}{2},\quad S_q=\frac{S_1-S_2}{2} \tag{2.96}$$

With this, we rewrite the term

$$\frac{-\delta\phi^{\alpha}_{\omega}\delta\phi^{\beta}_{-\omega}}{2}\int\frac{d\epsilon}{2\pi}\mathrm{Tr}Q_1^{-1}[A_1A_2(\frac{\partial S_{cl}}{\partial\alpha}+\{S_q,\frac{iP_{\alpha}}{2}\})+ \\ A_{-1}A_{-2}(\frac{\partial S^T_{cl}}{\partial\alpha}-\{S_q,\frac{iP_{\alpha}}{2}\})]Q_2^{-1}[A_1A_2(\frac{\partial S_{cl}}{\partial\alpha}-\{S_q,\frac{iP_{\alpha}}{2}\}) \\ +A_{-1}A_{-2}(\frac{\partial S^T_{cl}}{\partial\alpha}+\{S_q,\frac{iP_{\alpha}}{2}\})] \tag{2.97}$$

Next, we expand the terms that are taken at $\epsilon_1=\epsilon_2+\omega$. Thery come from three factors here. The expansion of the first factor $Q_1^{-1}\simeq Q_2^{-1}+\omega\frac{\partial Q_{\epsilon}^{-1}}{\partial\epsilon}$ gives rise to

$$\frac{\omega}{2}\delta\phi^{\alpha}_{\omega}\delta\phi^{\beta}_{-\omega}\int\frac{d\epsilon}{2\pi}\mathrm{Tr}Q_{\epsilon}^{-1}\frac{\partial Q_{\epsilon}}{\partial\epsilon}Q_{\epsilon}^{-1}\frac{\partial Q_{\epsilon}}{\partial\alpha}Q_{\epsilon}^{-1}\frac{\partial Q_{\epsilon}}{\partial\beta} \tag{2.98}$$

The expansion of the product of the classical parts is symmetric with respect to α, β, so it vanishes. The product of quantum parts vanishes in linear order in ω. So we only need to consider quantum times classical and expand the quantum one

$$S_q \simeq \frac{\omega}{2}\frac{\partial S_\epsilon}{\partial \epsilon} \tag{2.99}$$

it yields

$$\begin{aligned} &-\frac{2}{2}\delta\phi^\alpha_\omega \delta\phi^\beta_{-\omega}\int \frac{d\epsilon}{2\pi}\mathrm{Tr}Q^{-1}\frac{\omega}{2}(A^2_\epsilon\{\frac{iP_\alpha}{2},\frac{\partial S_\epsilon}{\partial\epsilon}\}- \\ &-A^2_{-\epsilon}\{\frac{iP_\alpha}{2},\frac{\partial S^T_{-\epsilon}}{\partial\epsilon}\})\frac{\partial Q}{\partial\beta}Q^{-1} = \\ &=\omega\delta\phi^\alpha_\omega\delta\phi^\beta_{-\omega}\int\frac{d\epsilon}{2\pi}\mathrm{Tr}\frac{\partial Q^{-1}}{\partial\beta}A^2_\epsilon\{\frac{\partial S_\epsilon}{\partial\epsilon},\frac{iP_\alpha}{2}\} \end{aligned} \tag{2.100}$$

where the first doubling is due to the same contribution with $\alpha \leftrightarrow \beta$. Summing it with (2.93) we obtain the total response function as given by (2.20)

$$\begin{aligned} &-\frac{2_S}{2}\omega\delta\phi^\alpha_\omega\delta\phi^\beta_{-\omega}\int\frac{d\epsilon}{2\pi}(\frac{1}{2}\mathrm{Tr}Q^{-1}_\epsilon\frac{\partial Q_\epsilon}{\partial\epsilon}Q^{-1}_\epsilon\frac{\partial Q_\epsilon}{\partial\alpha}Q^{-1}_\epsilon\frac{\partial Q_\epsilon}{\partial\beta}+ \\ &\frac{\partial}{\partial\beta}\mathrm{Tr}[Q^{-1}_\epsilon A^2(\epsilon)\{\frac{\partial S_\epsilon}{\partial\epsilon},\frac{iP_\alpha}{2}\}]) \end{aligned} \tag{2.101}$$

REFERENCES

[1] C. Xu and L. Balents, *Topological superconductivity in twisted multilayer graphene,* Phys. Rev. Lett. **121**, 087001 (2018).

[2] S. Yao and Z. Wang, *Edge states and topological invariants of non-hermitian systems,* Phys. Rev. Lett. **121**, 086803 (2018).

[3] M. J. Pacholski, C. W. J. Beenakker, and i. d. I. Adagideli, *Topologically protected landau level in the vortex lattice of a weyl superconductor,* Phys. Rev. Lett. **121**, 037701 (2018).

[4] M. S. Hossain, M. K. Ma, M. A. Mueed, L. N. Pfeiffer, K. W. West, K. W. Baldwin, and M. Shayegan, *Direct observation of composite fermions and their fully-spin-polarized fermi sea near $\nu = 5/2$,* Phys. Rev. Lett. **120**, 256601 (2018).

[5] X. Tan, D.-W. Zhang, Q. Liu, G. Xue, H.-F. Yu, Y.-Q. Zhu, H. Yan, S.-L. Zhu, and Y. Yu, *Topological maxwell metal bands in a superconducting qutrit,* Phys. Rev. Lett. **120**, 130503 (2018).

[6] M. R. Brems, J. Paaske, A. M. Lunde, and M. Willatzen, *Strain-enhanced optical absorbance of topological insulator films,* Phys. Rev. B **97**, 081402 (2018).

[7] C.-C. Tang, K. Ikushima, D. C. Ling, C. C. Chi, and J.-C. Chen, *Quantum hall dual-band infrared photodetector,* Phys. Rev. Applied **8**, 064001 (2017).

[8] M. Götte, T. Paananen, G. Reiss, and T. Dahm, *Tunneling magnetoresistance devices based on topological insulators: Ferromagnet–insulator–topological-insulator junctions employing* bi_2se_3, Phys. Rev. Applied **2**, 054010 (2014).

[9] J. Maciejko, E.-A. Kim, and X.-L. Qi, *Spin aharonov-bohm effect and topological spin transistor,* Phys. Rev. B **82**, 195409 (2010).

[10] H. Chen, W. Zhu, D. Xiao, and Z. Zhang, *Co oxidation facilitated by robust surface states on au-covered topological insulators,* Phys. Rev. Lett. **107**, 056804 (2011).

[11] C. Nayak, S. H. Simon, A. Stern, M. Freedman, and S. Das Sarma, *Non-abelian anyons and topological quantum computation,* Rev. Mod. Phys. **80**, 1083 (2008).

[12] D. Aasen, M. Hell, R. V. Mishmash, A. Higginbotham, J. Danon, M. Leijnse, T. S. Jespersen, J. A. Folk, C. M. Marcus, K. Flensberg, and J. Alicea, *Milestones toward majorana-based quantum computing,* Phys. Rev. X **6**, 031016 (2016).

[13] C. L. Kane and E. J. Mele, *Quantum spin hall effect in graphene,* Phys. Rev. Lett. **95**, 226801 (2005).

[14] C. Wu, B. A. Bernevig, and S.-C. Zhang, *Helical liquid and the edge of quantum spin hall systems,* Phys. Rev. Lett. **96**, 106401 (2006).

[15] L. Fu, C. L. Kane, and E. J. Mele, *Topological insulators in three dimensions,* Phys. Rev. Lett. **98**, 106803 (2007).

[16] X.-L. Qi, T. L. Hughes, S. Raghu, and S.-C. Zhang, *Time-reversal-invariant topological superconductors and superfluids in two and three dimensions,* Phys. Rev. Lett. **102**, 187001 (2009).

[17] X.-L. Qi, T. L. Hughes, and S.-C. Zhang, *Chiral topological superconductor from the quantum hall state,* Phys. Rev. B **82**, 184516 (2010).

[18] A. Das, Y. Ronen, Y. Most, Y. Oreg, M. Heiblum, and H. Shtrikman, *Zero-bias peaks and splitting in an al–inas nanowire topological superconductor as a signature of majorana fermions,* Nature Physics **8**, 887 EP (2012).

[19] L. Fu and E. Berg, *Odd-parity topological superconductors: Theory and application to* $cu_xbi_2se_3$, Phys. Rev. Lett. **105**, 097001 (2010).

[20] F. D. M. Haldane, *Model for a quantum hall effect without landau levels: Condensed-matter realization of the "parity anomaly",* Phys. Rev. Lett. **61**, 2015 (1988).

[21] N. Regnault and B. A. Bernevig, *Fractional chern insulator,* Phys. Rev. X **1**, 021014 (2011).

[22] Y. Zhang and X.-L. Qi, *Identifying non-abelian topological ordered state and transition by momentum polarization,* Phys. Rev. B **89**, 195144 (2014).

[23] T. Thonhauser and D. Vanderbilt, *Insulator/chern-insulator transition in the haldane model,* Phys. Rev. B **74**, 235111 (2006).

[24] X.-L. Qi and S.-C. Zhang, *Topological insulators and superconductors,* Rev. Mod. Phys. **83**, 1057 (2011).

[25] J. E. Moore and L. Balents, *Topological invariants of time-reversal-invariant band structures,* Phys. Rev. B **75**, 121306 (2007).

[26] E. Witten, *Global aspects of current algebra,* Nuclear Physics B **223**, 422 (1983).

[27] Z. Wang, X.-L. Qi, and S.-C. Zhang, *Topological order parameters for interacting topological insulators,* Phys. Rev. Lett. **105**, 256803 (2010).

[28] Z. Wang, X.-L. Qi, and S.-C. Zhang, *Equivalent topological invariants of topological insulators,* New Journal of Physics **12**, 065007 (2010).

[29] A. M. Essin and V. Gurarie, *Bulk-boundary correspondence of topological insulators from their respective green's functions,* Phys. Rev. B **84**, 125132 (2011).

[30] Q. Niu, D. J. Thouless, and Y.-S. Wu, *Quantized hall conductance as a topological invariant,* Phys. Rev. B **31**, 3372 (1985).

[31] D. J. Thouless, M. Kohmoto, M. P. Nightingale, and M. den Nijs, *Quantized hall conductance in a two-dimensional periodic potential,* Phys. Rev. Lett. **49**, 405 (1982).

[32] F. R. S. M. V. Berry, *Quantal phase factors accompanying adiabatic changes,* Proceedings of the Royal Society of London A: Mathematical, Physical and Engineering Sciences **392**, 45 (1984).

[33] R.-P. Riwar, M. Houzet, J. S. Meyer, and Y. V. Nazarov, *Multi-terminal josephson junctions as topological matter,* Nature Communications **7**, 11167 EP (2016).

[34] A. Andreev, *The thermal conductivity of the intermediate state in superconductors,* Sov. Phys. JETP **19**, 1228 (1964).

[35] P. de Gennes and D. Saint-James, *Elementary excitations in the vicinity of a normal metal-superconducting metal contact,* Physics Letters **4**, 151 (1963).

[36] C. W. J. Beenakker and H. van Houten, *Josephson current through a superconducting quantum point contact shorter than the coherence length,* Phys. Rev. Lett. **66**, 3056 (1991).

[37] A. Kitaev, *Periodic table for topological insulators and superconductors,* AIP Conference Proceedings **1134**, 22 (2009).

[38] L. Lu, Z. Wang, D. Ye, L. Ran, L. Fu, J. D. Joannopoulos, and M. Soljačić, *Experimental observation of weyl points,* Science **349**, 622 (2015).

[39] A. A. Soluyanov, D. Gresch, Z. Wang, Q. Wu, M. Troyer, X. Dai, and B. A. Bernevig, *Type-ii weyl semimetals,* Nature **527**, 495 EP (2015).

[40] Y. Nazarov and Y. Blanter, *Quantum Transport* (Cambridge University Press, 2009).

[41] G. Schön and A. Zaikin, *Quantum coherent effects, phase transitions, and the dissipative dynamics of ultra small tunnel junctions,* Physics Reports **198**, 237 (1990).

[42] C. W. J. Beenakker, *Random-matrix theory of quantum transport,* Rev. Mod. Phys. **69**, 731 (1997).

[43] G. Eilenberger, *Transformation of gorkov's equation for type ii superconductors into transport-like equations,* Zeitschrift für Physik A Hadrons and nuclei **214**, 195 (1968).

[44] X.-L. Qi, T. L. Hughes, and S.-C. Zhang, *Topological field theory of time-reversal invariant insulators,* Phys. Rev. B **78**, 195424 (2008).

[45] R. Landauer, *Spatial variation of currents and fields due to localized scatterers in metallic conduction,* IBM Journal of Research and Development **1**, 223 (1957).

[46] T. Yokoyama and Y. V. Nazarov, *Singularities in the andreev spectrum of a multiterminal josephson junction,* Phys. Rev. B **92**, 155437 (2015).

[47] A. A. Golubov, M. Y. Kupriyanov, and E. Il'ichev, *The current-phase relation in josephson junctions,* Rev. Mod. Phys. **76**, 411 (2004).

[48] Y. V. Nazarov, *Block-determinant formalism for an action of a multi-terminal scatterer,* Physica E: Low-dimensional Systems and Nanostructures **74**, 561 (2015).

3

SPIN-WEYL QUANTUM UNIT: THEORETICAL PROPOSAL

This chapter has been published as **Y. Chen** and Y. V. Nazarov, *Spin Weyl quantum unit: A theoretical proposal*, Phys. Rev. B **103**, 045410 (2021). The numerical data have reposited to zenodo.org/record/4538221

3.1. INTRODUCTION

Superconducting qubits are defined in the micro-fabricated macroscopic-scale superconducting circuits with quantum properties. Such circuits generally comprise superconducting loops with weak link coupling the superconductors. The artificial quantum mechanics emerging from an interplay of Josephson effect and Coulomb blockade makes it possible a rich variety of qubit designs. [1] Flux qubit[2, 3], charge qubit[4, 5] and phase qubit [6, 7] have been developed over the decades. The qubits defined in the circuits may be arranged to couple a common resonator mode, this enables multi-qubit quantum gates and non-invasive qubit measurements [8].

Another major direction in solid-state quantum information processing are spin qubits where the electron spin is used to store quantum information [9]. The spin qubits are usually realized in quantum dots in semiconductor materials where the electrons are confined in visibly discrete states. Both singlet[10, 11] and spin doublet[12, 13] schemes have been realized. The important experiments include [14–17]. The spin coherence time of these quantum dot systems may achieve milliseconds, which is beneficial for the quantum manipulation and quantum memory.

A less common but promising design of superconducting qubits exploits Andreev bound states: the localized quasiparticle states in the vicinity of superconducting contacts. It has been known that with the Andreev bound states one can realize both kinds of the qubits within the same device. Namely, if the number of excess localized quasiparticles is even, a (an Andreev) qubit emerges from the ground and excited spin-singlet states [18]. However, if the number of excess quasiparticles is odd, the superconducting device houses a conveniently isolated spin qubit [19]. Such realization is more interesting than a traditional electron confinement in quantum dots motivating theoretical research [20, 21]. These ideas have been realized experimentally [22–24] and remain in focus of attention of the superconducting qubit community.

Recently, a topological singularity in Andreev spectrum of multi-terminal superconducting structure — a Weyl point — has been predicted and theoretically investigated. [25]. For a 4-terminal structure, the spectrum of Andreev states depends on three independent superconducting phases. At a particular choice of these three phases, the energy of the lowermost Andreev level approaches zero signaling the degeneracy of the corresponding spin-singlet qubit. The spectrum is conical in the vicinity of this singularity manifesting the critical dependence of the wave functions: very small changes of the phases in the vicinity of the point strongly affect the wavefunctions of the states. This is already advantageous for quantum manipulation applications. The Weyl points in the superconducting structures have been investigated in [26–34].

As for any Andreev-based setup, the parity effect is crucial here. For even parity, the spectrum of two spin-singlets is conical and the dependence of the wave functions is critical in the vicinity of the point. For odd parity, the spin-doublet states are slightly split owing to spin-orbit interaction.[35] Their wave functions or energies exhibit no critical dependence on the phases. (Fig. 3.1a)

The quantum spaces of different parity are completely separated and cannot be made coherent: indeed, a transition between those would involve a quasiparticle coming from/escaping to the delocalized states of the continuous spectrum. So, despite the fact that the system can house both superconducting and spin qubit, there is no quantum coher-

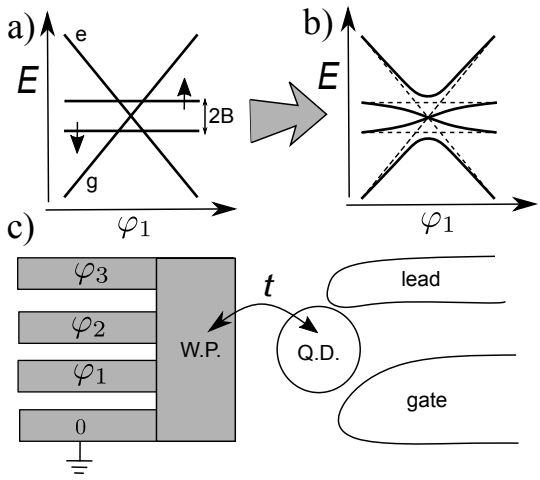

Figure 3.1: The spin-Weyl quantum unit. a. The low-energy spectrum of the multi-terminal superconducting structure with a Weyl point consists of a pair of flat spin-doublet states an a pair of conical spin-singlets. The spin-doublets are split by small energy $2B$ coming from spin-orbit interaction. The pairs are not coherent corresponding to different parities. b. The spin-Weyl quantum unit provides coherence and hybridization between the flat and conical states. Sketch of the spectrum presents the hybridization with solid lines and before hybridization with dashed lines. c. The setup of the spin-Weyl quantum unit. The superconducting structure with 4 leads and 3 independent phases $\varphi_{1,2,3}$ is tunnel-coupled with a single-electron quantum dot. The quantum dot is tuned by the gate electrode, a lead supplies electrons to the dot.

ence between the two.

Whatever tempting such coherence may be, it seems to be forbidden by fundamental laws. The main point of this chapter is that the coherence can be achieved with a rather simple extension of the Weyl point setup.

In this Article we propose a hybrid system that can be regarded as two coherently coupled qubits. It thus exhibits hybridization of flat spin-doublet states with conical spin-singlet states (Fig. 3.1b.). We term the system a *spin-Weyl quantum unit*. We show how the unit can be manipulated to achieve an arbitrary unitary transformation in the space of 4 states, by the superconducting phase controls only, and can be conveniently read out.

The system proposed combines a superconducting heterostructure and a single-electron quantum dot (Fig.3.1c). The two parts are coupled with a weak electron tunneling between the heterostructure and the dot. The degeneracy at the Weyl point guarantees that even the weak coupling results in strong change of the spectrum making it advantageous for quantum manipulation applications. The electron tunneling to localized states of the dot is essential for breaking the parity conservation that forbids the hybridization of flat and conical states near the Weyl point.

The structure of the Article is as follows. In Section 3.2 we describe the setup, establish a minimum Hamiltonian required to describe the unit, and explain its relevance in the wider context of more detailed description of the device. In Section 3.3, we describe the resulting spectrum and the choice we made for the subspace where quantum manipulations are performed. We discuss in Section 3.4 read-out, initialization, and var-

ious methods of quantum manipulation that can be implemented in the unit. In Section 3.5, we describe the implementation of single-qubit gates by means of resonant manipulation. In Section 3.6 we concentrate on diabatic manipulations and demonstrate the design of various two-qubit gates. We conclude in Section 3.7.

3.2. THE SETUP AND THE HAMILTONIAN

The unit consists of two subsystems: (Fig. 3.1c) the superconducting heterostructure and the quantum dot. The superconducting heterostructure is connected to four superconducting leads biased with three independent superconducting phases $\varphi_{1,2,3}$ and houses the discrete Andreev bound states with the spectrum depending on the phases. At a certain choice of the phases, the energy lowermost Andreev state reaches zero exhibiting a Weyl singularity [25, 30]. The quantum dot houses discrete number of electrons, this number can be tuned by a nearby gate electrode. A normal-metal lead supplies the electrons. The subsystems are coupled by electron tunneling.

Such setup can be realized with a variety of technologies, including the 2D semiconducting heterostructures, semiconducting nanowires, graphene, brought in proximity with superconducting metals. Here we do not specify a concrete technology but rather spell out the physical restrictions. The spacing δ between the Andreev bound states becomes small in comparison with the superconducting energy gap Δ if the conductances G in the superconducting structure exceed much the conductance quantum G_Q, $\delta \simeq (G_Q/G)\Delta$. So the conductances should be of the order of G_Q. As mentioned in [25], the existence of Weyl points relies on general scattering theory and does not impose any further restrictions on the properties of the structure. The vicinity of the Weyl point implies the working energy scale $\ll \Delta$. The level spacing in the quantum dot should be big at this energy scale. The tunneling energy should be also at this scale, that is, not too large. The spin-orbit splitting B is much smaller than Δ in materials with weak spin-orbit coupling. The tunneling energy should be comparable with B.

Let us consider the full Hamiltonian of the system, that is the sum of the Weyl point structure Hamiltonian, the quantum dot Hamiltonian, and the tunneling Hamiltonian.

$$H = H_{\text{wp}} + H_{\text{T}} + H_{\text{QD}} \tag{3.1}$$

We will construct a minimum Hamiltonian disregarding possible higher-energy states in the dot and in the structure. The Andreev levels in the vicinity of the Weyl point are described by a Weyl BdG Hamiltonian[30]. Assuming spin degeneracy, this Hamiltonian is a 2×2 matrix in Nambu space. Its general linear expansion near the Weyl point reads

$$\hat{H}^{\text{WP}} = \hat{\tau}^a M_{ab} \delta\varphi_b \tag{3.2}$$

here we use tensor convention for repeated indices. $a,b = 1,2,3$, $\hat{\tau}^a$ being a 3-vector of Pauli matrices in Nambu space, $\delta\varphi_b$ being small deviations of the superconducting phases from the Weyl point, M_{ab} being a matrix of proportionality coefficients. It is advantageous to introduce the convenient coordinates in the space of 3 superconducting phases, $\phi^a = M_{ab}\delta\varphi_b$. We will name these coordinates *phases* for brevity, although they have dimension energy. The spectrum of the Hamiltonian is conveniently isotropic in the resulting space, $E = \pm|\vec{\phi}|$, while the wave functions do depend on the direction. To

account for spin-orbit interaction, we promote the Hamiltonian to 4×4 matrix in spin and Nambu space,

$$\hat{H}^{\mathrm{WP}} = \vec{\hat{\tau}}\cdot\vec{\phi} + \frac{1}{2}\vec{B}\cdot\vec{\hat{\sigma}}, \tag{3.3}$$

$\vec{\hat{\sigma}}$ being the vector of Pauli matrices in spin space. The spin and orbital degrees of freedom separate, so the spectrum reads $E = \pm|\vec{\phi}| + s_z 2B$, $B \equiv |\vec{B}|$, $s_z = \pm 1/2$ being the spin projection on the direction of $\vec{B}$. We need the Hamiltonian in second quantization form. We introduce the quasiparticle annihilation operators $\hat{\gamma}_\sigma$ and associated Nambu bispinors $\bar{\gamma}_{a,\sigma} \equiv (\hat{\gamma}_\sigma, \sigma\hat{\gamma}^\dagger_{-\sigma})$ to recast it to the standart form,

$$H_{\mathrm{WP}} = \frac{1}{2}\bar{\gamma}^\dagger_\alpha \hat{H}^{\mathrm{WP}}_{\alpha\beta}\bar{\gamma}_\beta \tag{3.4}$$

This Hamiltonian can be reduced to a diagonal form for a certain direction in ϕ-space, $\vec{\phi} = \phi\vec{n}$ by a Bogoliubov transform of $\hat{\gamma}_\sigma$ to a direction-dependent $\hat{\tilde{\gamma}}_\sigma$. Choosing the spin quantization axis along $\vec{B}$, we arrive at

$$H_{\mathrm{WP}} = \frac{1}{2}(\phi + B\sigma)\left(\hat{\tilde{\gamma}}^\dagger_\sigma\hat{\tilde{\gamma}}_\sigma - \hat{\tilde{\gamma}}_\sigma\hat{\tilde{\gamma}}^\dagger_\sigma\right) \tag{3.5}$$

This gives the spectrum sketched in Fig. 3.1 a: $E = \pm\phi$ for the states $|0\rangle$, $|2_{\uparrow\downarrow}\rangle \equiv \hat{\tilde{\gamma}}^\dagger_\uparrow\hat{\tilde{\gamma}}^\dagger_\downarrow|0\rangle$, $E = \pm B$ for the states $|\uparrow\rangle \equiv \hat{\tilde{\gamma}}^\dagger_\uparrow|0\rangle$, $|\downarrow\rangle \equiv \hat{\tilde{\gamma}}^\dagger_\downarrow|0\rangle$.

To model the dot at the small energy scale, we only need to take into account three states that differ by an addition of an electron: a non-degenerate state $|0\rangle$ and two spin-degenerate states $\hat{d}^\dagger_\sigma|0\rangle$, $\hat{d}^\dagger_\sigma$ being the electron creation operator corresponding to spin σ. The charging energy of the quantum dot pushes the states of other occupancy too high in energy. As such, the Hamiltonian reads

$$H_{\mathrm{QD}} = \epsilon_d \hat{d}^\dagger_\sigma|0\rangle\langle 0|\hat{d}_\sigma, \tag{3.6}$$

the value of ϵ_d can be tuned with the gate voltage. The only function of the normal metal lead in our setup is to provide equilibration of the total parity, which is impossible otherwise. This equilibration is not required in course of quantum manipulation and measurement and thus can be a slow process. The speed of equilibration is determined by tunneling rate Γ_{L} to/from the lead. We assume the inverse of this rate to exceed all other relevant time scales in the setup. On this basis, we can disregard the dissipation and decoherence brought by the lead, as well as neglect the tunneling to/from the lead in the Hamiltonian description of the setup.

The least trivial and the most important part of the total Hamiltonian describes tunneling between the dot and the setup. To derive it, we assume spin conservation regarding spin-orbit as an irrelevant perturbation. Then the most general form of the tunneling Hamiltonian reads as follows:

$$H_{\mathrm{T}} = \int d\mathbf{y}d\mathbf{x}\hat{c}^\dagger_\sigma(\mathbf{y})\hat{d}(\mathbf{x})_\sigma\, t(\mathbf{x},\mathbf{y}) + h.c. \tag{3.7}$$

Here, $\mathbf{y}$ and $\mathbf{x}$ are the electron coordinates in the superconducting structure and in the dot, respectively, $\hat{c}_\sigma(\mathbf{y})$, $\hat{d}(\mathbf{x})_\sigma$ are the corresponding electron annihilation operators, and

$t(\mathbf{x},\mathbf{y})$ is the tunneling amplitude from the point $\mathbf{x}$ to the point $\mathbf{y}$. We need to project this operator to the low-energy electron states involved. To this end, we express the operators in terms of the wave functions of the quasiparticle states in the superconducting structure, and the electron states in the dot, and the corresponding creation/annihilation operators,

$$\hat{c}_\sigma(\mathbf{y}) = \sum_n (u_n(\mathbf{y})\hat{\gamma}_{n,\sigma} - \sigma v_n^*(\mathbf{y})\hat{\gamma}^\dagger_{n,-\sigma}); \tag{3.8}$$

$$\hat{d}_\sigma(\mathbf{x}) = \sum_n \Psi_n(\mathbf{x})\hat{d}_{n,\sigma} \tag{3.9}$$

where the summation is over all possible states. From this sum, we pick up the low-energy states, one for the superconducting structure, one for the dot, to arrive at:

$$H_{\mathrm{T}} = \left(t_1\hat{\gamma}^\dagger_\sigma - t_2\sigma\hat{\gamma}^\dagger_{-\sigma}\right)\hat{d}_\sigma + h.c. \tag{3.10}$$

with

$$t_1 = \int d\mathbf{y}d\mathbf{x}u^*(\mathbf{y})\Psi(\mathbf{x})t(\mathbf{x},\mathbf{y}); \tag{3.11}$$

$$t_2 = \int d\mathbf{y}d\mathbf{x}v(\mathbf{y})\Psi(\mathbf{x})t(\mathbf{x},\mathbf{y}) \tag{3.12}$$

The tunnel Hamiltonian is thus characterized with two complex effective tunneling amplitudes, $t_{1,2}$, whose common phase is irrelevant. It is important to understand that the remaining three parameters define the overall tunneling strength $T \equiv \sqrt{|t_1|^2+|t_2|^2}$ and the *direction* in the phase space. Thus, the tunneling breaks the isotropy in the phase space.

To analyze the spectrum, it is convenient to make the isotropy breaking explicit. For this, we fix the 3rd axis of the coordinate system to the direction defined by $t_{1,2}$, express ϕ in spherical coordinates, $\vec{\phi} = \phi(\sin\theta\cos\mu, \cos\theta\sin\mu, \cos\theta)$, and perform the unitary transformation of $\hat{\gamma}_\sigma$ that diagonalizes H_{WP}. With this, the transformed Hamiltonian reads

$$\begin{aligned} H = {} & \frac{1}{2}(\phi + B\sigma)\left(\hat{\tilde{\gamma}}^\dagger_\sigma\hat{\tilde{\gamma}}_\sigma - \hat{\tilde{\gamma}}_\sigma\hat{\tilde{\gamma}}^\dagger_\sigma\right)] \\ & + T\left(\cos\left(\frac{\theta}{2}\right)e^{-i\mu/2}\hat{\tilde{\gamma}}^\dagger_\sigma\hat{d}_\sigma - \right. \\ & \left. \sin\left(\frac{\theta}{2}\right)e^{i\mu/2}\sigma\hat{\tilde{\gamma}}_{-\sigma}\hat{d}_\sigma + h.c.\right) \\ & + H_{\mathrm{QD}} \end{aligned} \tag{3.13}$$

The azimuthal angle μ is not relevant for the spectrum and can be set to 0. The spectrum depends on the polar angle θ owing to the tunneling term.

It is useful to shortly discuss possible decoherence and dissipation sources in the resulting quantum system. As we will see, the resulting level energies are either essentially phase-dependent, as the singlet states in Fig. 3.1a. or "flat", as the spin states in the same figure. As to phase-dependent states, their dissipation and decoherence are determined by (quantum) fluctuations of the control phase differences. The corresponding

rates can be estimated as ZG_QE, E being the energy difference between the levels in the unit, Z being a typical impedance of the electromagnetic environment. Typically, $ZG_Q \simeq 10^{-2}$, that guarantees low decoherence at the time scale of quantum manipulation. The dissipation and decoherence of the "flat" states are determined by weaker sources, the electron-photon interaction may be a plausible one.

3.3. THE SPECTRUM

The whole spectrum consist of $3 \times 4 = 12$ states. They are separated into two groups of different total parity, 6 states in each group. In addition, the states are separated by the spin projection s_z on the B axis.

Let us consider the even parity first. There are two states with $s_z = \pm 1$, $|1_\uparrow 1_\uparrow\rangle$ and $|1_\downarrow 1_\downarrow\rangle$ (first and second number refer to the occupation of the superconducting structure and the dot, respectively) that are not affected by superconducting phases or tunneling, with energies $\epsilon_d \pm B$. The group of four states with $s_z = 0$ is of primary interest for us and comprises the spin-Weyl unit. Without tunneling, there are two conical states, $|00\rangle$, $|2_{\uparrow\downarrow}0\rangle$ with energies $\pm\phi$, and two flat states $|1_\uparrow 1_\downarrow\rangle$ and $|1_\downarrow 1_\uparrow\rangle$ with energies $\epsilon_d \pm B$ (the second number in this notation is the occupation of the dot). The tunneling hybridizes the states. The hybridization ceases at sufficiently large distances from the Weyl point, the energies of the states returning to their values without tunneling. The Hamiltonian in this basis is obtained by collecting the matrix elements of (3.13) into the 4×4 matrix. We assume $\mu = 0$. The signs of non-diagonal matrix elements depend on the choice of signs of the basis vectors, the current choice stresses the antisymmetry of a singlet state:

$$H_4 = \begin{bmatrix} -\phi & -T\sin(\frac{\theta}{2}) & T\sin(\frac{\theta}{2}) & 0 \\ -T\sin(\frac{\theta}{2}) & \epsilon_\mathrm{d} - B & 0 & T\cos(\frac{\theta}{2}) \\ T\sin(\frac{\theta}{2}) & 0 & \epsilon_\mathrm{d} + B & -T\cos(\frac{\theta}{2}) \\ 0 & T\cos(\frac{\theta}{2}) & -T\cos(\frac{\theta}{2}) & \phi \end{bmatrix} \tag{3.14}$$

The resulting axially symmetric spectrum is shown in Fig. 3.2 for various directions in the phase space given by the polar angle θ (to compact the plots, we concatenate the plots at θ and $\pi - \theta$ in such a way that the latter corresponds to negative ϕ) and three different settings of ϵ_d where the former conical point is above, below or in between the energies of the flat states.

The spectrum comprises 4 sub-bands that are eventually touch each other in 3 Weyl points. They are located at symmetry axis corresponding $\theta = 0$ (or $\theta = \pi$, if $\phi < 0$), leftmost column of the plots. For the middle row of the plots, the Weyl point is visible in all columns since it is located at $\vec{\phi} = 0$ for a particular symmetric choice $\epsilon_d = 0$ made. In general, the points are shifted from $\vec{\phi} = 0$. The existence of these points is a consequence of topology, so these points remain even if we perturb the Hamiltonian, for instance, with the terms breaking the axial symmetry. Apart from this feature, the sub-bands show rather expected hybridization at $\phi \simeq T$ and go asymptotically to flat and conical states for $\phi \gg T$.

This 4-dimensional subspace suits well to represent two coupled qubits, and we will use it to realize the spin-Weyl quantum unit.

For completeness, let us also describe the spectrum for odd parity. Six states are separated in two groups of three with $s_z = \pm 1/2$, that is, into two qutrits. The qutrit with

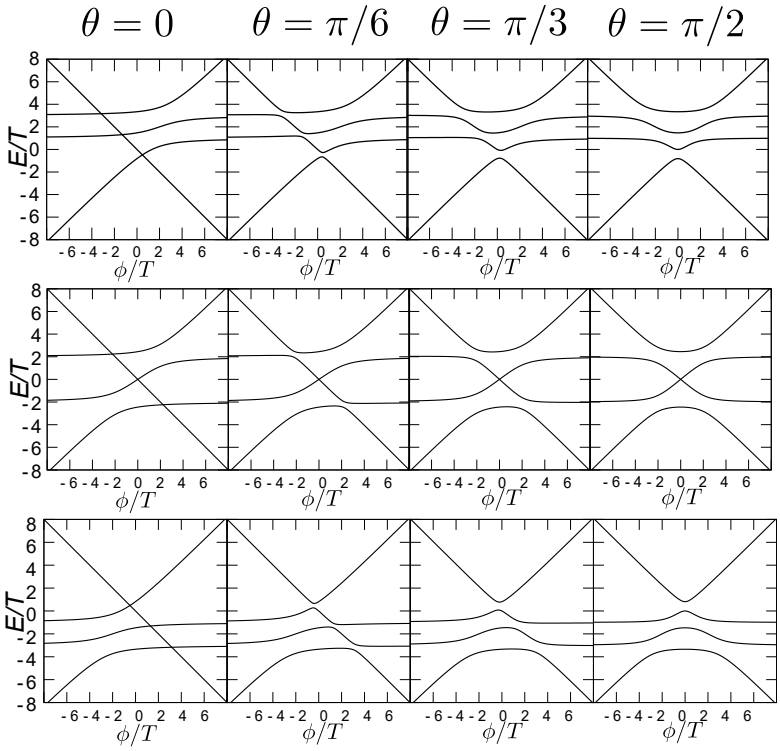

Figure 3.2: The spectrum of spin-Weyl unit (even parity, $s_z = 0$) consists of 4 sub-bands connected by three Weyl points, and emerges from hybridization of two flat and two conical subbands. The spectrum has axial symmetry. The columns correspond to four different settings of the polar angle θ. The choices of parameters for rows: upper row, $B = T$, $\epsilon_d = 2T$, both flat bands are above the conical point; middle row, $B = 2T$, $\epsilon_d = 0$, the conical point is between two flat subbands and remains at $\vec{\phi} = 0$ for this parameter choice; lower row, $B = T$, $\epsilon_d = -2T$, both flat bands are below the conical point.

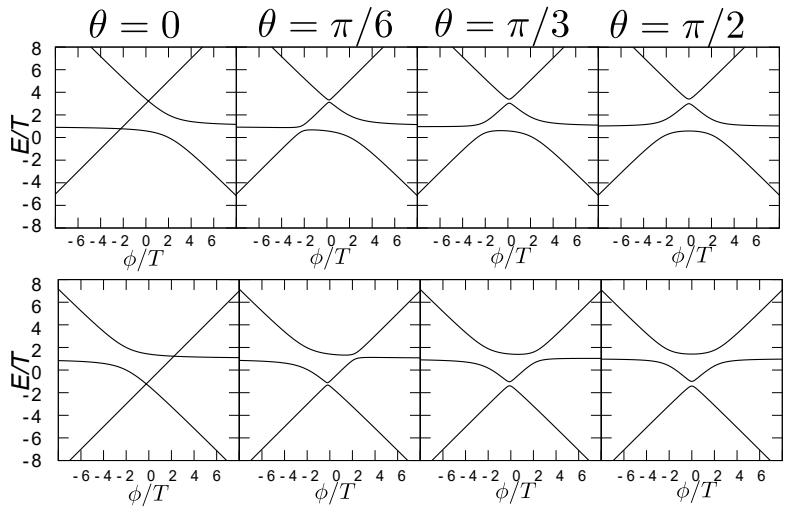

Figure 3.3: The spectrum of a qutrit (odd parity, $s_z = 1/2$) consists of 3 sub-bands connected by two Weyl points, and emerges from hybridization of one flat and two conical sub-bands. The spectrum has an axial symmetry. The columns correspond to four different settings of the polar angle θ. The choices of parameters for rows: upper row, $B = T$, $\epsilon_d = 3T$, the flat band is above the conical point; lower row, $B = T$, $\epsilon_d = -T$, the flat band is below the conical point.

$s_z = 1/2$ is composed from the flat state $|1_\uparrow 0\rangle$, and the conical states $|01_\uparrow\rangle$, $|2_{\uparrow\downarrow}1_\uparrow\rangle$ with energies B, $\epsilon_d \pm \phi$. The Hamiltonian is a 3×3 matrix:

$$H_3 = \begin{bmatrix} -\phi+\epsilon_d & -T\cos(\frac{\theta}{2}) & 0 \\ -T\cos(\frac{\theta}{2}) & B & -T\sin(\frac{\theta}{2}) \\ 0 & -T\sin(\frac{\theta}{2}) & \phi+\epsilon_d \end{bmatrix} \tag{3.15}$$

The spectrum is plotted in Fig. 3.3 for a set of polar angles and three different settings of ϵ_d where the former conical point is above or below the energy of the flat state. There are two Weyl points in the spectrum that are situated at the axis. Apart from the number of flat subbands, the spectrum is similar to that of the spin-Weyl unit. The spectrum of the qutrit with $s_z = -1/2$ is very similar to be obtained by inverting the value of B.

3.4. QUANTUM INFORMATION PROCESSING

Let us discuss the system under consideration from the point of view of quantum information processing. Without going to unnecessary details, we describe all elements required for the processing: state read-out, initialization, and various methods of manipulation.

Read-out. The most natural read-out in the system utilizes the supercurrents induced in the superconducting leads. For the state i, the supercurrent in the lead j is given $I_j = \frac{2e}{\hbar}\frac{\mathrm{d}E_j}{\mathrm{d}\varphi_i}$. The supercurrents thus distinguish the slopes the states. A realistic measurement scheme is usual for superconducting qubits and involves a change of non-linear inductance in a resonator by this current, so the current is detected as a shift

of resonant frequency [23]. One of the advantages of Weyl point is the conical property of the spectrum whereby the slops are of the same value far and close to the point, and can be significantly changed by a small change of the phase settings. The ground state and excited state in a conical pair give opposite supercurrent signals. In distinction, the spin-like flat states give almost zero supercurrent at $\phi \gg T$ and thus can not be distinguished. This is another advantage: the superposition of spin-like states is preserved by the measurement. Yet if necessary they can be distinguished as well: one needs to adiabatically change the phase settings close to zero where these states acquire slops owing to hybridization.

Initialization. In the unit, one can adopt a conservative approach to initialization: just wait till the relaxation brings the system to the ground state. After this, one can go to the desired state by performing a manipulation. The problem may be that the relaxation without quasiparticle exchange in principle conserves parity, so the unit could stuck in the ground state of odd parity. In addition, the spin conservation in the process of relaxation may lead to a stucking in $s_z = \pm 1$ states. To prevent this, one requires a tunnel connection to the lead which will change the parity and the spin projection. Another problem could be a slow relaxation from the flat states: this can be circumvented by setting the phases close to zero so these states are not flat any more.

Manipulation. Let us see how we can manipulate the states in the unit. The most natural way is to change the superconducting phases in time. As mentioned, the advantage of Weyl point is that the big changes of the wave functions can be achieved by small $\phi \simeq T$ changes of phases. We do not consider manipulation by magnetic field that is typical for spin qubits since it is rather impractical: the magnetic fields required for such manipulation are much bigger than those required to provide the small superconducting phase changes. More interesting and practical possibility is to change the gate voltage modulating ϵ_d, but we do not consider it here either.

The manipulation methods differ by the way the $\vec{\phi}$ is changing in time. Generally, there are three distinct methods: (Fig.3.4) i. resonant manipulation whereby a small oscillating phase addition is applied at a working point $\vec{\phi}_{\rm w}$, ii. adiabatic manipulation whereby the phase is slowly changing along a trajectory in the phase space, usually returning to the initial point $\vec{\phi}$, iii. diabatic manipulation where the phases are changed by sudden jumps, and the changed settings are kept for a time interval before jumping back to another point or the initial point. Let us discuss each method for the unit in hand. We acknowledge that an efficient implementation of each method requires Hamiltonian characterization and subsequent design on the basis of a concrete Hamiltonian. However, the Hamiltonian is defined by a handful of parameters, so this should be a doable task. One can also employ the combinations of these methods.

Resonant manipulation is the most common manipulation method working for almost all quantum systems. If one applies a modulation $\delta\vec{\phi}(t)$ that oscillates with the frequency matching the energies of the states $|a\rangle$ and $|b\rangle$ defined in a working point $\phi_{\rm w}$, one is able to achieve an arbitrary unitary transformation in the basis $|a\rangle$, $|b\rangle$ tuning the duration and phase of the modulation pulse. [1] One needs to do more for a more general unitary transformation. To implement single-qubit gates, we use the resonant manipulation in special working points where two energy differences are the same, this permits unitary transformations in the basis of four states. We discuss the details in the

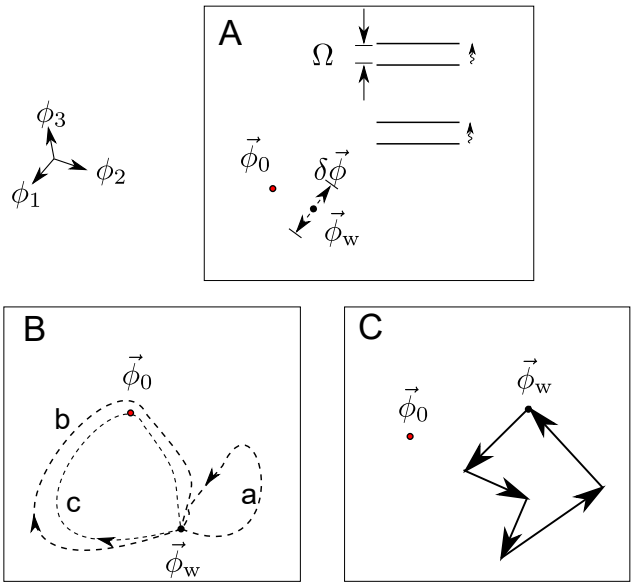

Figure 3.4: The quantum manipulation methods for spin-Weyl quantum unit. A. Resonant manipulation. The phases oscillate around the working point ϕ_w with amplitude $\delta\vec{\phi}$ and frequency ω that matches the level spacing Ω. B. Adiabatic manipulation. Adiabatic change of phases along a trajectory can realize a phase gate (trajectory a) if a trajectory (trajectory a in the plot) is far from a Weyl point $\vec{\phi}_0$ or a Landau-Zener gate if a trajectory passes close to the point (trajectory b). Trajectory c passes directly through the point and realizes an exchange of wave function amplitudes in the sub-bands. C. Diabatic manipulation. The phase settings jump from a working point $\vec{\phi}_w$ to a series of consecutive points coming back in the end of the manipulation.

Section 3.5.

Adiabatic manipulation involves a change of $\vec{\phi}$ along a closed trajectory. (Fig.3.4a) Usually, adiabaticity implies no transitions between the levels, this requires the velocity in phase space, $\vec{v} \equiv \dot{\phi}$ to be small in comparison with the energy difference between the levels. For our system, where the energy difference in interesting region of the phase space are $\simeq T$, this implies $v \ll T^2$. With this, one can easily arrange a phase gate: an amplitude of a quantum state on each level acquires a phase factor with no change of its modulus (trajectory *a* in Fig.3.4b). Notably, the presence of Weyl points in the spectrum of the unit permits design of more complicated gates. The point is that the level splitting becomes small near the point and, for any fixed v, the adiabaticity criterion is not satisfied if the trajectory comes sufficiently close to the Weyl point. (trajectory *b* in Fig.3.4c) This realizes a Landau-Zener gate [36]: there is a non-adiabatic transition between two subbands with an amplitude α given by Landau-Zener formula, $|\alpha| = \exp(-\pi\phi_d^2/v)$, ϕ_d being the smallest distance between the Weyl point and the trajectory. If the trajectory goes precisely through the Weyl point, a SWAP gate for two subbands is realized (trajectory *c* in Fig.3.4b). The phase factors accumulated in the course of the Landau-Zener transition can be adjusted by tuning the shape or velocity at the returning trajectory.

Diabatic manipulation is implemented as a sequence of sudden jumps between the points in the phase space, that brings the system back to the initial point. (Fig.3.4c) The

wave function does not change during the jumps. After each jump, the phase settings are kept constant during a time interval to let the wave function evolve with a Hamiltonian local to the point. To prevent the excitation to higher states in the course of jump, its actual duration should be yet longer than the inverse energy distance to higher levels. The Weyl point structure is advantageous for diabatic manipulation since big changes of the Hamiltonian can be produced by small jumps in the phase space.

This variety of manipulation methods permits multiple implementations of quantum gates. To illustrate, we have to make choices.

To start with, we define a bipartition of 4-dimensional Hilbert space into two qubits. We label the states as $|00\rangle$, $|01\rangle$, $|10\rangle$, $|11\rangle$ from the lowest energy to the highest energy, that is, the second qubit has the smaller excitation energy $E_{01} - E_{00}$. For separate non-interacting qubits, one expects $E_{11} + E_{00} = E_{01} + E_{01}$. This condition is generally not fulfilled for the spectrum in hand. However, it is fulfilled asymptotically at $\epsilon_d = 0$ and also in special points of the phase space. We assume $|\epsilon_d| < B$, so that the conical point is between the energies of the flat states.

For the implementation of single-qubit gates, we choose resonant manipulation in special points. For the implementation of the two-qubit gates, we choose diabatic manipulation. We describe the implementations in the subsequent sections.

3.5. THE SINGLE-QUBIT GATES

We will realize the single-qubit gates by means of resonant manipulation. This realization requires some tuning. Generally, the three energy differences between the levels are all different and resonant manipulation would result in a two-qubit gate. For instance, if the frequency of the oscillating field is in resonance with the energy difference between the states $|10\rangle$ and $|11\rangle$, one can swap by a pulse the amplitudes of the states $|10\rangle$ and $|11\rangle$ realizing the traditional CNOT gate [37].

The single-qubit manipulation is possible at a family of special working points where $E_{11} + E_{00} = E_{01} + E_{01}$, this corresponds to independent qubits with energy splittings $\Omega_1 = E_{10} - E_{00}$ and $\Omega_2 = E_{01} - E_{00}$. At these frequencies, the oscillating field resonates with two pairs of levels. Since the energy spectrum is independent of the azimuthal angle, these special working points form a surface of revolution around z-axis.

Let us explain how one realizes the X rotations of the first qubit. As an example, we take $B = 3T$, $\epsilon_d = 2T$. The special working point can be realized at $\vec{\phi}_{\mathbf{w}}/T = (1.3, 0, 2.25)$. The qubit splittings are: $\Omega_1 = 6.0T$, $\Omega_2 = 2.0T$. We apply an oscillatory modulation $\delta\vec{\phi}(t) = \mathrm{Re}(\delta\vec{\phi}e^{i\Omega_1 t})$, $\delta\vec{\phi}$ being a complex vector of the oscillation amplitudes. It results in a time-dependent perturbation $\hat{h} = \frac{1}{2}\delta\vec{\phi}\cdot\vec{\tau}e^{i\Omega_1 t} + h.c.$. For the result of the manipulation not to depend on the state of the second qubit, this perturbation should satisfy $\langle 10|\hat{h}|00\rangle = \langle 11|\hat{h}|01\rangle$. Since both matrix elements can be presented as scalar products of complex vectors, $h_{10,00} = \vec{v}_{10,00}\cdot\delta\vec{\phi}$, and similar for another matrix elements. To satisfy independence from the second qubit, the direction of $\delta\phi$ should be orthogonal to $\vec{v}_{10,00} - \vec{v}_{11,01}$. It also has to be orthogonal to the cross-product of the vectors, since the modulation in this direction does not appear in the matrix elements. For the example in hand, this fixes $\delta\phi$ to $|\delta\vec{\phi}|(0.16, 0.21i, 0.97)$. To perform the rotation $\exp(i\gamma\sigma_x)$, one chooses $\gamma = 0.34|\delta\vec{\phi}|\mathcal{T}$, $\mathcal{T}$ being the pulse duration.

To design the X-rotation of the second qubit, we proceed in the same way choosing

the direction of oscillations to achieve $\langle 01|\hat{h}|00\rangle = \langle 11|\hat{h}|10\rangle$. This fixes $\delta\phi$ to $|\delta\vec{\phi}|(0.6, 0.7i, -0.35)$. To perform the X-rotation $\exp(i\gamma\sigma_x)$, one chooses $\gamma = 0.04|\delta\vec{\phi}|\tau$, τ being the pulse duration.

As it is usual in the context of resonant manipulation, the Y and Z rotations can be achieved by changing the total phase of the oscillation and frequency modulation, respectively.

3.6. THE TWO-QUBIT GATES

More complex gates require realization of an arbitrary 4×4 s-unitary transformations. In principle, this can be achieved only by means of resonance manipulation and adiabatic manipulation. However, this requires a tedious design and the time of the manipulation should greatly exceed the inverse energy differences $\simeq T^{-1}$. So we turn to diabatic manipulation.

For diabatic manipulation, it is proficient to work with the spin-Weyl Hamiltonian in the phase-independent basis where it takes the form

$$H_4 = \begin{bmatrix} -\phi_3 & 0 & 0 & \phi_1 + i\phi_2 \\ 0 & \epsilon_d - B & 0 & T \\ 0 & 0 & \epsilon_d + B & -T \\ \phi_1 - i\phi_2 & T & -T & \phi_3 \end{bmatrix} \tag{3.16}$$

In this basis, the wave function remains continuous upon a diabatic change of $\vec{\phi}$.

The manipulation starts in a working point $\vec{\phi}_w$ where the Hamiltonian is diagonalized as

$$H_4(\vec{\phi}_w) = DE_dD^{-1} \tag{3.17}$$

E_d being the diagonal matrix of two qubit eigenstates. The phase then goes through a set of points $\vec{\phi}_i$ staying for a time interval t_i in each point and finally returning to

The result of the manipulation is a unitary 4×4 matrix in the basis of two-qubit eigenstates,

$$S = D^{-1}e^{iH_4(\vec{\phi}_w)\sum_i t_i}\prod_i S_i e^{-iH_4(\vec{\phi}_w)\sum_i t_i}D; \tag{3.18}$$

$$S_i \equiv \exp(-iH_4(\vec{\phi}_i)t_i) \tag{3.19}$$

To design a manipulation given a target S, we need to choose $\vec{\phi}_i, t_i$ in a proper way. An arbitrary SU(4) transformation depends on $4^2-1=15$ parameters, while each jumping point brings 4 parameters: 3 phases and 1 time interval. Consequently, an arbitrary SU(4) transformation requires at least 4 jumping points(Fig. 3.4C). To accomplish the design task numerically, we specify the target unitary matrix S_t and define a minimization function in the space of the manipulation parameters $\{\vec{\phi}_i, t_i\}$,

$$U(\{\vec{\phi}_i, t_i\}) = 8 - \mathrm{Tr}(S_tS^\dagger + SS_t^\dagger). \tag{3.20}$$

We start the minimization routine with a random point in 16-dimensional space, iterate to a minimum and check if $U=0$ in this minimum. We accomplish this by setting a

Gate	Phase(ϕ/T)	Time(t/T)
cX	$\vec{\phi}_{\rm w}$	
	$\rightarrow (1.04,-0.11,1.07)$	5.10
	$\rightarrow (4.56,6.76,5.52)$	$\rightarrow$ 5.96
	$\rightarrow (6.62,2.67,-1.11)$	$\rightarrow$ 0.03
	$\rightarrow (5.24,2.13,6.34)$	$\rightarrow$ 7.85
	$\rightarrow \vec{\phi}_{\rm w}$	
cY	$\vec{\phi}_{\rm w}$	
	$\rightarrow (4.40,9.82,12.15)$	2.80
	$\rightarrow (5.63,1.35,-0.87)$	$\rightarrow$ 3.77
	$\rightarrow (0.84,-1.15,-0.46)$	$\rightarrow$ 5.43
	$\rightarrow (11.99,14.25,7.60)$	$\rightarrow$ 2.05
	$\rightarrow \vec{\phi}_{\rm w}$	
cZ	$\vec{\phi}_{\rm w}$	
	$\rightarrow (9.41,2.82,4.57)$	7.18
	$\rightarrow (-1.28,0.18,0.90)$	$\rightarrow$ 6.96
	$\rightarrow (9.72,9.90,10.22)$	$\rightarrow$ 2.53
	$\rightarrow (1.55,0.91,7.67)$	$\rightarrow$ 5.27
	$\rightarrow \vec{\phi}_{\rm w}$	

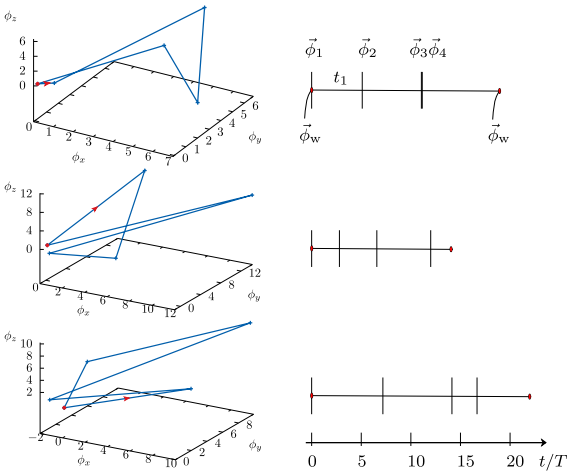

Figure 3.5: Design of two-qubit gates by diabatic manipulation. We implement controlled logic gates cX, cY and cZ gates, the first qubit being control one. The choice of the parameters: $B = 3T, \epsilon_d = 2T$, working point: $\vec{\phi}_{\rm w} = (1.3, 0, 2.25)T$. The table specifies for each three gates the set of jumping points $\vec{\phi}_i$ and the time intervals t_i. The plots illustrate the diabatic paths and time intervals. The red mark in each graph indicates the initial working point. The arrow indicates the diabatic jumping sequence initiated from the working point.

threshold of $U_{\rm th} \ll T^2$ and see if U falls into the interval of $[0, U_{\rm th}]$. If $0 \leq U \leq U_{\rm th}$, we have found the solution: the minimum $U = 0$ is achieved only if $S = S_t$. If otherwise $U > U_{\rm th}$, we repeat the procedure starting another random point.

A set of universal quantum gates can be achieved combining elementary quantum logic gates. The minimum circuit requirement for a general two-qubit manipulation can be constructed with 3 CNOT (cX) gates and 15 elementary one-qubit gates[38]. In principle, the single-qubit gates can be also designed by diabatic manipulation method. However, we have already achieved these gates as described in the previous Section. Here, we present the design of 3 controlled Pauli gates, cX, cY and cZ that $c(\sigma_i) = \begin{pmatrix} \sigma_i & \\ & \mathbb{1} \end{pmatrix}$ in the qubit basis with the first qubit serving as control one.

We choose the same parameters and the working point as in the previous Section: $B = 3T$, $\epsilon_d = 2T$, $\vec{\phi}_{\mathbf{w}}/T = (1.3, 0, 2.25)$. The results are presented in Fig. 3.5. The advantage of the diabatic manipulation is the speed: the longest manipulation takes no more than $\simeq 20\, T^{-1}$.

3.7. CONCLUSIONS

In conclusion, we propose a spin-Weyl quantum unit: a four-state system that can be regarded as a coherent combination of spin and Andreev superconducting qubits. The

coherence, that seemingly breaks the parity conservation, can be achieved by coupling a 4-terminal superconducting structure housing a Weyl point to a quantum dot. We derive a simple but non-trivial universal Hamiltonian for the setup and choose 4-dimensional subspace for the realization of the spin-Weyl quantum unit. We have described the methods and advantages of the quantum manipulation by controlling the superconducting phases in the vicinity of the Weyl point. We illustrate this by providing concrete designs of single-qubit and two-qubit quantum gates.

Such devices can be fabricated and tuned, and, as it is common in superconducting qubit technologies, can be made work together in a many-unit quantum computer by coupling them to electric resonant modes. The system described calls for an experimental realization.

REFERENCES

[1] Y. V. Nazarov and Y. M. Blanter, *Quantum Transport: Introduction to Nanoscience* (Cambridge University Press, 2009).

[2] J. Q. You, X. Hu, S. Ashhab, and F. Nori, *Low-decoherence flux qubit,* Phys. Rev. B **75**, 140515(R) (2007).

[3] R. Harris, J. Johansson, A. J. Berkley, M. W. Johnson, T. Lanting, S. Han, P. Bunyk, E. Ladizinsky, T. Oh, I. Perminov, E. Tolkacheva, S. Uchaikin, E. M. Chapple, C. Enderud, C. Rich, M. Thom, J. Wang, B. Wilson, and G. Rose, *Experimental demonstration of a robust and scalable flux qubit,* Phys. Rev. B **81**, 134510 (2010).

[4] A. A. Houck, J. A. Schreier, B. R. Johnson, J. M. Chow, J. Koch, J. M. Gambetta, D. I. Schuster, L. Frunzio, M. H. Devoret, S. M. Girvin, and R. J. Schoelkopf, *Controlling the spontaneous emission of a superconducting transmon qubit,* Phys. Rev. Lett. **101**, 080502 (2008).

[5] M. B. Metcalfe, E. Boaknin, V. Manucharyan, R. Vijay, I. Siddiqi, C. Rigetti, L. Frunzio, R. J. Schoelkopf, and M. H. Devoret, *Measuring the decoherence of a quantronium qubit with the cavity bifurcation amplifier,* Phys. Rev. B **76**, 174516 (2007).

[6] H. Paik, S. K. Dutta, R. M. Lewis, T. A. Palomaki, B. K. Cooper, R. C. Ramos, H. Xu, A. J. Dragt, J. R. Anderson, C. J. Lobb, and F. C. Wellstood, *Decoherence in dc squid phase qubits,* Phys. Rev. B **77**, 214510 (2008).

[7] M. H. S. Amin, A. Y. Smirnov, and A. Maassen van den Brink, *Josephson-phase qubit without tunneling,* Phys. Rev. B **67**, 100508(R) (2003).

[8] L. DiCarlo, J. M. Chow, J. M. Gambetta, L. S. Bishop, B. R. Johnson, D. I. Schuster, J. Majer, A. Blais, L. Frunzio, S. M. Girvin, and R. J. Schoelkopf, *Demonstration of two-qubit algorithms with a superconducting quantum processor,* Nature **460**, 240 (2009).

[9] L. M. K. Vandersypen, H. Bluhm, J. S. Clarke, A. S. Dzurak, R. Ishihara, A. Morello, D. J. Reilly, L. R. Schreiber, and M. Veldhorst, *Interfacing spin qubits in quantum dots and donors—hot, dense, and coherent,* npj Quantum Information **3**, 34 (2017).

[10] D. Loss and D. P. DiVincenzo, *Quantum computation with quantum dots,* Phys. Rev. A **57**, 120 (1998).

[11] R. Hanson and G. Burkard, *Universal set of quantum gates for double-dot spin qubits with fixed interdot coupling,* Phys. Rev. Lett. **98**, 050502 (2007).

[12] G. C. Aers, S. A. Studenikin, G. Granger, A. Kam, P. Zawadzki, Z. R. Wasilewski, and A. S. Sachrajda, *Coherent exchange and double beam splitter oscillations in a triple quantum dot,* Phys. Rev. B **86**, 045316 (2012).

[13] E. A. Laird, J. M. Taylor, D. P. DiVincenzo, C. M. Marcus, M. P. Hanson, and A. C. Gossard, *Coherent spin manipulation in an exchange-only qubit,* Phys. Rev. B **82**, 075403 (2010).

[14] E. Kawakami, P. Scarlino, D. R. Ward, F. R. Braakman, D. E. Savage, M. G. Lagally, M. Friesen, S. N. Coppersmith, M. A. Eriksson, and L. M. K. Vandersypen, *Electrical control of a long-lived spin qubit in a si/sige quantum dot,* Nature Nanotechnology **9**, 666 EP (2014).

[15] Y.-L. Wu and S. Das Sarma, *Decoherence of two coupled singlet-triplet spin qubits,* Phys. Rev. B **96**, 165301 (2017).

[16] A. P. Higginbotham, F. Kuemmeth, M. P. Hanson, A. C. Gossard, and C. M. Marcus, *Coherent operations and screening in multielectron spin qubits,* Phys. Rev. Lett. **112**, 026801 (2014).

[17] S. E. Lillie, D. A. Broadway, J. D. A. Wood, D. A. Simpson, A. Stacey, J.-P. Tetienne, and L. C. L. Hollenberg, *Environmentally mediated coherent control of a spin qubit in diamond,* Phys. Rev. Lett. **118**, 167204 (2017).

[18] A. Zazunov, V. S. Shumeiko, E. N. Bratus', J. Lantz, and G. Wendin, *Andreev level qubit,* Phys. Rev. Lett. **90**, 087003 (2003).

[19] N. M. Chtchelkatchev and Y. V. Nazarov, *Andreev quantum dots for spin manipulation,* Phys. Rev. Lett. **90**, 226806 (2003).

[20] C. Padurariu and Y. V. Nazarov, *Theoretical proposal for superconducting spin qubits,* Phys. Rev. B **81**, 144519 (2010).

[21] C. Padurariu and Y. V. Nazarov, *Spin blockade qubit in a superconducting junction, EPL (Europhysics Letters)*, Europhysics Letters **100**, 57006 (2012).

[22] L. Bretheau, Ç. Ö. Girit, H. Pothier, D. Esteve, and C. Urbina, *Exciting andreev pairs in a superconducting atomic contact,* Nature **499**, 312 (2013).

[23] C. Janvier, L. Tosi, L. Bretheau, Ç. Ö. Girit, M. Stern, P. Bertet, P. Joyez, D. Vion, D. Esteve, M. F. Goffman, H. Pothier, and C. Urbina, *Coherent manipulation of andreev states in superconducting atomic contacts,* Science **349**, 1199 (2015), https://science.sciencemag.org/content/349/6253/1199.full.pdf .

[24] L. Tosi, C. Metzger, M. F. Goffman, C. Urbina, H. Pothier, S. Park, A. L. Yeyati, J. Nygård, and P. Krogstrup, *Spin-orbit splitting of andreev states revealed by microwave spectroscopy,* Phys. Rev. X **9**, 011010 (2019).

[25] R.-P. Riwar, M. Houzet, J. S. Meyer, and Y. V. Nazarov, *Multi-terminal josephson junctions as topological matter,* Nature Communications **7**, 11167 (2016).

[26] M. Amundsen, J. A. Ouassou, and J. Linder, *Analytically determined topological phase diagram of the proximity-induced gap in diffusive n-terminal Josephson junctions,* Scientific Reports **7** (2017), 10.1038/srep40578.

[27] E. Strambini, S. D'Ambrosio, F. Vischi, F. S. Bergeret, Y. V. Nazarov, and F. Giazotto, *The omega-SQUIPT as a tool to phase-engineer Josephson topological materials,* Nature Nanotechnology **11**, 1055 (2016).

[28] F. Nichele, E. Portolés, A. Fornieri, A. M. Whiticar, A. C. C. Drachmann, S. Gronin, T. Wang, G. C. Gardner, C. Thomas, A. T. Hatke, M. J. Manfra, and C. M. Marcus, *Relating andreev bound states and supercurrents in hybrid josephson junctions,* Phys. Rev. Lett. **124**, 226801 (2020).

[29] P. Kotetes, M. T. Mercaldo, and M. Cuoco, *Synthetic weyl points and chiral anomaly in majorana devices with nonstandard andreev-bound-state spectra,* Phys. Rev. Lett. **123**, 126802 (2019).

[30] E. V. Repin, Y. Chen, and Y. V. Nazarov, *Topological properties of multiterminal superconducting nanostructures: Effect of a continuous spectrum,* Phys. Rev. B **99**, 165414 (2019).

[31] M. Houzet and J. S. Meyer, *Majorana-weyl crossings in topological multiterminal junctions,* Phys. Rev. B **100**, 014521 (2019).

[32] R. L. Klees, G. Rastelli, J. C. Cuevas, and W. Belzig, *Microwave Spectroscopy Reveals the Quantum Geometric Tensor of Topological Josephson Matter,* Physical Review Letters **124** (2020), 10.1103/PhysRevLett.124.197002.

[33] A. W. Draelos, M.-T. Wei, A. Seredinski, H. Li, Y. Mehta, K. Watanabe, T. Taniguchi, I. V. Borzenets, F. Amet, and G. Finkelstein, *Supercurrent flow in multiterminal graphene josephson junctions,* Nano Letters **19**, 1039 (2019).

[34] N. Pankratova, H. Lee, R. Kuzmin, K. Wickramasinghe, W. Mayer, J. Yuan, M. G. Vavilov, J. Shabani, and V. E. Manucharyan, *Multiterminal josephson effect,* Phys. Rev. X **10**, 031051 (2020).

[35] T. Yokoyama and Y. V. Nazarov, *Singularities in the andreev spectrum of a multiterminal josephson junction,* Phys. Rev. B **92**, 155437 (2015).

[36] W. D. Oliver, Y. Yu, J. C. Lee, K. K. Berggren, L. S. Levitov, and T. P. Orlando, *Mach-zehnder interferometry in a strongly driven superconducting qubit,* Science **310**, 1653 (2005), https://science.sciencemag.org/content/310/5754/1653.full.pdf .

[37] M. A. Nielsen and I. L. Chuang, *Quantum Computation and Quantum Information: 10th Anniversary Edition* (Cambridge University Press, 2010).

[38] F. Vatan and C. Williams, *Optimal quantum circuits for general two-qubit gates,* Phys. Rev. A **69**, 032315 (2004).

4

SPINTRONICS WITH A WEYL POINT IN SUPERCONDUCTING NANOSTRUCTURES

This chapter has been published as **Yuguang Chen**, Yuli Nazarov, *Spintronics with a Weyl point in superconducting nanostructures*, Phys. Rev. B **103**, 165424 (2021).

4.1. INTRODUCTION

Spin currents in metals are conserved at significant length scale of spin-flip length and therefore can be induced and measured at this scale. The whole field of spintronics [1, 2] concentrates on conversion of electric currents to spin currents, electrical detection of spin polarization produced by the spin currents, and dynamics of these processes [3]. Much theoretical research addressed this conversion and detection at ferromagnet-normal metal interfaces, for collinear[4, 5] and non-collinear[6, 7] configurations of the ferromagnets. Detection of the complex counting statistics of spin currents has been addressed as well[8, 9].

New functionalities can be achieved by combining ferromagnets, normal metal and superconductors, most are based on spin-singlet nature of Cooper pairs forming the superconducting condensate[10]. For instance, the absolute spin-valve effect [11, 12] can be achieved in this way, and long-distance triplet proximity effect [13–15] can be arranged.

While most research and applications in spintronics concentrates on extended structures, all spintronic effects can be reproduced with the systems involving few quantum states, for instance, realized in semiconducting quantum dots [16, 17]. Spin filtering and detection have been demonstrated[17–19] and more research is underway[20]. The ferromagnets are not needed here since spin effects arise from Zeeman splitting of the discrete energy levels by external magnetic field.

Recently, Weyl points - the topological singularities in the spectrum of Andreev bound states - have been predicted in superconducting nanostructures[21]. At a Weyl point, the energy of the lowest Andreev state crosses Fermi level, so it costs vanishing energy to excite a quasiparticle near the Weyl point. From general topological reasoning, such crossing requires tuning of three parameters. This is why the Weyl points are usually considered in multi-terminal superconducting nanostructures where the parameters are the superconducting phase differences of the terminals. Four terminals are thus needed to realize a Weyl point. This prediction gave rise to related experimental and theoretical research [22–33].

It is important that weak spin-orbit interaction splits the energies of single-quasiparticle states.This can be realized within AIIIBV semiconductors, heavy metals, and curved graphene. [21, 34–36] Owing to this, the ground state configuration is always magnetic in a small finite region around the point and is non-magnetic otherwise.[28, 34] The opposite magnetization is realized in a small region at opposite settings of the phase differences, as required by time reversibility. Thus Weyl point provides a minimum magnet that involves a single electron spin and can be driven to a non-magnetic state by a tiny change of the external parameters — superconducting phases. More details are provided in Section 4.2.

In this Article, we investigate if this minimum magnet can be utilized in spintronic context. We consider low-voltage transport in a setup where one or two normal leads are tunnel-coupled to a superconducting structure hosting a Weyl point (Fig. 4.1). We demonstrate that this suffice to realize all spintronic effects: the magnetic state of the superconducting structure can be detected, a spin-polarized current can be induced in the leads, and its polarization can be close to absolute one, non-equilibrium spin accumulation in the leads can be detected electrically. The peculiarity and a possible ad-

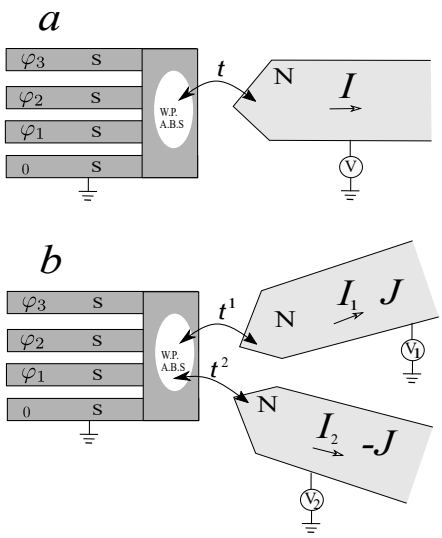

Figure 4.1: Single-lead (a) and two-lead (b) setups for spintronics with a Weyl point investigated in the Article. The normal leads are tunnel-coupled to a superconducting structure hosting an Andreev bound state (W.P.A.B.S. in the Figure) that can be tuned to a Weyl point by choosing the superconducting phases $\phi_{1,2,3}$. Since the model in use applies to any nanostructure, the picture is rather symbolic, the W.P.A.B.S region is anything that connects the leads thus making the Andreev bound states possible. We demonstrate the spintronic effects in the transport: spin current J in addition to electric current I, and the detection of possible spin accumulation in the leads.

vantage of the Weyl-point spintronics is the sensitivity of all effects to tiny variations of the superconducting phases. This enables spintronic effects that are not usually present in common situations: we discuss how to provide spin on demand and alternative spin current.

The structure of the Article is as follows. In Section 4.2 we review the generic Hamiltonian of the Weyl point and explain the magnetism in its vicinity. In Section 4.3 we establish a microscopic model of tunneling to/from the nanostructure, identify the elementary transport processes, compute their rates and derive a master equation describing the transport. We study the transport in a single-lead setup in Section 4.4. Next, we describe how to achieve spin on demand and alternative spin current (Section 4.5). Owing to spin conservation in the superconductor, the d.c. spin current requires two leads: we consider this situation in Section 4.6 and show how to approach the absolute spin polarization of the resulting current. We discuss the detection of spin accumulation in the leads in Section 4.7. We conclude in Section 4.8.

4.2. MAGNETISM NEAR A WEYL POINT

In this Section, we will give the effective low-energy Hamiltonian of the superconducting nanostructure in the vicinity of Weyl point and describe its magnetic state following the references[21, 28, 34]. Three independent superconducting phase differences can be regarded as a 3D vector $\vec{\varphi}$. Suppose the Weyl points are situated at $\pm\vec{\varphi}_0$. In the vicinity

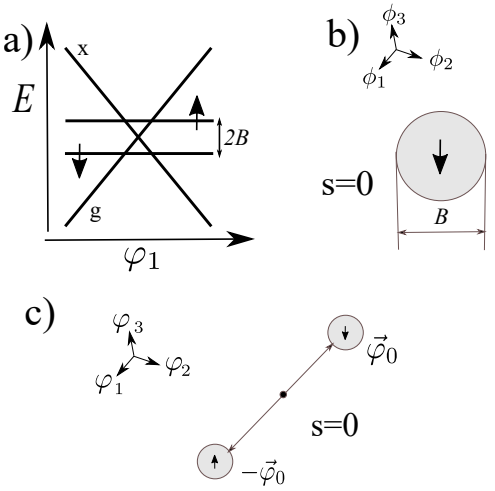

Figure 4.2: Magnetism near a Weyl point (a) Energies of the singlet (g,x) and doublet ($\downarrow$, $\uparrow$) states in the vicinity of a Weyl point versus one of the phases. (b) The region of a doublet (magnetic) ground state around a Weyl point at $\vec{\varphi}_0$ surrounded by the region of a singlet ground state. (c) Opposite magnetizations at Weyl points at $\pm\vec{\varphi}_0$.

of the point at $\vec{\varphi}_0$ we expand $\vec{\varphi} = \vec{\varphi}_0 + \delta\vec{\varphi}$, $|\delta\vec{\varphi}| \ll 1$ and can describe the lowest Andreev bound states by a 2×2 matrix BdG Hamiltonian

$$\hat{H}_W = \phi_a \hat{\tau}_a;\ \phi_a = M_{ab}\delta\varphi_b, \tag{4.1}$$

where $\hat{\tau}_a$ is a vector of Pauli matrices. This form suggests convenient coordinates $\vec{\phi}$ for the vicinity of a Weyl point that are linearly related and thus equivalent to $\delta\vec{\varphi}$. These rescaled coordinates $\vec{\phi}$ are very convenient although they have dimension energy. We will make consistent use of them in the rest of the paper. In these coordinates of dimension energy, the spectrum is isotropic and conical, $E = \pm|\vec{\phi}|$. The coordinates are thus defined upon an orthogonal transformation. We thus consider only a pair of Andreev bound states. We stress that this approximation is valid at low energy and in the small vicinity of the Weyl point in any nanostructure, while the criteria on low energy and small vicinity are specific for a nanostructure. If there are few Andreev bound states in the overall spectrum, the energy should be lower than the superconducting energy gap Δ, and the phase distance from the Weyl point should be smaller than 2π. The approximation is also valid if there are many Andreev bound states forming a quasi-continuous spectrum: in this case, the energy should be smaller than the average level spacing in the spectrum and the phase distance is restricted by a correspondingly smaller value.

The 2×2 BdG Hamiltonian is obtained by projection on two two-component eigenfunctions $|\Psi_\pm\rangle$ related by BdG symmetry. In coordinate representation,

$$|\Psi_+\rangle = (u(\mathbf{r}), v(\mathbf{r}));\ |\Psi_-\rangle = (-v^*(\mathbf{r}), u^*(\mathbf{r})), \tag{4.2}$$

$\mathbf{r}$ being the coordinates within the nanostructure.

Weak spin-orbit interaction within the nanostructure modifies the Hamiltonian splitting the Andreev states in spin[34],

$$\hat{H}_{\mathrm{W}} = \phi_a \hat{\tau}_a + B_a \hat{\sigma}_a, \tag{4.3}$$

$\hat{\sigma}_a$ being a vector of Pauli matrices in spin space, and B_a looks like an external magnetic field causing Zeeman splitting. However, $\vec{B} \neq 0$ even in the absence of external magnetic field and represents the effect of the superconducting phase differences on spin orientation. Owing to global time reversibility, the vectors $\vec{B}$ are opposite for opposite Weyl points, $\vec{B}(-\varphi_0) = -\vec{B}(\varphi_0)$. The magnitude of $\vec{B}$ can be estimated as the superconducting energy gap Δ times a dimensionless factor characterizing the weakness of the spin-orbit interaction. For a concrete number in mind, we can take $B \simeq 0.1\Delta \simeq 0.2meV$ which corresponds to niobium. If there is an external magnetic field, it adds to $\vec{B}$. We note however that our estimation of B is about $3T$, so it requires a significant field to change it. While the presence of SO is important for the spectrum of the Weyl point, its concrete value is not that important for our model since it enters only as a single parameter B and all spintronic properties scale eventually scale with this parameter.

To rewrite the Hamiltonian in the second-quantization form, we introduce quasiparticle annihilation operators $\hat{\gamma}_\sigma$ and associated Nambu bispinors $\bar{\gamma}_{a,\sigma} \equiv (\hat{\gamma}_\sigma, \sigma\hat{\gamma}^\dagger_{-\sigma})$ to recast it to the standard form,

$$H_{\mathrm{WP}} = \frac{1}{2}\bar{\gamma}^\dagger_\alpha \hat{H}^{\mathrm{WP}}_{\alpha\beta}\bar{\gamma}_\beta \tag{4.4}$$

This Hamiltonian can be reduced to a diagonal form for a certain direction in ϕ-space, $\vec{\phi} = \phi\vec{n}$ by a Bogoliubov transform of $\hat{\gamma}_\sigma$ to a direction-dependent $\hat{\tilde{\gamma}}_\sigma$. Choosing the spin quantization axis along $\vec{B}$, we arrive at

$$H_{\mathrm{WP}} = \frac{1}{2}(\phi + B\sigma)\left(\hat{\tilde{\gamma}}^\dagger_\sigma\hat{\tilde{\gamma}}_\sigma - \hat{\tilde{\gamma}}_\sigma\hat{\tilde{\gamma}}^\dagger_\sigma\right) \tag{4.5}$$

This gives the spectrum sketched in Fig. 4.2a. The energies are $E = \pm\phi$ for two spin-singlet states, ground one $|g\rangle$, and excited one $|x\rangle \equiv \hat{\tilde{\gamma}}^\dagger_\uparrow\hat{\tilde{\gamma}}^\dagger_\downarrow|g\rangle$. The energies are $E = \pm B$ for two components of the spin doublet $|\uparrow\rangle \equiv \hat{\tilde{\gamma}}^\dagger_\uparrow|g\rangle$, $|\downarrow\rangle \equiv \hat{\tilde{\gamma}}^\dagger_\downarrow|g\rangle$. The spin-doublet is split and its energies exhibit no singularity or phase dependence in the vicinity of the Weyl point $\vec{\phi} = 0$, while the spin-singlet states retain the conical spectrum.

This leads us to a simple but important conclusion: the ground state of the nanostructure is magnetic in a narrow vicinity of a Weyl point, namely, at $|\phi| < B$ (Fig. 4.2a). Corresponding to our estimation of B, $\delta\varphi \simeq 0.1$. Thus, the magnetism can be switched on and off by variation of magnetic flux controlling the superconducting phase differences by a tenth of the flux quantum. This is a much smaller action than, for instance, in quantum dots where it requires a change of electron number and strong magnetic fields, not mentioning the bulk magnetic structures. The opposite direction of the equilibrium magnetic polarization is found at the opposite Weyl point (Fig. 4.2c).

This makes a nanostructure with Weyl points a minimum example of a magnet.

4.3. MICROSCOPIC MODEL AND TUNNELING RATES

Let us consider tunneling between the electron states in the nanostructure and those in a normal lead. Conventionally, we assume a quasi-continuous spectrum in the lead and

label the electron states with k and spin direction σ, $\hat{d}_{\sigma,k}$ being an associated electron creation operator. We start with a rather general model tunneling Hamiltonian

$$H_T = \int d\mathbf{r}(t_k(\mathbf{r})\hat{c}_\sigma(\mathbf{r})^\dagger \hat{d}_{\sigma,k} + h.c.) \tag{4.6}$$

that describes electron tunnelling to/from a point $\mathbf{r}$ in the nanostructure from/to the state k in the lead, $\hat{c}_\sigma(\mathbf{r})$ being the electron annihilation operator at the point $\mathbf{r}$. The tunneling amplitudes can be equivalently given in coordinate representation, $t(\mathbf{r},\mathbf{r}')$, with the transform involving the eigenfunctions of the states k in coordinate representation. We assume spin conservation in the course of tunneling, this is consistent with the assumption of weak spin-orbit interaction.

To proceed, one represents $\hat{c}_\sigma(\mathbf{r})$ in terms of the quasiparticle creation/annihilation operators $\hat{\gamma}_{\sigma,n}$ associated with the quasiparticle states in the nanostructure, those are labelled with n:

$$\hat{c}_\sigma(\mathbf{r}) = \sum_n \left(u_n(\mathbf{r})\hat{\gamma}_{\sigma,n} - \sigma v_n^*(\mathbf{r})\hat{\gamma}^\dagger_{-\sigma,n}\right). \tag{4.7}$$

Here, $(u_n(\mathbf{r}), v_n(\mathbf{r})$ is the wave function of the quasiparticle state n.

We concentrate on the tunneling that involves only the lowest quasiparticle state near the Weyl point, this is relevant at low energies $\ll \Delta$. We also neglect higher-order tunneling processes corresponding to two-electron tunneling to the superconducting nanostructure [37] or Andreev reflection from the nanostructure. With this, we can replace

$$c_\sigma(\mathbf{r}) \to u(\mathbf{r})\hat{\tilde{\gamma}}_\sigma - \sigma v^*(\mathbf{r})\hat{\tilde{\gamma}}^\dagger_{-\sigma} \tag{4.8}$$

where $\hat{\tilde{\gamma}}_\sigma$ is the direction-dependent quasiparticle creation operator, and $(u(\mathbf{r}), v(\mathbf{r}))$ is the associated wave function which also depends on the direction $\vec{n} = \vec{r}/|\vec{r}|$.

With this, we can express all the tunneling rates involving electron energy E in terms of two combinations of the tunneling amplitudes:

$$\Gamma_{u,v} = \frac{2\pi}{\hbar}\sum_k \delta(E - E_k)|T_k^{u,v}|^2 \tag{4.9}$$

$$T_k^u = \int d\mathbf{r} u(\mathbf{r})\, t_k^*(\mathbf{r});\; T_k^v = \int d\mathbf{r} v(\mathbf{r})\, t_k(\mathbf{r}) \tag{4.10}$$

Here, Γ_u enters the rates of the processes where adding/extracting of an electron in the lead is accompanied by extracting/adding a quasiparticle, while Γ_v determines the rates of the processes where the adding/extracting of an electron goes together with the adding/extracting a quasiparticle. These rates depend on the direction in the vicinity of the Weyl point. Transforming the wave functions, we derive the $\vec{n}$ dependence of these rates:

$$\Gamma_{u,v} = \frac{\Gamma}{2} \pm \vec{\Gamma}_1 \cdot \vec{n};\; |\vec{\Gamma}_1| < \Gamma/2 \tag{4.11}$$

We observe that the tunneling breaks isotropy near the Weyl point. This has been also noted in [38] where we have considered tunneling to/from a Weyl point nanostructure to discrete electron states. In the following, we will neglect the energy dependence of $\Gamma_{u,v}$ which is a common assumption for the tunneling at energies close to the Fermi energy.

With this, we can straightforwardly evaluate the rates of all relevant processes. Those include transitions between $|g\rangle$ and doublet states, $|e\rangle$ and doublet states, each transition can proceed with addition of spin σ and either electron or hole to the lead. Let us consider a transition from $|e\rangle$ to $|-\sigma\rangle$ with addition of an electron with spin σ to the lead. This should involve Γ_u. The energy of the resulting electron is $E = E_e - E_{-\sigma}$, and the probability to find an empty state for this transition is defined by the filling factor in the lead at the energy E and with spin direction σ. Therefore,

$$\Gamma_{x\to-\sigma,e} = \Gamma_u \left(1 - f_\sigma(E_x - E_{-\sigma})\right) \tag{4.12}$$

The other rates are obtained by similar consideration. Let us list them all (here for brevity $\bar{f} \equiv (1-f)$) :

$$\Gamma_{x\to\sigma,e} = \Gamma_u \bar{f}_{-\sigma}(E_x - E_\sigma) \tag{4.13}$$
$$\Gamma_{x\to\sigma,h} = \Gamma_v f_\sigma(E_\sigma - E_x) \tag{4.14}$$
$$\Gamma_{\sigma\to x,e} = \Gamma_v \bar{f}_\sigma(E_\sigma - E_x) \tag{4.15}$$
$$\Gamma_{\sigma\to x,h} = \Gamma_u f_{-\sigma}(E_x - E_\sigma) \tag{4.16}$$
$$\Gamma_{g\to\sigma,e} = \Gamma_v \bar{f}_{-\sigma}(E_g - E_\sigma) \tag{4.17}$$
$$\Gamma_{g\to\sigma,h} = \Gamma_u f_\sigma(E_\sigma - E_g) \tag{4.18}$$
$$\Gamma_{\sigma\to g,e} = \Gamma_u \bar{f}_\sigma(E_\sigma - E_g) \tag{4.19}$$
$$\Gamma_{\sigma\to g,h} = \Gamma_v f_{-\sigma}(E_g - E_\sigma) \tag{4.20}$$

We note that since $E_g = -E_x$ and $E_\sigma = -E_{-\sigma}$, this is the manifestation of the absence of electron-electron interactions in our model,

$$\Gamma_{\sigma\to x} = \Gamma_{g\to-\sigma};\ \Gamma_{x\to\sigma} = \Gamma_{-\sigma\to g} \tag{4.21}$$

for both e and h processes separately. One can easily include more leads into the consideration: each rate will be a sum of contributions of the rates to each lead.

The rates will enter a standard master equation for the probabilities $p_g, p_x, p_\uparrow, p_\downarrow$. We will not write down the equation, since owing to the absence of the interactions, its solution is easily obtained in a very general situation and reads ($\bar{F} = 1 - F$):

$$p_g = \bar{F}_u \bar{F}_d,\ p_\downarrow = F_d \bar{F}_u,\ p_\uparrow = F_u \bar{F}_d,\ p_x = F_u F_d, \tag{4.22}$$

where the effective "filling factors" $F_{d,u}$ are given by

$$F_d = \Sigma^{-1} \sum_j \left(\Gamma_u^{(j)} f_\downarrow^{(j)}(\epsilon_d) + \Gamma_v^{(j)} \bar{f}_\uparrow(-\epsilon_d)\right); \tag{4.23}$$

$$F_u = \Sigma^{-1} \sum_j \left(\Gamma_u^{(j)} f_\uparrow^{(j)}(\epsilon_u) + \Gamma_v^{(j)} \bar{f}_\downarrow(-\epsilon_u)\right); \tag{4.24}$$

$$\epsilon_{u,d} = E_{\uparrow,\downarrow} - E_g;\ \Sigma \equiv \sum_j \left(\Gamma_u^{(j)} + \Gamma_v^{(j)}\right) \tag{4.25}$$

j being metallic lead index.

We mostly concentrate on the vanishing temperature case, $k_B T \ll B$. Then in the absence of spin accumulation the filling factor does not depend on spin and can be approximated $f(E) = \Theta(-E + eV)$, V being the voltage applied to the lead. It is convenient to set the superconducting nanostructure at zero voltage.

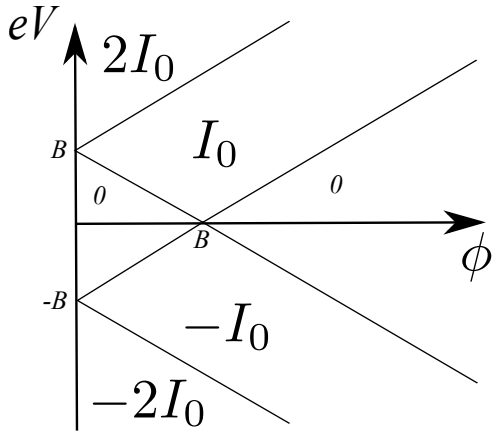

Figure 4.3: Transport in the single-lead setup. The lines of thresholds at $eV = \pm|B-\phi|$ and $eV = \pm(B+\phi)$ define the domains with the electric current $I = \pm I_0, \pm 2I_0$. There is no current at low voltage except $\phi \approx B$ and vanishing temperature.

4.4. SINGLE-LEAD TRANSPORT

Let us concentrate on a single lead setup and evaluate the current at various voltages applied to the lead. To understand the relevant transport processes, let us fist assume vanishing temperature, $eV > 0$ and $\phi > B$, that is, the singlet ground state. No current will flow until the voltage exceeds the threshold required to put a quasiparticle with spin down to the nanostructure, $eV > \epsilon_d = \phi - B$. At slightly higher voltage, the states at energy e_d are filled in the lead and an electron at this energy tunnels to the nanostructure adding a quasiparticle. The rate of this process is Γ_u. The second quasiparticle can not be added yet since it requires higher energy. The state of the nanostructure only changes when an electron at energy $-\epsilon_d$ enters annihilating the quasiparticle. This process occurs with the rate Γ_v. Then the transport cycle repeats itself. We thus have two electrons transferred per cycle of the average duration $\Gamma_u^{-1} + \Gamma_v^{-1}$, so that the current in this regime is given by

$$I = e\frac{2\Gamma_u\Gamma_v}{\Gamma_u + \Gamma_v} \equiv I_0. \tag{4.26}$$

If we start with the magnet ground state, $\phi < B$, the threshold voltage for the same transport regime is determined by opening the pair annihilation process, $eV > -\epsilon_d$. Both thresholds are combined in one by relation $eV > |\phi - B|$. (Fig. 4.3) Upon further increase of voltage, we achieve another threshold $eV > \epsilon_d = B + \phi$ where electrons coming to the leads can add a quasiparticle with spin up, either to ground or spin-down state. Owing to the absence of interaction, this opens up another equivalent and independent transport channel, and the current doubles in this regime (Fig. 4.3):

$$I = 2I_0 \tag{4.27}$$

An interesting feature in this regime is a singular dependence of the current at the

Weyl point $\phi = 0$. Indeed, the current is a function of $\vec{n}$ (see Eq. 4.11),

$$I = e\frac{4\Gamma_u\Gamma_v}{\Gamma_u+\Gamma_v} = e\Gamma_0 - 4e\frac{(\vec{\Gamma}_1\cdot\vec{n})^2}{\Gamma} \tag{4.28}$$

At $\phi = 0$, an infinitesimally small change of $\vec{\phi}$ leads to a finite change of the current. Remarkably, such divergent admittance response persist at finite voltages. In reality, the singularity is probably smoothed at $\phi \simeq \Gamma$, elaboration on this being beyond the approach of this article. Nevertheless, this anomalously big response can be used for a simple and reliable identification of the Weyl point position in a realistic experiment.

At negative eV, all the processes are accompanied by electrons leaving the nanostructure rather than entering it. This reverses the sign of the current upon reverting the voltage.

There is a relatively simple expression for the current beyond the vanishing temperature limit,

$$\begin{aligned} I/I_0 = &(f_F(\epsilon_d - eV) - f_F(\epsilon_d + eV)) \\ &+ (f_F(\epsilon_u - eV) - f_F(\epsilon_u + eV)) \end{aligned} \tag{4.29}$$

where $f_F(\epsilon) \equiv (1+\exp(\epsilon/k_BT))^{-1}$ is the Fermi distribution function, two terms correspond to quasiparticle transfer with down or up spin. At finite but small temperature $k_BT \ll B$ the zero-voltage conductance exhibits a resonant peak in the vicinity of $B = \phi$, that is, at $\epsilon_d \simeq k_BT \ll B$

$$dI/dV = \frac{eI_0}{2k_BT}\frac{1}{\cosh^2(\epsilon_d/2k_BT)} \tag{4.30}$$

This can be used for identification of the transition to the magnetic state.

There is no dc spin current in the sigle-lead setup owing to a simple fact: the current to the singlet superconductor bears no spin. In the next Sections, we show how this can be circumvented.

4.5. SPIN ON DEMAND AND A.C. SPIN CURRENT

Let us understand that despite the fact that the dc spin current is absent for the single-lead setup, the spin injection is easy to organize. Suppose we want a spin on demand: single spin injected to the lead in a time window around a time moment t_0. We can do so by changing the superconducting phases, that is, ϕ. Before t_0, we keep $\phi > B$ so the state is the ground singlet. At $t = t_0$, we switch ϕ to a value $< B$ making down state energetically favorable. Within a time interval $\simeq \Gamma_0$ a spin will be injected to the lead, either as an electron or hole excitation. To inject a spin of opposite sign, we keep $\phi < B$ before t_0 and change it to the value $B > 0$.

An obvious drawback of this scheme is that we cannot inject the spin of the same sign twice: we would need to evacuate the quasiparticle somewhere. In the single-lead setup, it would have to go to the same lead injecting the opposite spin. This drawback becomes an advantage if the goal is to produce an a.c. spin current J.

Suppose we cycle ϕ in the following way:

$$\phi(t) = B + \tilde{\phi}\sin(\Omega t) \tag{4.31}$$

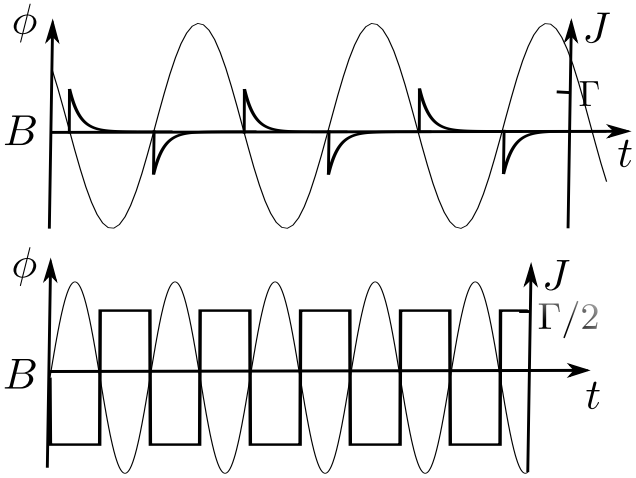

Figure 4.4: Time-averaged a.c. spin current (thick curve) from the lead produced by a periodic modulation of the distance ϕ (thin curve) from the Weyl point. Upper plot: low frequencies $\Omega \ll \Gamma$, spin transfers at the time scale $\simeq \Gamma$ upon crossing the boundary of magnetic state region. Lower plot: high frequencies $\Omega \gg \Gamma$, equal populations of spin-down and ground singlet state.

In the limit of low frequencies $\Omega < \Gamma$, we have alternating single-spin injections at time moments $t_n = 2\pi n/\Omega$ (Fig. 4.4). In the opposite limit of high frequencies $\Omega > \Gamma$, the down and ground singlet state are equally populated, the spin transfers are stochastic with the time-averaged spin current being given by

$$J(t) = -\mathrm{sgn}\,(\sin(\Omega t))\ \Gamma/2 \tag{4.32}$$

Even in the limit of high frequencies, the amplitude of this a.c. spin current is comparable with d.c. spin currents we will evaluate later.

4.6. TWO-LEAD TRANSPORT

Let us start our discussion of the transport in the two-lead setup with a simple but perhaps the most interesting example. Let us organize an absolute spin-valve, that is, the transport involving only electrons of a single spin direction. The tunneling to/from the two leads is characterized by the rates $\Gamma^{(1)}_{u,v}$, $\Gamma^{(2)}_{u,v}$. We assume vanishing temperature and $\phi > B$. We also set $V_2 = 0$ and increase the voltage of the first lead. Nothing happens till $eV_1 < \epsilon_d$: the nanostructure remains in the ground singlet state. Upon crossing this threshold, spin-down electrons from the first lead can create a quasiparticle in the nanostructure. The quasiparticle can go either to the first or two the second lead. Let us assume $\Gamma^{(1)}_{u,v} \ll \Gamma^{(2)}_{u,v}$. In this case, the created quasiparticle will go to the second lead almost instantly bringing the nanostructure back to the ground singlet state. Therefore the transport in the first lead will involve only spin-down electrons, $I_1 = e\Gamma^{(1)}_u$, $J_1 = -I_1/e$. The absolute spin-valve is realized.

The spin current in the second lead is exactly opposite, $J_2 = -J_1$. As to the electric current, the quasiparticle decaying to this lead can create both electron and hole excita-

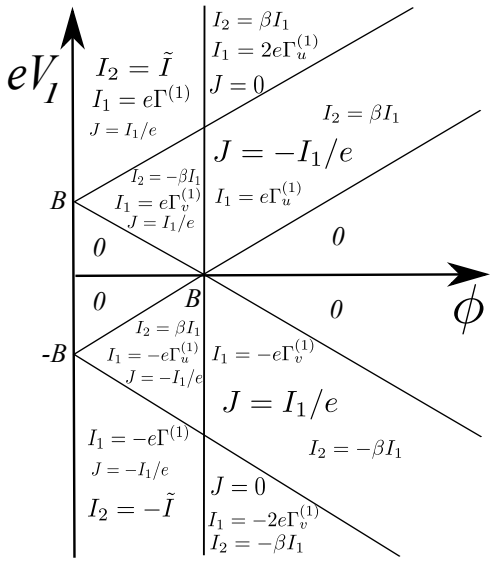

Figure 4.5: Two-lead setup. The absolute spin-valve regime can be realized at small $|eV_2| < |\epsilon_d|$ and $\Gamma^{(1)}_{u,v} \ll \Gamma^{(2)}_{u,v}$. Except the regions with zero spin current $J = 0$, only electrons with either spin-down or spin-up are transported in the first lead. In all regions, $J = J_1 = -J_2$. The current in the second lead is not completely polarized, $I_2 = \pm\beta I_1$ with $\beta \equiv (\Gamma^{(2)}_v - \Gamma^{(2)}_u)/(\Gamma^{(2)}_v + \Gamma^{(2)}_u)$, or $I_2 = \pm\tilde{I}$, $\tilde{I} = e(\Gamma^{(1)}_v - \Gamma^{(1)}_u)\beta$.

tions. So that the current in the second lead is smaller in magnitude than I_2 and can be of either sign depending on the direction near the Weyl point,

$$I_2 = I_1(\Gamma^{(2)}_v - \Gamma^{(2)}_u)/(\Gamma^{(2)}_v + \Gamma^{(2)}_u) = -2I_1(\vec{\Gamma}^{(2)} \cdot \vec{n})/\Gamma^{(2)}. \tag{4.33}$$

It is easy to revert the direction of the spin current. If $\phi < B$, the ground state is spin-down doublet and the transport in the first lead involves the spin-up electrons only, $I_1 = e\Gamma^{(1)}_v$, $J_1 = I_1/e$. The currents in the second lead follow I_1, J_1 as in the previous case.

If we rise eV_1 above the second threshold, $eV_1 > \epsilon_u$, at $\phi > B$ the quasiparticles with both spins can be created in the nanostructure, eventually, with equal probability. This quenches the spin current in this regime, while the electric current $I_1 = 2e\Gamma^{(1)}_u$ is doubled. If $\phi < B$, the crossing of the second threshold does not change the absolute spin valve regime since the transitions from the spin-down state to either ground or excited singlet are both accompanied by the same spin change. The current increases to $I_1 = e\Gamma^{(1)}$

Reverting V_1 changes the sign and magnitude of I_1 while J follows the magnitude but remains of the same sign. The results for the absolute spin valve regime are summarized in Fig 4.5. At vanishing temperature, the transport is the same through the range $-|\epsilon_d| < eV_2 < |\epsilon_d|$.

General picture of the transport in the two-lead setup beyond the assumption $\Gamma^{(1)} \ll \Gamma^{(2)}$ is more complex. The polarization of the transport electrons is not absolute. For instance, in the region defined by $-|\epsilon_d| < eV_2 < |\epsilon_d|$, $\phi > B$, $\phi - B < eV_1 < \phi + B$ the

currents read:

$$J = J_1 = -J_2 = -\Gamma_u^{(1)} \frac{\Gamma^{(2)}}{\Gamma^{(2)}+\Gamma^{(1)}} \tag{4.34}$$

$$I_1 = e\Gamma_u^{(1)} \frac{\Gamma^{(2)}+2\Gamma_v^{(1)}}{\Gamma^{(2)}+\Gamma^{(1)}} \tag{4.35}$$

$$I_2 = -e\Gamma_u^{(1)} \frac{\Gamma_u^{(2)}-\Gamma_v^{(1)}}{\Gamma^{(2)}+\Gamma^{(1)}} \tag{4.36}$$

The polarization of the current in the second lead is thus

$$\left|\frac{eJ}{I_1}\right| = \frac{1}{1+2\Gamma_v^{(1)}/\Gamma^{(2)}} < 1 \tag{4.37}$$

4

In all voltage regions and arbitrary temperatures the currents are obtained from the general formulas

$$\begin{aligned}(\Gamma^{(2)}+\Gamma^{(1)})J =& \Gamma^{(1)}\Gamma_u^{(2)}(f_F(\epsilon_d - eV_2) - f_F(\epsilon_u - eV_2)) \\ &- \Gamma^{(2)}\Gamma_u^{(1)}(f_F(\epsilon_d - eV_1) - f_F(\epsilon_u - eV_1)) \\ &+ \Gamma^{(1)}\Gamma_v^{(2)}(f_F(\epsilon_d + eV_2) - f_F(\epsilon_u + eV_2) \\ &- \Gamma^{(2)}\Gamma_v^{(1)}(f_F(\epsilon_d + eV_1) - f_F(\epsilon_u + eV_1))\end{aligned} \tag{4.38}$$

$$\begin{aligned}(\Gamma^{(2)}+\Gamma^{(1)})I_1/e =& 2\Gamma_u^{(1)}\Gamma_v^{(1)}(f_F(\epsilon_d - eV_1) - f_F(\epsilon_d + eV_1) \\ &+ f_F(\epsilon_u - eV_1) - f_F(\epsilon_u + eV_1)) \\ &+ \Gamma_u^{(1)}\Gamma_u^{(2)}(f_F(\epsilon_d - eV_2) - f_F(\epsilon_d - eV_1) \\ &+ f_F(\epsilon_u - eV_2) - f_F(\epsilon_u - eV_1)) \\ &+ \Gamma_u^{(1)}\Gamma_v^{(2)}(f_F(\epsilon_d + eV_2) - f_F(\epsilon_d - eV_1) \\ &+ f_F(\epsilon_u + eV_2) - f_F(\epsilon_u - eV_1)) \\ &+ \Gamma_v^{(1)}\Gamma_u^{(2)}(f_F(\epsilon_d - eV_2) - f_F(\epsilon_d + eV_1) \\ &+ f_F(\epsilon_u - eV_2) - f_F(\epsilon_u + eV_1)) \\ &+ \Gamma_v^{(1)}\Gamma_v^{(2)}(f_F(\epsilon_d + eV_2) - f_F(\epsilon_d + eV_1) \\ &+ f_F(\epsilon_u + eV_2) - f_F(\epsilon_u + eV_1))\end{aligned} \tag{4.39}$$

4.7. DETECTION OF SPIN ACCUMULATION

So far we have considered equilibrium electron distribution in the normal leads. It is plausible to arrange a distribution that is not in equilibrium with respect to spin. [1, 3] For instance, there may be another contact with this lead, that injects spin utilizing the properties of a traditional normal metal - ferromagnet interface. Owing to the approximate spin conservation, the distributions of the spins of two different directions can be regarded as independent and may differ in chemical potentials. This difference $2P$ characterizes spin accumulation in energy units. If we assume thermalization of the distributions, the filling factors read

$$f_{\downarrow,\uparrow}(\epsilon) = f_F(\epsilon \pm P). \tag{4.40}$$

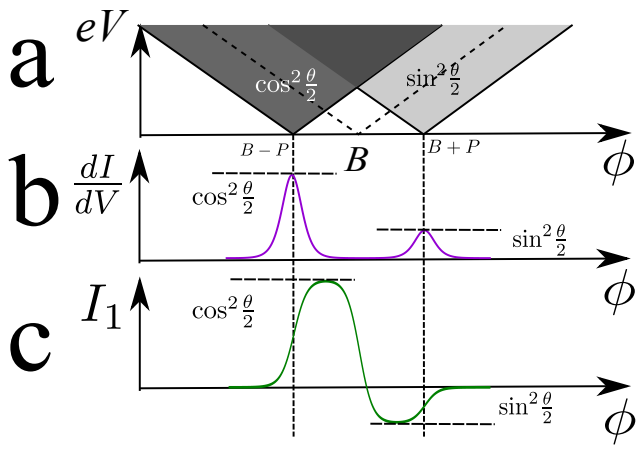

Figure 4.6: The detection of spin accumulation. a. The single-lead setup. The domain of the current with $I = I_0$ (see Fig.4.3) is spit into two corresponding to majority and minority spin accumulated, those are shifted in ϕ by $\pm P$. The currents in the resulting domains are $\cos^2\frac{\theta}{2} I_0$, $\sin^2\frac{\theta}{2} I_0$. b. The detection in the single-lead setup requires voltage. Low-voltage conductance corresponding to a. gives two peaks that are well-separated provided $k_B T \ll P$. In the plot, $k_B T = 0.1P$. c. In the two-lead setup, the spin accumulation gives rise to a current in the absence of voltage. The current in the first lead exhibits two plateaux $\simeq \cos^2\frac{\theta}{2}, -\sin^2\frac{\theta}{2}$. Here, $k_B T = 0.1P$.

If the axis of the resulting spin accumulation $\vec{P}$ is not in the direction of $\vec{B}$, the effective filling factors for two spin directions read

$$\begin{bmatrix} f_\downarrow(\epsilon) \\ f_\uparrow(\epsilon) \end{bmatrix} = \begin{bmatrix} \cos^2\frac{\theta}{2} & \sin^2\frac{\theta}{2} \\ \sin^2\frac{\theta}{2} & \cos^2\frac{\theta}{2} \end{bmatrix} \begin{bmatrix} f_F(\epsilon + P) \\ f_F(\epsilon - P) \end{bmatrix} \tag{4.41}$$

θ being the angle between $\vec{P}$ and $\vec{B}$.

A common spintronic effect is an electric current response on spin accumulation at one side of a contact.[1] This response may be present even without a voltage difference applied to the contact owing to spin dependence of the transmission coefficients. [2] It provides a convenient way to detect and measure the spin accumulation.

Let us start with the single-lead setup. In this case, the spin accumulation gives no current at zero voltage despite the difference in transport of spin-down and spin-up electrons. The reason for this is a rather fine symmetry of the distribution given by Eq. 4.41: $f_\sigma(\epsilon) = \bar{f}_{-\sigma}(-\epsilon)$. This guarantees equal amount of electron emission and absorption by the superconducting nanostructure and thus zero net current. The spin accumulation in this setup is however detected in the presence of voltage. At vanishing temperature, each boundary between the regions of different current is split by the spin accumulation. Two resulting boundaries correspond to thresholds for the transport of minority/majority spin and are shifted by $\pm P$ in eV, as shown in Fig. 4.6 a. At finite temperature and small voltage, spin accumulation is manifested in splitting and $\pm P$ shifts of the conductance peak. Two separate peaks are formed if the accumulation is not in the direction of $\vec{B}$,

otherwise the conductance peak is shifted by P,

$$\frac{dI}{dV} = \frac{eI_0}{k_B T}\left(\frac{\cos^2\frac{\theta}{2}}{\cosh^2((\epsilon_d + P)/2k_B T)} + \frac{\sin^2\frac{\theta}{2}}{\cosh^2((\epsilon_d - P)/2k_B T)}\right), \tag{4.42}$$

c.f. Eq. 4.30, see also Fig. 4.6b. More general expression for the current reads

$$\begin{aligned} I/I_0 &= \cos^2\frac{\theta}{2}A_+ + \sin^2\frac{\theta}{2}A_-; \\ A_\pm &= f(\epsilon_d \pm P - eV) - f(\epsilon_d \pm P + eV) \\ &\quad + f(\epsilon_u \mp P - eV) - f(\epsilon_u \mp P + eV) \end{aligned} \tag{4.43}$$

Interestingly, in a two-lead setup the spin accumulation is detected as a current signal without the voltages applied. We assume the spin accumulation is in the first lead. The accumulation $P < B$ gives rise to the current response near $\phi = B$ (Fig.4.6c.) in the window $|\phi - B| < 2P$. In this regime, we can disregard the contribution of the spin-up excitations. The current in the first lead reads

$$\begin{aligned} I_1 = \frac{e\Gamma^{(1)}\Gamma^{(2)}}{\Gamma^{(1)} + \Gamma^{(2)}}\Big[&\cos^2\frac{\theta}{2}(f_F(e_d + P) - f_F(\epsilon_d)) \\ &+ \sin^2\frac{\theta}{2}(f_F(e_d - P) - f_F(\epsilon_d)\Big] \end{aligned} \tag{4.44}$$

and $I_2 = -I_1$. Finally, we notice that the current response on the spin accumulation also remains the limit of high temperatures $k_B T \gg B, P$ where it is small in comparison with I_0 and linear in $\vec{P}$:

$$I_1 = -\frac{e\phi\Gamma^{(1)}\Gamma^{(2)}}{8(\Gamma^{(1)} + \Gamma^{(2)})(k_B T)^3}\left(2\vec{P}\cdot\vec{B} + \vec{P}^2\right) \tag{4.45}$$

4.8. CONCLUSION

To conclude, we have investigated transport from the normal leads to a superconducting nanostructure housing a Weyl point. A minimum magnet state is realized in the vicinity of this point. Owing to this, the transport exhibit all fundamental spintronic effects: the magnetic state can be detected, spin-on-demand and a.c. spin currents can be arranged in single-lead setups, spin-polarized current can be produced in two-lead setups, this includes the absolute polarization, the spin accumulation in a lead can be detected by electric measurement. The experimental realization of the setup and the corresponding spintronic experiments are feasible. Such a minimum spintronic device will be a demonstration of the power of superconducting nanotechnology and is advantageous because of its sensitivity to small changes of superconducting phase differences and energy selectivity of the transport.

REFERENCES

[1] I. Žutić, J. Fabian, and S. Das Sarma, *Spintronics: Fundamentals and applications,* Rev. Mod. Phys. **76**, 323 (2004).

[2] G. E. W. Bauer, *Perpendicular transport through magnetic multilayers,* Phys. Rev. Lett. **70**, 1733(E) (1993).

[3] Y. Tserkovnyak, A. Brataas, G. E. W. Bauer, and B. I. Halperin, *Nonlocal magnetization dynamics in ferromagnetic heterostructures,* Rev. Mod. Phys. **77**, 1375 (2005).

[4] T. Valet and A. Fert, *Theory of the perpendicular magnetoresistance in magnetic multilayers,* Phys. Rev. B **48**, 7099 (1993).

[5] M. Johnson and R. H. Silsbee, *Coupling of electronic charge and spin at a ferromagnetic-paramagnetic metal interface,* Phys. Rev. B **37**, 5312 (1988).

[6] A. Brataas, Y. V. Nazarov, and G. E. W. Bauer, *Finite-element theory of transport in ferromagnet–normal metal systems,* Phys. Rev. Lett. **84**, 2481 (2000).

[7] A. Brataas, G. E. Bauer, and P. J. Kelly, *Non-collinear magnetoelectronics,* Physics Reports **427**, 157 (2006).

[8] A. Di Lorenzo and Y. V. Nazarov, *Full counting statistics of spin currents,* Phys. Rev. Lett. **93**, 046601 (2004).

[9] A. Di Lorenzo, G. Campagnano, and Y. V. Nazarov, *Full counting statistics of non-commuting variables: The case of spin counts,* Phys. Rev. B **73**, 125311 (2006).

[10] J. Linder and J. W. A. Robinson, *Superconducting spintronics,* Nature Physics **11**, 307 (2015).

[11] D. Huertas-Hernando, Y. V. Nazarov, and W. Belzig, *Absolute spin-valve effect with superconducting proximity structures,* Phys. Rev. Lett. **88**, 047003 (2002).

[12] G. De Simoni, E. Strambini, J. S. Moodera, F. S. Bergeret, and F. Giazotto, *Toward the absolute spin-valve effect in superconducting tunnel junctions,* Nano Letters **18**, 6369 (2018).

[13] F. S. Bergeret, A. F. Volkov, and K. B. Efetov, *Long-range proximity effects in superconductor-ferromagnet structures,* Phys. Rev. Lett. **86**, 4096 (2001).

[14] J. Linder and A. V. Balatsky, *Odd-frequency superconductivity,* Rev. Mod. Phys. **91**, 045005 (2019).

[15] V. Braude and Y. V. Nazarov, *Fully developed triplet proximity effect,* Phys. Rev. Lett. **98**, 077003 (2007).

[16] A. Ludwig, B. Sothmann, H. Höpfner, N. C. Gerhardt, J. Nannen, T. Kümmell, J. König, M. R. Hofmann, G. Bacher, and A. D. Wieck, *Quantum dot spintronics: Fundamentals and applications,* in *Magnetic Nanostructures: Spin Dynamics and Spin Transport*, edited by H. Zabel and M. Farle (Springer Berlin Heidelberg, Berlin, Heidelberg, 2013) pp. 235–268.

[17] R. Hanson, L. P. Kouwenhoven, J. R. Petta, S. Tarucha, and L. M. K. Vandersypen, *Spins in few-electron quantum dots,* Rev. Mod. Phys. **79**, 1217 (2007).

[18] R. Hanson, L. M. K. Vandersypen, L. H. W. van Beveren, J. M. Elzerman, I. T. Vink, and L. P. Kouwenhoven, *Semiconductor few-electron quantum dot operated as a bipolar spin filter,* Phys. Rev. B **70**, 241304(R) (2004).

[19] K. Ono, D. G. Austing, Y. Tokura, and S. Tarucha, *Current rectification by pauli exclusion in a weakly coupled double quantum dot system,* Science **297**, 1313 (2002), https://science.sciencemag.org/content/297/5585/1313.full.pdf .

[20] A. Bordoloi, V. Zannier, L. Sorba, C. Schönenberger, and A. Baumgartner, *A double quantum dot spin valve,* Communications Physics **3**, 135 (2020).

[21] R.-P. Riwar, M. Houzet, J. S. Meyer, and Y. V. Nazarov, *Multi-terminal Josephson junctions as topological matter,* Nature Communications **7** (2016), 10.1038/ncomms11167.

[22] N. Pankratova, H. Lee, R. Kuzmin, K. Wickramasinghe, W. Mayer, J. Yuan, M. G. Vavilov, J. Shabani, and V. E. Manucharyan, *Multiterminal Josephson Effect,* Physical Review X **10** (2020), 10.1103/PhysRevX.10.031051.

[23] R. L. Klees, G. Rastelli, J. C. Cuevas, and W. Belzig, *Microwave Spectroscopy Reveals the Quantum Geometric Tensor of Topological Josephson Matter,* Physical Review Letters **124** (2020), 10.1103/PhysRevLett.124.197002.

[24] G. Graziano, V, J. S. Lee, M. Pendharkar, C. Palmstrom, and V. S. Pribiag, *Transport studies in a gate-tunable three-terminal Josephson junction,* Physical Review B **101** (2020), 10.1103/PhysRevB.101.054510.

[25] P. Marra and M. Nitta, *Topologically nontrivial Andreev bound states,* Physical Review B **100** (2019), 10.1103/PhysRevB.100.220502.

[26] Z. Scherubl, A. Palyi, G. Frank, I. E. Lukacs, G. Fulop, B. Fulop, J. Nygard, K. Watanabe, T. Taniguchi, G. Zarand, and S. Csonka, *Observation of spin-orbit coupling induced Weyl points in a two-electron double quantum dot,* Communications Physics **2** (2019), 10.1038/s42005-019-0200-2.

[27] M. Houzet and J. S. Meyer, *Majorana-weyl crossings in topological multiterminal junctions,* Phys. Rev. B **100**, 014521 (2019).

[28] E. Repin, V, Y. Chen, and Y. Nazarov, V, *Topological properties of multiterminal superconducting nanostructures: Effect of a continuous spectrum,* Physical Review B **99** (2019), 10.1103/PhysRevB.99.165414.

[29] X. Fan, C. Qiu, Y. Shen, H. He, M. Xiao, M. Ke, and Z. Liu, *Probing Weyl Physics with One-Dimensional Sonic Crystals,* Physical Review Letters **122** (2019), 10.1103/PhysRevLett.122.136802.

[30] A. W. Draelos, M.-T. Wei, A. Seredinski, H. Li, Y. Mehta, K. Watanabe, T. Taniguchi, I. V. Borzenets, F. Amet, and G. Finkelstein, *Supercurrent Flow in Multiterminal Graphene Josephson Junctions,* Nano Letters **19**, 1039 (2019).

[31] J. Erdmanis, A. Lukacs, and Y. Nazarov, V, *Weyl disks: Theoretical prediction,* Physical Review B **98** (2018), 10.1103/PhysRevB.98.241105.

[32] J. S. Meyer and M. Houzet, *Nontrivial Chern Numbers in Three-Terminal Josephson Junctions,* Physical Review Letters **119** (2017), 10.1103/PhysRevLett.119.136807.

[33] E. Eriksson, R.-P. Riwar, M. Houzet, J. S. Meyer, and Y. V. Nazarov, *Topological transconductance quantization in a four-terminal Josephson junction,* Physical Review B **95** (2017), 10.1103/PhysRevB.95.075417.

[34] T. Yokoyama and Y. V. Nazarov, *Singularities in the andreev spectrum of a multiterminal josephson junction,* Phys. Rev. B **92**, 155437 (2015).

[35] J. D. S. Bommer, H. Zhang, O. Gül, B. Nijholt, M. Wimmer, F. N. Rybakov, J. Garaud, D. Rodic, E. Babaev, M. Troyer, D. Car, S. R. Plissard, E. P. A. M. Bakkers, K. Watanabe, T. Taniguchi, and L. P. Kouwenhoven, *Spin-orbit protection of induced superconductivity in majorana nanowires,* Phys. Rev. Lett. **122**, 187702 (2019).

[36] M. M. Desjardins, L. C. Contamin, M. R. Delbecq, M. C. Dartiailh, L. E. Bruhat, T. Cubaynes, J. J. Viennot, F. Mallet, S. Rohart, A. Thiaville, A. Cottet, and T. Kontos, *Synthetic spin–orbit interaction for majorana devices,* Nature Materials **18**, 1060 (2019).

[37] F. W. J. Hekking and Y. V. Nazarov, *Interference of two electrons entering a superconductor,* Phys. Rev. Lett. **71**, 1625 (1993).

[38] Y. Chen and Y. V. Nazarov, *Spin-weyl quantum unit: theoretical proposal,* (2020), arXiv:2008.06070 .

5

WEYL POINT IMMERSED IN A CONTINUOUS SPECTRUM: AN EXAMPLE FROM SUPERCONDUCTING NANOSTRUCTURES

This chapter has been published as **Y. Chen**, Y. Nazarov, *Weyl point immersed in a continuous spectrum: an example from superconducting nanostructures*, https://arxiv.org/abs/2102.03947 (2021). The manuscript is submitted to Phys. Rev. B

5.1. INTRODUCTION

The study of topological materials has been on the front edge of the modern research in condensed matter physics for the past decade [1–5]. These materials are appealing from fundamental point of view and for possible applications [6, 7], [8], [9],[10], including quantum information processing[11, 12]). The basis for applications is the topological protection of quantum states, which makes the states robust against small perturbations and leads to many unusual phenomena, e.g. topologically protected edge states[13–15]. The topological superconductors[16–19] and Chern insulators[20–23] are the classes of topological materials that are under active investigation.

Most topological effects under consideration require discrete quantum states, for instance, electron, photon or phonon bands in a Brillouin zone of a periodic structure. Topological protection requires a gap in energy spectrum, that is, absence of continuous excitation spectrum at low energies. It is intuitively clear that immersing the discrete states in a continuous spectrum, and compromising the energy gaps in this way will lead to compromising the topology. One of the goals of the present paper to propose and investigate a simple model for this that can be elaborated analytically to all details.

We concentrate on Weyl points those are most generally defined as topologically protected crossings of the discrete energy levels in a parametric space. From general topological reasoning, such crossing requires tuning of three parameters, so it is natural to consider a three-dimensional parametric space.

Recently, Weyl points - the topologically protected crossings in the spectrum of Andreev bound states - have been predicted in superconducting nanostructures[24]. The specifics of superconductivity that these crossings may be pinned to Fermi level. This restricts the relevant physics to low energies and the properties of the ground state of the system. At a Weyl point, the energy of the lowest Andreev state crosses Fermi level, so it costs vanishing energy to excite a quasiparticle in the vicinity of the point. A requirement of realization. This is why the Weyl points are usually considered in multi-terminal superconducting nanostructures where the parameters are the superconducting phase differences of the terminals. Four terminals are thus needed to realize a Weyl point. This prediction gave rise to related experimental and theoretical research [25–36] A separate set of proposals aims to realization of Weyl points in devices combining Josephson effect and Coulomb blockade [37, 38].

It is important that weak spin-orbit interaction splits the energies of single-quasiparticle states.[24, 39] Owing to this, the ground state configuration is always a component of a spin doublet in a small finite region around the point and is spin-singlet otherwise.[31, 39] The topological singularity still remains since the energies of two singlet states still cross in a point owing to topological protection.

In [31] we have noticed that continuous spectrum above the gap may modify the signatures of topology leading to a non-quantized contribution to the transconductance. The continuous spectrum at low energies shall bring more drastic modification. The most experimentally relevant way to bring a continuous spectrum into play is to couple a system of discrete Andreev levels in the superconducting nanostructure to normal leads. As we will see in detail in this Article, this brings new energy scale Γ, that is the rate of tunnelling to the leads from a discrete state. Since we are at a point of energy crossing, this small energy scale also implies a small scale in the parameter space: the scale at

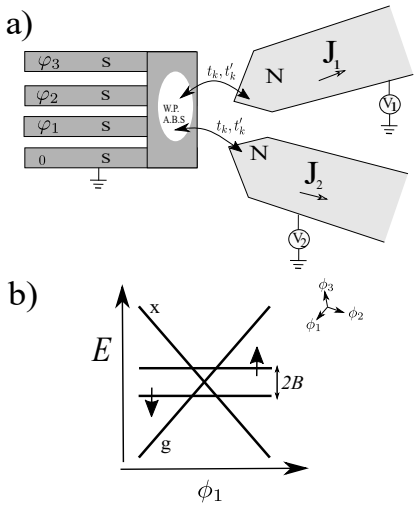

Figure 5.1: a. In a four-terminal superconducting heterostructure, the Andreev states may cross Fermi level in a point - a Weyl point - in 3D parameter space of superconducting phase. The resulting spectrum in the vicinity of the point is isotropic and conical for two singlet states (x and g in the Figure) and flat for doublet states. The doublet states are split by spin-orbit interaction, and one doublet state is ground one in the mere vicinity of the point. b. The setup under consideration. The Andreev bound states near Weyl point (A.B.S.W.P) are tunnel-coupled with the continuous spectrum of the electron states in several normal-metal leads (two are shown in the Figure). The tunnel coupling results in an energy scale Γ at which the spectral singularities are smoothed.

which the energy splitting matches Γ.

We have studied tunnel coupling to discrete normal states in [40] where we propose a Spin-Weyl quantum unit. Importantly, we have found there that the tunnel coupling may break isotropy in the vicinity of the Weyl point. In the context of spintronics, we have recently studied the charge and spin transport in normal leads tunnel-coupled to a Weyl-point superconducting nanostructure. This is essentially the same setup as we consider here. However, in [40] we access the transport in the framework of master equation, that is, assuming that the energy differences of Andreev states exceed much the tunnel energy scale. In this approximation the quantities characterizing the setup retain singularities: the superconducting current has a jump at the point, the normal currents jump at voltages corresponging to the energy levels, the Berry curvature diverges upon approaching the point indicating the point-like topological charge.

In this Article, we investigate the setup at the energy scale Γ revealing how the above-mentioned singularities are smoothed at this scale. We formulate a generic model of tunneling suitable for many leads that includes isotropy violation. Technically, the problem at hand is a case of non-equlibrium Green function technique [41, 42] for non-interacting Fermions. However, we chose to present an explicit derivation in terms of Heisenberg equation of motion for the operators of the superconducting current and those of the currents in the normal leads. We compute these quantities for equilibrium, stationary and adiabatic cases. Owing to simplicity of the generic setup under consideration, all results are analytical.

As expected, all singularities are smoothed. We find the maximum derivative of the supercurrent with respect to the controlling phases, that is set by Γ, and the maximum differential conductance in the tunneling currents. An experimentally relevant point is the sharp dependence of tunneling currents in the vicinity of the point in the limit of high voltages and temperatures. This can be used for detection of Weyl points at temperatures that exceed the level splitting.

We redefine Berry curvature in terms of the response function in the limit of small frequencies. The divergence of the redefined curvature gives the density of topological charge, so we explicitly compute how the point-like topological singularity is spread over the parameter space.

In addition, we evaluate the tunneling currents generated by an adiabatic change of the controlling phases. This is the case of parametric charge pumping[43–45]: the result of a change of the controlling phases along a closed contour is a charge transferred to the leads that depends on the contour only. We show that this is a convenient tool for exploration of the vicinity of the Weyl point, including the smoothing of the singularities.

The structure of the Article is as follows. We formulate the model in Section 5.2 and perform necessary derivations in Section 5.3. We evaluate the superconducting currents in equilibrium in Section 5.4. There are no tunneling currents in equilibrium. They arise if the voltages are applied to the leads, and we evaluate these currents for stationary voltages in Section 5.5. Next, we turn to the adiabatic case computing the response functions in the limit of low frequency. We redefine Berry curvature, evaluate the response function and the density of topological charge in Section 5.6. The Section 5.7 concentrates on charge pumping to the normal leads. We conclude in Section 5.8.

5.2. THE MODEL

We start with the effective Hamiltonian in the vicinity of a Weyl point following [24, 31, 39].

Three independent superconducting phase differences can be regarded as a 3D vector $\vec{\varphi}$. Suppose the Weyl points are situated at $\pm\vec{\varphi}_0$. In the vicinity of the point at $\vec{\varphi}_0$ we expand $\vec{\varphi} = \vec{\varphi}_0 + \delta\vec{\varphi}$, $|\delta\vec{\varphi}| \ll 1$ and can describe the lowest Andreev bound states by a 2×2 matrix BdG Hamiltonian

$$\hat{H}_{\mathrm{W}} = \phi_a \hat{\tau}_a;\ \phi_a = M_{ab}\delta\varphi_b, \tag{5.1}$$

where $\hat{\tau}_a$ is a vector of Pauli matrices. This form suggests convenient coordinates $\vec{\phi}$ for the vicinity of a Weyl point that are linearly related and thus equivalent to $\delta\vec{\varphi}$. We will make use of these coordinates through the paper. In these coordinates of dimension energy, the spectrum is isotropic and conical, $E = \pm|\vec{\phi}|$. The coordinates are thus defined upon an orthogonal transform.

Weak spin-orbit interaction within the nanostructure splits the Andreev states in spin[39], resulting in the following Hamiltonian,

$$\hat{H}^{\mathrm{W}} = \phi_a \hat{\tau}_a + B_a \hat{\sigma}_a, \tag{5.2}$$

$\hat{\sigma}_a$ being a vector of Pauli matrices in spin space, and B_a looks like an external magnetic field causing Zeeman splitting. However, $\vec{B} \neq 0$ even in the absence of external magnetic

field and represents the effect of the superconducting phase differences on spin orientation. Owing to global time reversibility, the vectors $\vec{B}$ are opposite for opposite Weyl points, $\vec{B}(-\varphi_0) = -\vec{B}(\varphi_0)$. The magnitude of $\vec{B}$ can be estimated as the superconducting energy gap Δ times a dimensionless factor characterizing the weakness of the spin-orbit interaction. For a concrete number in mind, we can take $B \simeq 0.1\Delta \simeq 0.2meV$ which corresponds to niobium. If there is an external magnetic field, it adds to $\vec{B}$. We note however that our estimation of B is about $3T$, so it requires a significant field to change it.

To represent the Hamiltonian in the second-quantization form, we introduce quasiparticle annihilation operators $\hat{\gamma}_\sigma$ and associated 4-component Nambu bispinors γ_α, where $\alpha = (i,\sigma)$ combines spin and Nabmu index $i = e,h$, $\bar{\gamma}_{i,\sigma} \equiv (\hat{\gamma}_\sigma, -\sigma\hat{\gamma}_{-\sigma})$ to recast it to the standard form,

$$H_{\mathrm{W}} = \frac{1}{2}\bar{\gamma}^\dagger_\alpha H^{\mathrm{W}}_{\alpha\beta}\bar{\gamma}_\beta. \tag{5.3}$$

We note that $\gamma^\dagger_{i,\sigma} = -\sigma\gamma^{-i,-\sigma}$ This gives an isotropic spectrum which depends only on $\phi \equiv |\vec{\phi}|$.(see Fig. 5.1 a) The energies are $E = \pm\phi$ for two spin-singlet states, ground one $|g\rangle$, and excited one $|x\rangle$, and $E = \pm B$ for two components of the spin doublet $|\uparrow\rangle, |\downarrow\rangle$. The energies of the split doublet exhibit no singularity nor phase dependence in the vicinity of the Weyl point, while the spin-singlet states retain the conical spectrum.

The ground state is magnetic ($|\downarrow\rangle$) in a narrow vicinity of the Weyl point, namely, at $|\phi| < B$ and spin-singlet otherwise. (Fig. 5.1 a)

We will need the current operators in 3 superconducting leads. They are given by the derivatives of the Hamiltonian with respect to the phases,[45]

$$I_a = \frac{2e}{\hbar}\frac{\partial\hat{H}_W}{\partial\varphi_a} = \frac{2e}{\hbar}M_{ab}\tilde{I}_b; \tag{5.4}$$

$$\tilde{I}_a \equiv \frac{1}{2}\gamma^\dagger_\alpha\tau^a_{\alpha\beta}\gamma_\beta \tag{5.5}$$

Since there is a trivial linear relation between I_a and $\tilde{I}_a$, we will futher concentrate on the dimensionless quantities $\tilde{I}_a$.

Let us bring in the coupling with the continuous spectrum of electron states in several leads (Fig. 5.1). We will describe the leads with a usual free-fermion Hamiltonian

$$\hat{H}_{\mathrm{leads}} = \sum_k E_k \hat{d}^{a\dagger}_{k,\sigma}\hat{d}^a_{k,\sigma} \tag{5.6}$$

where k labels the states of the quasi-continuous spectrum in the leads, d_k are the corresponding electron annihilation operators, E_k are the corresponding energies. The states k are distributed over the leads, those are labelled with a. We characterize a general non-equilibrium state of the leads with the energy-dependent filling factors $f_a(E)$ such that

$$\langle\hat{d}^\dagger_{k,\sigma}\hat{d}_{k,\sigma}\rangle = f_a(E_k), \text{ for } k \in a. \tag{5.7}$$

The crucial part of the Hamiltonian is the tunnelling between the electron states in the leads and the Andreev state in the nanostructure. We will keep it in the most general form,

$$\hat{H}_{\mathrm{T}} = \sum_{k,\sigma}\left(t_k\hat{\gamma}^\dagger_\sigma - t'_k\sigma\hat{\gamma}_{-\sigma}\right)\hat{d}_{k,\sigma} + h.c. \tag{5.8}$$

5

not specifying the spin-independent tunnel amplitudes t_k, t'_k. In the course of the derivation, we will see which combinations of the amplitudes are the relevant parameters of the model. It is convenient to present the Hamiltonian in the form of Nambu spinors

$$2\hat{H}_{\mathrm{T}} = \sum_k \gamma^\dagger_\alpha T^{\alpha\beta}_k d^\alpha_k + h.c. \tag{5.9}$$

where the matrix $T^{\alpha\beta}$ depends on the Nambu index only,

$$T_k = \begin{pmatrix} t^k & t'^*_k \\ t'_k & -t^*_k \end{pmatrix} \tag{5.10}$$

With this, we derive the operators of the current to a normal lead a

$$J_a = e \sum_{k\in a,\sigma} i\left(t_k \hat{\gamma}^\dagger_\sigma - t'_k \sigma \hat{\gamma}_{-\sigma}\right)\hat{d}_{k,\sigma} + h.c; \tag{5.11}$$

$$J_a = \frac{ie}{2}\sum_{k\in a} \gamma^\dagger_\alpha (T^{\alpha\beta}_k \tau_3)^{\alpha\beta} d^\alpha_k + h.c. \tag{5.12}$$

5

5.3. DERIVATION

The derivation of expressions for the currents in superconducting and normal leads can be accomplished by standard methods of superconducting non-equilibrium Keldysh Green functions [41, 42, 46]. However, for the sake of comprehensibility we give here an explicit derivation from scratch. This is easy for the system under consideration and makes explicit the transition from quasi-continuous to continuous spectrum in the leads.

Let us write down the Heisenberg evolution equations for the operators $\hat{\gamma}^\alpha, \hat{d}^\alpha_{k,\sigma}$ governed by the total Hamiltonian $\hat{H} = \hat{H}_{\mathrm{W}} + \hat{H}_{\mathrm{leads}} + \hat{H}_{\mathrm{T}}$. We use bold-face notations for bispinors and "check" for the corresponding 4×4 matrices. In these notations,

$$i\dot{\boldsymbol{\gamma}} = \check{H}_{\mathrm{W}}\boldsymbol{\gamma} + \sum_k \check{T}_k \boldsymbol{d}_k \tag{5.13}$$

$$i\dot{\boldsymbol{d}}_k = E_k \check{\tau}_3 \boldsymbol{d}_k + \check{T}^\dagger_k \boldsymbol{\gamma} \tag{5.14}$$

Here, we implicitly assume a time-dependence of H^{W}. Solving equations for each of $\hat{d}$ gives

$$\boldsymbol{d}_k(t) = e^{-iE_k\check{\tau}_3 t}\boldsymbol{d}^0_k + \int dt' \check{g}_k(t,t')\check{T}^\dagger_k \boldsymbol{\gamma}(t') \tag{5.15}$$

where

$$\check{g}_k(t,t') = -ie^{-iE_k\check{\tau}_3(t-t')}\Theta(t-t'). \tag{5.16}$$

Here, $\boldsymbol{d}^0$ describes the state of the leads. We substitude this to Eq. (5.13) to obtain a closed equation for $\boldsymbol{\gamma}$ and express it in terms of $\boldsymbol{d}^0$:

$$\boldsymbol{\gamma}(t) = \int dt' \check{G}(t,t')\sum_k \check{T}_k e^{-iE_k\check{\tau}_3 t'}\boldsymbol{d}^0_k \tag{5.17}$$

where we have introduced the advanced Green function defined as

$$[i\partial_t - \check{H}_W]\check{G}(t,t') - \int dt''\check{\Sigma}(t-t'')\check{G}(t'',t') = \delta(t-t') \tag{5.18}$$

where the self-energy $\check{\Sigma}$ reads

$$\check{\Sigma}(t,t') = \sum_k \check{T}_k \check{g}_k(t,t')\check{T}_k^\dagger \tag{5.19}$$

We substitute the expression (5.17) to the expressions for the current operators (5.5) and average over the non-equilibrium state of the leads using Eq. (5.7). This yields

$$\langle \tilde{I}_a \rangle = \frac{1}{2}\int dt'dt''\mathrm{Tr}[\check{\tau}_a\check{G}(t,t')\check{F}(t',t'')\check{\tilde{G}}(t'',t)] \tag{5.20}$$

where $\check{\tilde{G}}(t,t') \equiv \check{G}^\dagger(t',t)$ and

$$\check{F} = \check{T}_k \begin{pmatrix} f_k e^{iE_k(t'-t)} & 0 \\ 0 & (\bar{f}_k)e^{iE_k(t-t')} \end{pmatrix} \check{T}_k^\dagger \tag{5.21}$$

Here and further on, $\bar{f}_k \equiv 1 - f_k$. In a similar way, we derive the averages of the currents in the normal leads. They read:

$$\begin{aligned}\langle J_a(t)\rangle = e\int dt_1 dt_2 dt_3 \mathrm{Tr}[\check{M}_a(t,t_1)\check{G}(t_1,t_2)\check{F}(t_2,t_3)\check{\tilde{G}}(t_3,t)] \\ + \int dt_1 \left(\mathrm{Tr}[\check{D}_a(t,t')\check{G}(t,t')] + H.c.\right).\end{aligned} \tag{5.22}$$

Here, we define

$$\check{M}_a = -\frac{1}{2}\sum_{k\in a}\check{T}_k\tau_3 e^{-iE_k\tau_3(t-t')}\check{T}_k^\dagger; \tag{5.23}$$

$$\check{D}_a(t,t') = \frac{-i}{2}\sum_{k\in a}\check{T}_k\tau_3\begin{pmatrix} f_k e^{iE_k(t'-t)} & 0 \\ 0 & f_k e^{iE_k(t-t')} \end{pmatrix}\check{T}_k^\dagger. \tag{5.24}$$

So far, the expressions are valid for any spectrum in the normal lead, either quasi-continuous or continuous. Let us now specify to continuous spectrum. For this, we define the following combinations of tunnel amplitudes in each lead:

$$\Gamma_a(E) = \sum_{k\in a}(|t_k|^2 + |t_k'|^2)\delta(E-E_k); \tag{5.25}$$

$$\vec{\Gamma}_a(E) = \sum_{k\in a}(2\mathrm{Re}(t_k' t_k^*), 2\mathrm{Im}(t_k' t_k^*), |t_k|^2 - |t_k'|^2)\delta(E-E_k) \tag{5.26}$$

All the constituents of the expressions for the operators can be expressed through $\Gamma_a(E)$, $\vec{\Gamma}_a(E)$. Those are thus the actual parameters of our model. The continuous spectrum is implemented by assumption that $\Gamma_a(E), \vec{\Gamma}_a(E)$ are continuous and smooth functions of energy. Moreover, a convenient and relevant assumption is that these functions vary at an energy scale that exceeds by far that of the Weyl point. In this case, the energy dependence can be disregarded and $\Gamma_a, \vec{\Gamma}_a$ are taken at zero energy.

Let us see how $\check{\Sigma}$, $\check{F}$, $\check{M}_a$ and $\check{D}_a$ are simplified under these assumptions. In energy representation, the self-energy becomes

$$\check{\Sigma}(\epsilon) = \frac{1}{4\pi}\sum_{\pm}\left(\Gamma(E) \pm \vec{\Gamma}(E)\cdot\vec{\check{\tau}}\right)\frac{1}{\epsilon \mp E - i0} \tag{5.27}$$

where $\Gamma, \vec{\Gamma} \equiv \sum_a \Gamma_a, \vec{\Gamma}_a$. The Hermitian part of $\check{\Sigma}$ in the limit ϵ adds a constant term to H and therefore describes a shift, or renormalization of the Weyl point position in the space of three phases due to tunneling,

$$\delta\phi = -\int dE \frac{\vec{\Gamma}(E)}{E}. \tag{5.28}$$

We will disregard this irrelevant redefinition of the Weyl point position. The anti-Hermitian part of the self-energy is more important describing the decay of discrete states into the continuous spectrum,

$$\check{\Sigma} = \frac{1}{4}\sum_{\pm}\left(\Gamma(\pm\epsilon) \pm \vec{\Gamma}(\pm\epsilon)\cdot\vec{\check{\tau}}\right) \approx \frac{\Gamma}{2} \tag{5.29}$$

where the limit of small ϵ has been implemented in the last equality. The matrices $\check{F}, \check{D}_a$ bring the information about the filling factors in the leads and are expressed as

$$\check{F} = \sum_a \Gamma_a f_a^+ + \vec{\Gamma}_a\cdot\vec{\check{\tau}} f_a^- \tag{5.30}$$

$$\check{D}_a = -\frac{i}{2}\left[\vec{\Gamma}_a\cdot\vec{\check{\tau}} f_a^+ + \Gamma_a f_a^-\right]. \tag{5.31}$$

$$f^{\pm}(\epsilon) \equiv \frac{f_a(\epsilon) \pm \bar{f}_a(-\epsilon)}{2} \tag{5.32}$$

Finally, $\check{M}_a = -\vec{\Gamma}_a\cdot\vec{\check{\tau}}/2$. With this, the terms with $\check{M}_a$ in Eq. (5.22) are related to superconducting currents,

$$\langle J_a\rangle = -\vec{\Gamma}_a\cdot\vec{\check{I}} + \int dt_1 \left(\mathrm{Tr}[\check{D}_a(t,t')\check{G}(t,t')] + h.c.\right) \tag{5.33}$$

From now on, we will denote the expectation values of the currents simply as J_a, $\vec{\check{I}}$.

5.4. CURRENTS IN EQUILIBRIUM

In equilibrium and stationary state, the Green functions are diagonal in energy representation,

$$\check{G}, \check{\bar{G}} = \frac{1}{\epsilon - \check{H}_W \mp i\frac{\Gamma}{2}}. \tag{5.34}$$

There is also a convenient relation

$$i(\check{G}^{-1} - \check{\bar{G}}^{-1}) = \Gamma \tag{5.35}$$

We note that in equilibrium $f(\epsilon) = \bar{f}(-\epsilon)$ and filling factors in all leads correspond to Fermi distribution at zero chemical potential, $f_a(\epsilon) = f_F(\epsilon)$. With this, $\check{F} = \Gamma f_F$. Invoking Eq. (5.35), we prove

$$\check{G}\check{F}\check{\bar{G}} = -i f_F(\check{G} - \check{\bar{G}}) \tag{5.36}$$

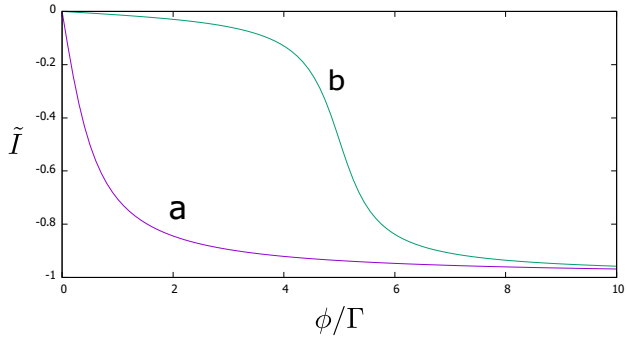

Figure 5.2: Smoothing of the superconducting current singularity at the scale of Γ. The curve a. corresponds to $B \ll \Gamma$, while the curve b. to $B = 5\Gamma$.

and the currents are expressed as

$$\vec{\tilde{I}} = -i \int \frac{d\epsilon}{2\pi} \mathrm{Tr}[\vec{\tilde{\tau}}(\check{G} - \check{\tilde{G}}) f_F(\epsilon)] \tag{5.37}$$

Let us first recognize that the equilibrium super currents are expressed from the derivatives of free energy with respect to $\vec{\phi}$. For an isolated superconducting nanostructure, that is, in the limit $\Gamma \ll B, \phi$, and at zero temperature, the ground state energy is given through the positive energies of Andreev bound states,

$$E_g = -\frac{1}{2} \sum_i E_i \Theta(E_i) \tag{5.38}$$

For the nanostructure under consideration, the Andreev bound states are $E_{\sigma,\pm} = B\sigma \pm \phi$ and the currents in this limit read

$$\vec{\tilde{I}} = -\vec{n}\Theta(\phi - B) \tag{5.39}$$

The current has a cusp: that is, its derivative with respect to ϕ diverges in a point. This divergence may be in principle used for finding the Weyl point and is smoothed at the scale of Γ.

At finite Γ, the Andreev energies correspond to the poles of the Green functions. Their poles are shifted by $\pm i\Gamma/2$ from the real axis. The currents are expressed through the phases of the pole positions $\xi_{\sigma,\pm} \equiv \arctan(2(B\sigma \pm \phi)/\Gamma)$,

$$\vec{\tilde{I}} = \frac{\vec{n}}{2\pi} \sum_\sigma (\xi_{\sigma,-} - \xi_{\sigma,+}) \tag{5.40}$$

The cusps are smoothed by a finite Γ (see Fig. 5.2). The maximum derivative with respect to ϕ is now finite and is of the order of Γ^{-1}:

$$\frac{\partial \tilde{I}}{\partial \phi} = \frac{2}{\pi\Gamma} \text{ for } B \ll \Gamma, \quad \frac{1}{\pi\Gamma} \text{ for } B \gg \Gamma. \tag{5.41}$$

In equlibrium, we expect no currents to normal leads. Indeed, if there were currents, one could extract energy from the equilibrium system by applying voltages to the normal leads. Technically, two terms in Eq. (5.33) cancel each other upon applying the relation (5.36).

5.5. STATIONARY CURRENTS

Now we turn to the case of non-equilibrium filling factors in the leads still assuming stationary Weyl point Hamiltonian. The currents are given by Eqs. (5.33), (5.20) with energy-diagonal Green functions (5.34). To keep the formulas simple, we will specify to differential conductances at vanishing temperature. The voltages in the leads only change the filling factors, at vanishing temperature $\partial f_a/\partial_{eV_a} = \delta(\epsilon - eV_a)$, that is, the differential conductances are contributed by the specific energies $\epsilon = \pm eV_a$ only.

For the derivatives of supercurrents, we have

$$2\pi\frac{\partial\vec{I}}{\partial eV_a} = \vec{\phi}\Gamma_a K_o(eV_a) + ((2\vec{\phi}\cdot\vec{\Gamma}_a)\vec{\phi} + (\vec{\phi}\times\vec{\Gamma}_a))K_e(eV_a) + \vec{\Gamma}_a K_3(eV_a) \tag{5.42}$$

where the functions $K_{o,e,3}$ are defined as ($K_\sigma^{-1} \equiv ((\epsilon - B\sigma)^2 - \Gamma^2/4 - \phi^2)^2 + \Gamma^2(\epsilon - B\sigma)^2$):

$$K_o = 2\sum_\sigma(\epsilon - B\sigma)K_\sigma; K_e = \sum_\sigma K_\sigma; \tag{5.43}$$

$$K_3 = \sum_\sigma((\epsilon - B\sigma)^2 + \Gamma^2/4 - \phi^2)K_\sigma \tag{5.44}$$

We note that

$$\int_0^\infty d\epsilon K_o = \frac{2(\arctan(\phi + B) + \arctan(\phi - B))}{\Gamma\phi}; \tag{5.45}$$

$$\int_0^\infty d\epsilon K_e = \frac{\pi}{\Gamma(\Gamma^2/4 + \phi^2)}; \tag{5.46}$$

$$\int_0^\infty d\epsilon K_3 = \frac{\pi\Gamma}{2(\Gamma^2/4 + \phi^2)} \tag{5.47}$$

The derivatives are illustrated in Fig. 5.3 for a single lead and simple case $\vec{\Gamma} = 0$. They peak at the positions of resonant levels $eV = \phi + B, |\phi - B|$. The peak width is of the order of Γ. For singlet ground state (the curves a,b the finite current at zero voltage falls to zero in one or two steps. For the doublet ground state, the current that is small at zero voltage rises at the first and drops at the second resonant level.

The differential conductances in the normal leads are given by:

$$\frac{\partial J_a}{\partial e^2 V_b} = -\vec{\Gamma}_a\cdot\frac{\partial\vec{\tilde{I}}}{\partial eV_b} + \frac{\Gamma\delta_{ab}}{2\pi}\left(\Gamma_a(K_3(eV_a) + 2\phi^2 K_e(eV_a)) + (\vec{\Gamma}_a\cdot\vec{\phi})K_o\right) \tag{5.48}$$

We plot in Fig. 5.4 an example of zero-voltage conductances G_{11}, G_{22}, G_{12} for two leads. The diagonal conductances peak when the resonant levels are at zero energy, $|\phi - B| = 0$. The peak widths are of the order of the conductance quantum $G_Q \equiv e^2/\hbar\pi$.

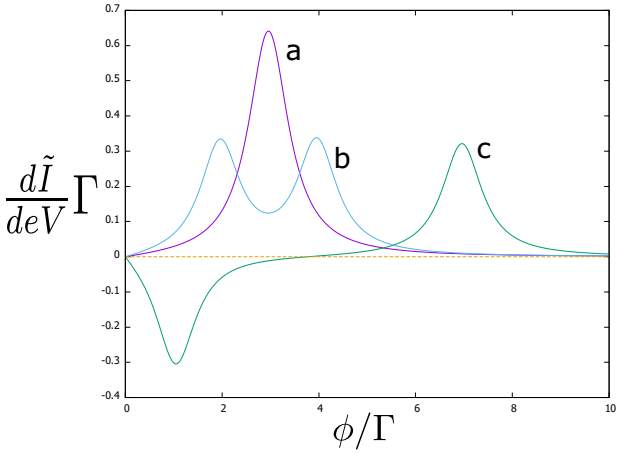

Figure 5.3: The voltage derivative of the superconducting current. There is a single lead, $\vec{\Gamma} = 0$, we set $\phi = 3.0$. The spin splitting B is set to 0, Γ, 4Γ, for the curves a,b,c respectively.

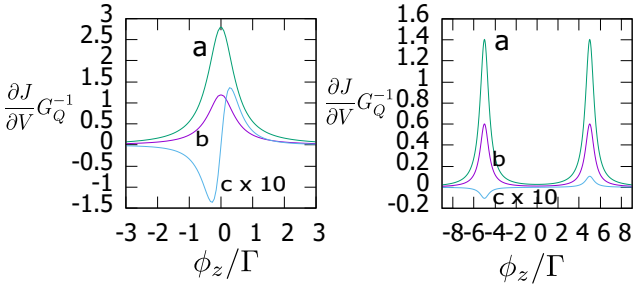

Figure 5.4: An example of zero-voltage conductances. There are two leads, $\Gamma_1 = 0.7\Gamma$, $\Gamma_2 = 0.3\Gamma$, $\vec{\Gamma}_1 \parallel x$,$\vec{\Gamma}_2 \parallel y$, the plots are for $\vec{\phi}$ in z-direction. The curves a,b,c, correspond two G_{11}, G_{22}, G_{12}. The transconductance is antisymmetric in this case, $G_{12} = -G_{21}$. Left pane: $B \ll \Gamma$, right pane: $B = 5\Gamma$. The vertical scale of the curve c is increased by a factor of 10.

An interesting feature is a Hall-like antisymmetric transconductance $G_{12} = -G_{21}$. It incorporates the effects of vector parts of Γ in two leads, $G_{12} \propto \vec{\phi} \cdot (\vec{\Gamma}_1 \times \vec{\Gamma}_2)$ and changes sign if $\vec{\phi} \to -\vec{\phi}$.

For finite-voltage conductance, we restrict ourselves to the case of a single lead. The example for $|\vec{\Gamma}| = \Gamma/2$ is given in Fig. 5.5. The peaks of differential conductance are situated at $eV = |\phi \pm B|$, their width being of the order of Γ. The peak values are of the order of G_Q. The vector part of Γ brings anisotropy and asymmetry of conductances with respect to voltage and $\vec{\phi}$.

At high voltages $eV \gg \Gamma, \phi, B$ applied, the current in the normal lead saturates at finite value J_∞, as it is expected for the transport via resonant levels. We note a peculiar feature: this current retains the dependence on ϕ and its direction, this dependence is smoothed at the small scale of $\phi \simeq \Gamma$ only. Using the relations (5.42),(5.43),(5.45), we obtain

$$J_\infty / e = \Gamma - \frac{(\vec{\Gamma} \cdot \vec{\phi})^2 + (\vec{\Gamma})^2 \Gamma^2/4}{\Gamma(\phi^2 + \Gamma^2/4)} \tag{5.49}$$

This feature survives rather high temperatures $\phi \ll k_B T \ll eV$ at which the thermal equilibration eventually cancels the superconducting currents near the Weyl point. This makes the feature highly proficient for experimental detection of Weyl points in a practical situation where the finite temperature prevents the detection through the supercurrent. One would look at the variation of the tunnel current under variation of ϕ to find a signal that is concentrated near the point and shows anisotropy defined by Eq. (5.49). The maximum derivative for $\vec{\phi} \perp \Gamma$

$$\frac{\partial J}{\partial \phi} = \frac{e}{\hbar} \frac{\vec{\Gamma}^2}{\Gamma^2} \tag{5.50}$$

does not depend on the strength of the tunnel coupling, this guarantees a big amplitude of the detection signal.

5.6. REDIFINITION OF BERRY CURVATURE AND DENSITY OF TOPOLOGICAL CHARGE

In this Section, we consider adiabatic case. We assume equilibrium filling factor in the leads and concentrate on the case of vanishing temperature. If we change the control phases slowly,the superconducting currents acquire a correction proportional to time derivatives of the phases:

$$\tilde{I}^\alpha(t) = \tilde{I}^\alpha(\vec{\phi}(t)) + B^{\alpha\beta}(\vec{\phi})\dot{\phi}^\beta \tag{5.51}$$

Thereby we define a tensor response function $B^{\alpha\beta}$. The symmetric part of this tensor defines the dissipation in the course of the slow change of the phases,

$$\frac{dE}{dt} = \dot{\phi}^\alpha B^{\alpha\beta}(\vec{\phi})\dot{\phi}^\beta. \tag{5.52}$$

If the system under consideration is gapped, the dissipative part is absent, while the antisymmetric part of the response function gives the Berry curvature of the ground state of the system (see e.g. [24])

$$B^{\alpha\beta} = 2\mathrm{Im}\langle \partial_\alpha \Psi | \partial_\Psi \Psi \rangle. \tag{5.53}$$

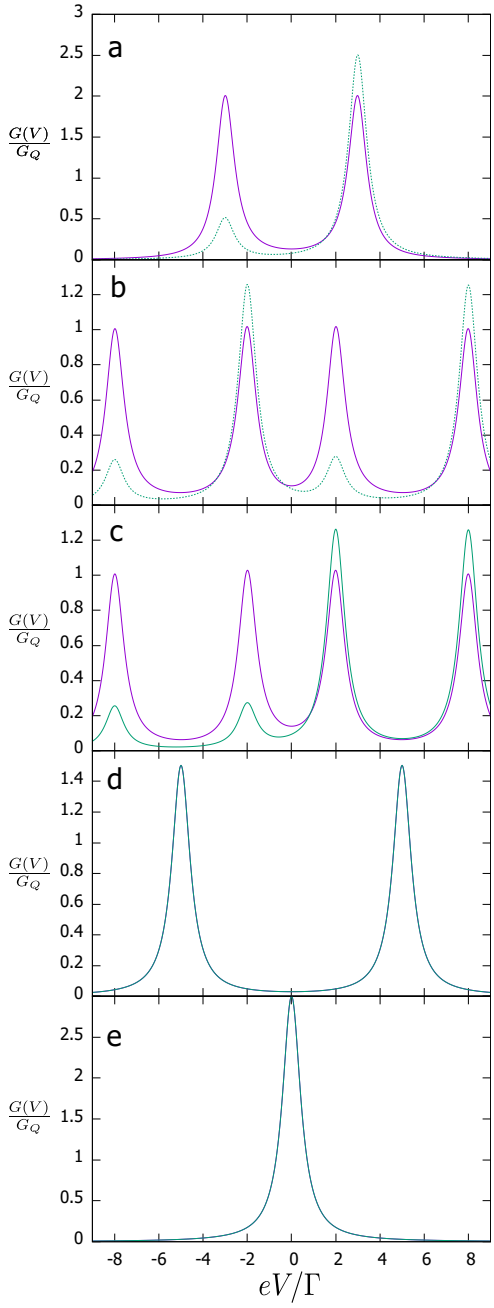

Figure 5.5: Differential conductance for the case of a single lead. $|\vec{\Gamma}| = \Gamma/2$ was taken. The solid curves correspond to $\vec{\phi} \perp \vec{\Gamma}$, the conductance is even in V and ϕ. The dashed curves correspond to $\vec{\phi} \parallel \vec{\Gamma}$, and $G(V,\phi) = G(-V,-\phi)$. The parameters are: a. $B = 0$, $\phi = 3\Gamma$; b. $B = 5\Gamma$, $\phi = 3\Gamma$; c. $B = 3\Gamma$, $\phi = 5\Gamma$; d. $B = 5\Gamma$, $\phi = 0$; e. $B = 0$, $\phi = 0$. The perpendicular and parallel conductances coincide for the last two plots, since $\phi = 0$.

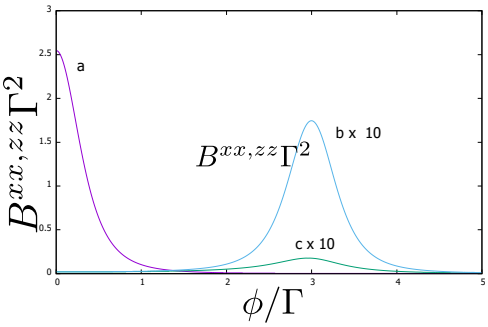

Figure 5.6: Dissipative part of the response function. We assume $\phi \parallel z$ and plot B^{zz}, $B^{xx} = B^{yy}$. Curve a: $B = 0$, $B^{zz} = B^{xx}$. Curves b,c: $B = 3$

It is convenient to introduce a pseudovector of Berry curvature $B^\alpha = e^{\alpha\beta\gamma}B^{\beta\gamma}$ For the superconducting Weyl point, the Berry curvature has been evaluated in [24, 31]. For the singlet ground state, and in the coordinates in use it assumes the standard expression $\vec{B} = \vec{\phi}/(2\phi^2)$. The flux of $\vec{B}$ through a surface enclosing the origin is 2π manifesting a unit point-like topological charge at the origin. However, $\vec{B} = 0$ at $\phi < B$ where the ground state is doublet. The continuity of the ground state is broken at $\phi = B$ and topological consideration that guarantees a divergentless $\vec{B}$ cannot be applied anymore.

We evalute $B^{\alpha\beta}$ for the setup under consideration making use of Eq. (5.20). Given a modulation of the Hamiltonian $\delta\check{H}$ oscillating at frequency ω, the response of the currents oscillating at the same frequency can be represented as

$$\tilde{I}^\alpha_\omega = \int \frac{d\epsilon}{2\pi}\frac{1}{2}\mathrm{Tr}[\check{\tau}^\alpha(\check{G}_{\epsilon+\omega}\delta\check{H}\check{G}_\epsilon\check{F}_\epsilon\check{\tilde{G}}_\epsilon + \tag{5.54}$$

$$\check{G}_\epsilon\check{F}_\epsilon\check{\tilde{G}}_\epsilon\delta\check{H}\check{\tilde{G}}_{\epsilon-\omega})]. \tag{5.55}$$

We obtain $B^{\alpha\beta}$ by substituting $\check{H} = \delta\phi^\alpha\check{\tau}^\alpha$ and taking the limit $\omega \to 0$. This is valid for $\omega \ll \Gamma$. We assume vanishing temperature when integrating over the energy.

To present the answers in a compact form, we introduce a convenient expression $K \equiv (\phi^2 - B^2 + \Gamma^2/4)^2 + B^2\Gamma^2$. The dissipative part of the response function reads:

$$B^{\alpha\beta} = \frac{\Gamma^2}{2\pi K}\left(\delta_{\alpha\beta} + \frac{\phi^\alpha\phi^\beta B^2}{K}\right) \tag{5.56}$$

It is plotted in Fig. 5.6 for two values of magnetic field. We note that the dissipative part at small Γ is proportional to Γ^2 except $\phi = B$ This is because the dissipation requires an excitation of an electron-hole pair in the normal leads, which is a second-order tunneling process [45]. At the resonance threshold $\phi = B$, and $B \gg \Gamma$, the dissipative part of the response function is strongly anisotropic: it is $\simeq \Gamma^{-2}$ for the direction $\parallel \vec{\phi}$ and $\simeq B^{-2}$ otherwise.

Following [31], we redefine Berry curvature as an asymmetric part of the response function. For any discrete spectrum and zero temperature, this redefinition would be exact retaining all topological properties of the curvature provided the limit $\omega \to 0$ implies $\omega \ll \delta$, δ being the level spacing in the spectrum. However, in our case the spectrum

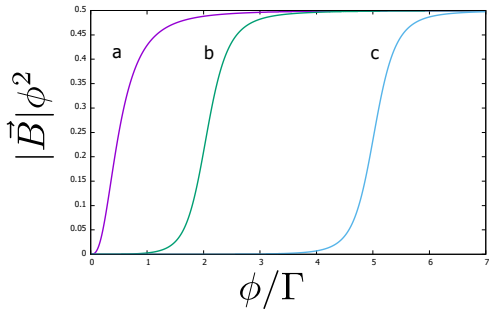

Figure 5.7: Redefined Berry phase $\times\phi^2$. The curves a,b,c correspond to $B = 0, 2, 5\Gamma$. They quickly approach the standard expression at $\phi \gg \Gamma$.

is continuous, that is, $\delta = 0$, and the limit $\omega \to 0$ rather implies $\omega \ll \Gamma$. Nevertheless, the redefined curvature coincides with the standard expression at $\phi, B \gg \Gamma$, that is, far from a close vicinity of the point or the resonance $\phi = B$. General expression reads

$$\vec{B} = \frac{\vec{\phi}}{2\pi\phi^3}\left[\sum_{\pm}\arctan\frac{2(\phi \pm B)}{\Gamma} + \frac{\phi^2 - \Gamma^2/4 - B^2}{K}\right] \tag{5.57}$$

We plot it in Fig. 5.7 for several B. At the origin, $\vec{B} \propto \vec{\phi}$, the maximum at $B = 0$ is $|\vec{B}| \approx 1.2\Gamma^{-2}$ and is achieved at $\phi \approx 0.3\Gamma$.

So-redefined Berry curvature gives rise to a continuous density of topological charge,

$$\rho(\phi) = \frac{1}{2\pi}\mathrm{div}\vec{B} \tag{5.58}$$

This is the most important manifestation of embedding a topological singularity into a continous spectrum. The point-line unit charge is spead over the parameter space concentrating either near the origin or, at $B \gg \Gamma$ at the surface $\phi = B$. We evaluate

$$\rho(\phi, B) = \frac{\Gamma^3}{4\pi^2}\frac{B^2 + \phi^2 + \Gamma^2/4}{K^2} \tag{5.59}$$

At small Γ, the density is proportional to Γ^3 arising from a complex tunneling process. Its maximum value $\simeq \Gamma^{-3}$ at $B = 0$ and $\simeq B^{-2}\Gamma^{-1}$ at $B \gg \Gamma$. We plot the density at several values of B in Fig. 5.8

5.7. CURRENTS IN NORMAL LEADS: PUMPING

A slow change of control phases may lead to the currents in the normal leads proportional to the time derivatives of the phases,

$$J_a = e\left(\vec{A}_a(\vec{\phi})\cdot\frac{d\vec{\phi}}{dt}\right) \tag{5.60}$$

$\vec{A}_a$ being $\vec{\phi}$-dependent proportionality coefficients. Let us recognize this as a case of parametric pumping, a phenomenon that has been intensively discussed in quantum

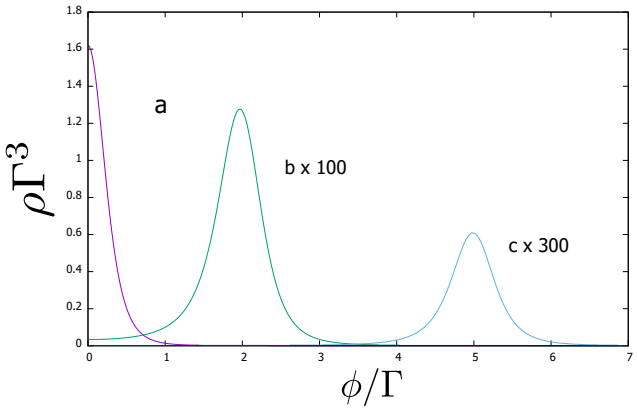

Figure 5.8: The density of topological charge. Curves a, b, c correspond to $B = 0, 2, 5\Gamma$, b and c are rescaled as shown in the plot.

5

transport [43, 45], also in the context of superconducting nanostructures with normal leads [44]. An ac modulation of ϕ is expected to result in an ac normal current, that is difficult to measure. However, it can also give rise to a dc current, that is, to pumping. If $\vec{\phi}$ is changing periodically along a closed contour, the charge per cycle depends on the contour only, and, by virtue of Stokes theorem, is given by a flux of the curl of $\vec{A}$ through the contour,

$$Q_a = \int_0^T dt J_a(t) = \oiint dS(\vec{N}\cdot \mathrm{curl}\vec{A}). \tag{5.61}$$

We evaluate $\vec{A}$ making use of Eq. (5.33) and expanding the Green functions up to first order in $\delta\check{H}$. We notice that the currents, since the filling factors are in equilibrium, are only due to the vector parts of Γ. Two groups of terms in Eq. (5.33) that cancel each other in stationary equilibrium case can be rewriten as

$$J_a = \frac{1}{2}\mathrm{Tr}[(\vec{\Gamma}_a\cdot\check{\vec{\tau}}[\check{f},\check{G}]\check{\tilde{G}}] \tag{5.62}$$

The commutator in this expression in energy representation can be rewritten as

$$[\check{f},\check{G}] = (f(\epsilon) - f(\epsilon-\omega))\check{G}_{\epsilon,\epsilon-\omega} \tag{5.63}$$

Since we are to expand to the first order in ω, this will give a weight of $\partial_\epsilon f$ in the integration over ϵ, and we can neglect small ω in the Green functions. The quantities under evaluation just sample Green functions in an energy interval $\simeq k_B T$ near zero energy, this interval going to zero at vanishing temperature. This is in contrast to the response functions explored in the previous Section, those are determined by integration over all relevant energies. Nevertheless, the expression of $\vec{A}$ has qualitatively similar features, the values being concentrated at $\phi \simeq \Gamma$ if $B \ll \Gamma$ or at $\phi = B$

$$\vec{A}_a = -\frac{\Gamma}{\pi K}\left(\vec{\Gamma}_a\Gamma + \vec{\phi}(\vec{\Gamma}_a\cdot\vec{\phi})\Gamma\frac{4B^2}{K} + (\Gamma_a\times\vec{\phi})\right) \tag{5.64}$$

Since we discuss the pumping, the curl of $\vec{A}$ — let us call it the effective field —is more relevant for us:

$$\mathrm{curl}\vec{A}_a = -\frac{\Gamma}{2\pi K^2}[(\vec{\Gamma}_a \times \vec{\phi})4\Gamma(\phi^2+\Gamma^2/4)+\vec{\Gamma}_a((B^2+\Gamma^2/4)^2-\phi^4)+\vec{\phi}(\vec{\phi}\cdot\vec{\Gamma}_a)(\phi^2+\Gamma^2-B^2)]. \tag{5.65}$$

The natural axis in $\vec{\phi}$ space is set by the direction of $\vec{\Gamma}_a$. In the above expression, we have separated the effective field into azimuthal, axial, and radial component. The dimension of effective field is E^{-2}. Far from the resonance, the azimuthal field is estimated as $\simeq \Gamma^3\phi^{-5}$, and axial/radial field as $\simeq \Gamma^2\phi^{-4}$. Thus, the typical Q_a/e for the contours that do not cross the resonance are small, $(\Gamma/\phi)^3$, $(\Gamma/\phi)^2$ respectively. At the resonance $\phi = B \gg \Gamma$, the azimuthal field is estimated as $B^{-1}\Gamma^{-1}$, and axial/radial field as B^{-2}. At $B \simeq \Gamma$, and near the origin, all field components are estimated as Γ^2. This implies that we can achieve $Q_a \simeq e$ for small contours with dimension Γ provided they are close to the origin.

We illustrate this with the following examples (Fig. 5.9). For pumping in the lead a, it is convenient to choose the coordinate system such that $z \parallel \vec{\Gamma}_a$. We probe the axial component of the effective field by taking a circular orbit with radius R in the plane $z = 0$, that is centered at the origin.(Fig. 5.9 a). The axial field is positive at the origin, and changes sign at $\phi = \sqrt{B^2+\Gamma^2/4}$. The total flux in $z = 0$ plane is zero. The charge per cycle for this orbit is given by

$$Q_a/e = \frac{2|\vec{\Gamma}_a|\Gamma R^2}{(R^2+\Gamma^2/4+B^2)^2-4R^2B^2}. \tag{5.66}$$

It reaches maximum that does not depend on magnetic field,

$$Q_a = 2e\frac{|\vec{\Gamma}_a|}{\Gamma}, \tag{5.67}$$

and gets back to zero for the contours of bigger radius. To probe the azimuthal field, one chooses a contour in e.g. $x = 0$ plane, that follows the axis at the scale $\max(B,\Gamma)$ to enclose the maximum positive flux. The charge per cycle in this case does not depend on the contour details and equals

$$Q_a = -\pi e\frac{|\vec{\Gamma}_a|}{4\Gamma}\frac{\Gamma^2/2+B^2}{\Gamma^2/4+B^2}. \tag{5.68}$$

The vector parts of Γ are generally different in different leads, so that the same contour is oriented differently for different leads. We conclude that the pumping to the normal leads provides an interesting possibility to explore the vicinity of the Weyl point.

5.8. CONCLUSIONS

To conclude, we have investigated the properties of a Weyl point immersed to a continuous spectrum. We take a Weyl point in a superconducting nanostructure that is tunnel-coupled to the electronic states in the normal leads. The tunnel coupling gives rise to a new energy scale Γ, that corresponds to a scale in parametric space. We investigate in

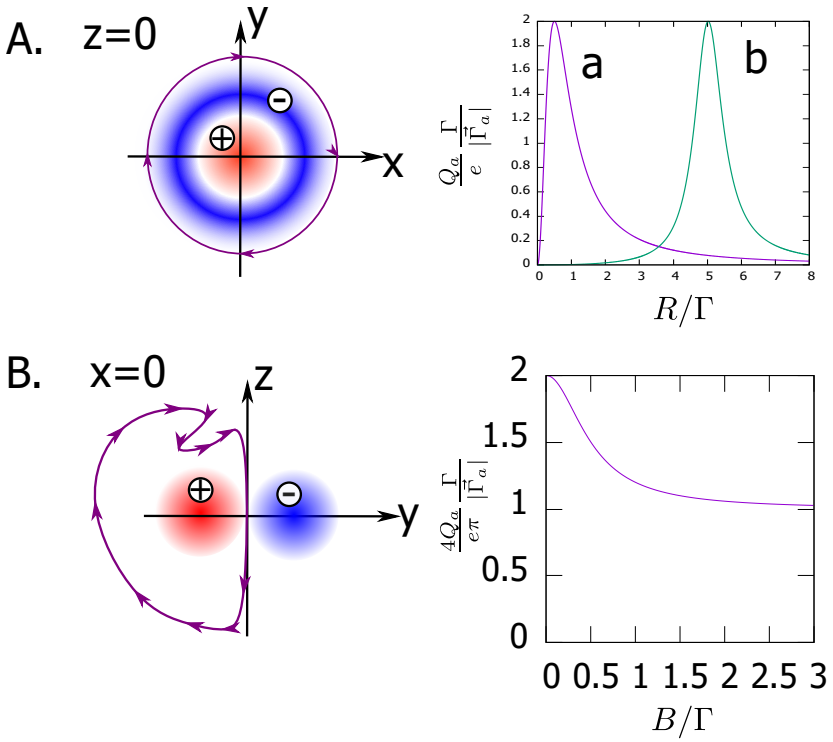

Figure 5.9: Pumping to a normal lead, $\vec{\Gamma}_a \parallel z$. A. Probing the axial effective field. A circular contour with radius R in $z = 0$ plane is centered at the origin. The plot: dependence of the charge per cycle on R for $B = 0,5\Gamma$. B. Probing the azimuthal effective field. The contour in $x = 0$ plane that goes along the axis at the scale $\max B, \Gamma$ encircles the whole flux in this direction. The value of the charge per cycle does not depend on the contour details and is given as function of B in the plot.

detail how the topological and spectral singularities of the Weyl point are smoothed on this scale. We evaluate the superconducting currents in equilibrium, the superconducting and normal-lead currents at constant voltages applied to the leads. We find sharp features in high-voltage tunnel currents that may be used to detect the Weyl points in experiment.

Importantly, we consider the adiabatic variation of control phases. This permits us to redefine Berry curvature and evaluate the density of topological charge that is not point-like but rather spread around the origin as the manifestation of coupling to the continuous spectrum.

We investigate the pumping to normal leads and find that it witnesses the peculiarities of Weyl point at the scale of Γ and opens up new perspectives for experimental exploration of Weyl point singularities.

REFERENCES

[1] C. Xu and L. Balents, *Topological superconductivity in twisted multilayer graphene,* Phys. Rev. Lett. **121**, 087001 (2018).

[2] S. Yao and Z. Wang, *Edge states and topological invariants of non-hermitian systems,* Phys. Rev. Lett. **121**, 086803 (2018).

[3] M. J. Pacholski, C. W. J. Beenakker, and i. d. I. Adagideli, *Topologically protected landau level in the vortex lattice of a weyl superconductor,* Phys. Rev. Lett. **121**, 037701 (2018).

[4] M. S. Hossain, M. K. Ma, M. A. Mueed, L. N. Pfeiffer, K. W. West, K. W. Baldwin, and M. Shayegan, *Direct observation of composite fermions and their fully-spin-polarized fermi sea near $\nu = 5/2$,* Phys. Rev. Lett. **120**, 256601 (2018).

[5] X. Tan, D.-W. Zhang, Q. Liu, G. Xue, H.-F. Yu, Y.-Q. Zhu, H. Yan, S.-L. Zhu, and Y. Yu, *Topological maxwell metal bands in a superconducting qutrit,* Phys. Rev. Lett. **120**, 130503 (2018).

[6] M. R. Brems, J. Paaske, A. M. Lunde, and M. Willatzen, *Strain-enhanced optical absorbance of topological insulator films,* Phys. Rev. B **97**, 081402 (2018).

[7] C.-C. Tang, K. Ikushima, D. C. Ling, C. C. Chi, and J.-C. Chen, *Quantum hall dual-band infrared photodetector,* Phys. Rev. Applied **8**, 064001 (2017).

[8] M. Götte, T. Paananen, G. Reiss, and T. Dahm, *Tunneling magnetoresistance devices based on topological insulators: Ferromagnet–insulator–topological-insulator junctions employing* bi_2se_3, Phys. Rev. Applied **2**, 054010 (2014).

[9] J. Maciejko, E.-A. Kim, and X.-L. Qi, *Spin aharonov-bohm effect and topological spin transistor,* Phys. Rev. B **82**, 195409 (2010).

[10] H. Chen, W. Zhu, D. Xiao, and Z. Zhang, *Co oxidation facilitated by robust surface states on au-covered topological insulators,* Phys. Rev. Lett. **107**, 056804 (2011).

[11] C. Nayak, S. H. Simon, A. Stern, M. Freedman, and S. Das Sarma, *Non-abelian anyons and topological quantum computation,* Rev. Mod. Phys. **80**, 1083 (2008).

[12] D. Aasen, M. Hell, R. V. Mishmash, A. Higginbotham, J. Danon, M. Leijnse, T. S. Jespersen, J. A. Folk, C. M. Marcus, K. Flensberg, and J. Alicea, *Milestones toward majorana-based quantum computing,* Phys. Rev. X **6**, 031016 (2016).

[13] C. L. Kane and E. J. Mele, *Quantum spin hall effect in graphene,* Phys. Rev. Lett. **95**, 226801 (2005).

[14] C. Wu, B. A. Bernevig, and S.-C. Zhang, *Helical liquid and the edge of quantum spin hall systems,* Phys. Rev. Lett. **96**, 106401 (2006).

[15] L. Fu, C. L. Kane, and E. J. Mele, *Topological insulators in three dimensions,* Phys. Rev. Lett. **98**, 106803 (2007).

[16] X.-L. Qi, T. L. Hughes, S. Raghu, and S.-C. Zhang, *Time-reversal-invariant topological superconductors and superfluids in two and three dimensions,* Phys. Rev. Lett. **102**, 187001 (2009).

[17] X.-L. Qi, T. L. Hughes, and S.-C. Zhang, *Chiral topological superconductor from the quantum hall state,* Phys. Rev. B **82**, 184516 (2010).

[18] A. Das, Y. Ronen, Y. Most, Y. Oreg, M. Heiblum, and H. Shtrikman, *Zero-bias peaks and splitting in an al–inas nanowire topological superconductor as a signature of majorana fermions,* Nature Physics **8**, 887 EP (2012).

[19] L. Fu and E. Berg, *Odd-parity topological superconductors: Theory and application to* $\mathrm{cu}_x\mathrm{bi}_2\mathrm{se}_3$, Phys. Rev. Lett. **105**, 097001 (2010).

[20] F. D. M. Haldane, *Model for a quantum hall effect without landau levels: Condensed-matter realization of the "parity anomaly",* Phys. Rev. Lett. **61**, 2015 (1988).

[21] N. Regnault and B. A. Bernevig, *Fractional chern insulator,* Phys. Rev. X **1**, 021014 (2011).

[22] Y. Zhang and X.-L. Qi, *Identifying non-abelian topological ordered state and transition by momentum polarization,* Phys. Rev. B **89**, 195144 (2014).

[23] T. Thonhauser and D. Vanderbilt, *Insulator/chern-insulator transition in the haldane model,* Phys. Rev. B **74**, 235111 (2006).

[24] R.-P. Riwar, M. Houzet, J. S. Meyer, and Y. V. Nazarov, *Multi-terminal Josephson junctions as topological matter,* Nature Communications **7** (2016), 10.1038/ncomms11167.

[25] N. Pankratova, H. Lee, R. Kuzmin, K. Wickramasinghe, W. Mayer, J. Yuan, M. G. Vavilov, J. Shabani, and V. E. Manucharyan, *Multiterminal Josephson Effect,* Physical Review X **10** (2020), 10.1103/PhysRevX.10.031051.

[26] R. L. Klees, G. Rastelli, J. C. Cuevas, and W. Belzig, *Microwave Spectroscopy Reveals the Quantum Geometric Tensor of Topological Josephson Matter,* Physical Review Letters **124** (2020), 10.1103/PhysRevLett.124.197002.

[27] G. Graziano, V, J. S. Lee, M. Pendharkar, C. Palmstrom, and V. S. Pribiag, *Transport studies in a gate-tunable three-terminal Josephson junction,* Physical Review B **101** (2020), 10.1103/PhysRevB.101.054510.

[28] P. Marra and M. Nitta, *Topologically nontrivial Andreev bound states,* Physical Review B **100** (2019), 10.1103/PhysRevB.100.220502.

[29] Z. Scherubl, A. Palyi, G. Frank, I. E. Lukacs, G. Fulop, B. Fulop, J. Nygard, K. Watanabe, T. Taniguchi, G. Zarand, and S. Csonka, *Observation of spin-orbit coupling induced Weyl points in a two-electron double quantum dot,* Communications Physics **2** (2019), 10.1038/s42005-019-0200-2.

[30] M. Houzet and J. S. Meyer, *Majorana-weyl crossings in topological multiterminal junctions,* Phys. Rev. B **100**, 014521 (2019).

[31] E. Repin, V, Y. Chen, and Y. Nazarov, V, *Topological properties of multiterminal superconducting nanostructures: Effect of a continuous spectrum,* Physical Review B **99** (2019), 10.1103/PhysRevB.99.165414.

[32] X. Fan, C. Qiu, Y. Shen, H. He, M. Xiao, M. Ke, and Z. Liu, *Probing Weyl Physics with One-Dimensional Sonic Crystals,* Physical Review Letters **122** (2019), 10.1103/PhysRevLett.122.136802.

[33] A. W. Draelos, M.-T. Wei, A. Seredinski, H. Li, Y. Mehta, K. Watanabe, T. Taniguchi, I. V. Borzenets, F. Amet, and G. Finkelstein, *Supercurrent Flow in Multiterminal Graphene Josephson Junctions,* Nano Letters **19**, 1039 (2019).

[34] J. Erdmanis, A. Lukacs, and Y. Nazarov, V, *Weyl disks: Theoretical prediction,* Physical Review B **98** (2018), 10.1103/PhysRevB.98.241105.

[35] J. S. Meyer and M. Houzet, *Nontrivial Chern Numbers in Three-Terminal Josephson Junctions,* Physical Review Letters **119** (2017), 10.1103/PhysRevLett.119.136807.

[36] E. Eriksson, R.-P. Riwar, M. Houzet, J. S. Meyer, and Y. V. Nazarov, *Topological transconductance quantization in a four-terminal Josephson junction,* Physical Review B **95** (2017), 10.1103/PhysRevB.95.075417.

[37] V. Fatemi, A. R. Akhmerov, and L. Bretheau, *Weyl josephson circuits,* (2020), arXiv:2008.13758 [cond-mat.mes-hall] .

[38] T. Herrig and R.-P. Riwar, *A "minimal" topological quantum circuit,* (2020), arXiv:2012.10655 [cond-mat.mes-hall] .

[39] T. Yokoyama and Y. V. Nazarov, *Singularities in the andreev spectrum of a multiterminal josephson junction,* Phys. Rev. B **92**, 155437 (2015).

[40] Y. Chen and Y. V. Nazarov, *Spin weyl quantum unit: A theoretical proposal,* Phys. Rev. B **103**, 045410 (2021).

[41] L. V. Keldysh, *Diagram technique for nonequilibrium processes,* Soviet Phys. JETP **20**, 1018 (1965).

[42] J. Rammer and H. Smith, *Quantum field-theoretical methods in transport theory of metals,* Rev. Mod. Phys. **58**, 323 (1986).

[43] P. W. Brouwer, *Scattering approach to parametric pumping,* Phys. Rev. B **58**, R10135 (1998).

[44] M. Blaauboer, *Charge pumping in mesoscopic systems coupled to a superconducting lead,* Phys. Rev. B **65**, 235318 (2002).

[45] Y. V. Nazarov and Y. M. Blanter, *Quantum Transport: Introduction to Nanoscience* (Cambridge University Press, 2009).

[46] J. Barański and T. Domański, *Decoherence effect on fano line shapes in double quantum dots coupled between normal and superconducting leads,* Phys. Rev. B **85**, 205451 (2012).

CURRICULUM VITÆ

Yuguang CHEN

19-11-1990 Born in Baotou, China.

EDUCATION

2008 High School
Zhonghua High School, Nanjing China

2009–2012 Bsc. in Mathematics & Physics
Beloit College, Beloit USA

Bsc. Thesis: Brachistochrone problem and some generalizations
Promotor: Prof. dr. D. Ellis

Sc. Assistant: Relay and vacuum pump rebuilt for the accelerator reconstruction
Calculate and measure circular hydraulic jump
Promotor: Prof. dr. P. Stanley

2013–2015 Msc. in Physics
University of Minnesota, Minneapolis USA

Msc. Thesis: CO_2 leak test for the Mu2e straw-tube tracker and muon capture simulation
Promotor: Prof. dr. D. Cronin-Hennessy

2017-2021 PhD. Physics
Delft University of Technology, Delft Netherlands
Thesis:
Promotor: Prof. dr. Y. V. Nazarov
Promotor: Prof. dr. Y. M. Blanter

List of Publications

4. **Y. Chen**, Y. Nazarov, *Weyl point immersed in a continuous spectrum: an example from superconducting nanostructures*, https://arxiv.org/abs/2102.03947 (2021).

3. **Yuguang Chen**, Yuli Nazarov, *Spintronics with a Weyl point in superconducting nanostructures*, Phys. Rev. B **103**, 165424 (2021).

2. **Y. Chen** and Y. V. Nazarov, *Spin Weyl quantum unit: A theoretical proposal*, Phys. Rev. B **103**, 045410 (2021).

1. E. V. Repin, **Y. Chen**, and Y. V. Nazarov, *Topological properties of multi-terminal superconducting nanostructures: effect of a continuous spectrum*, Phys. Rev. B **99**, 165414 (2019).

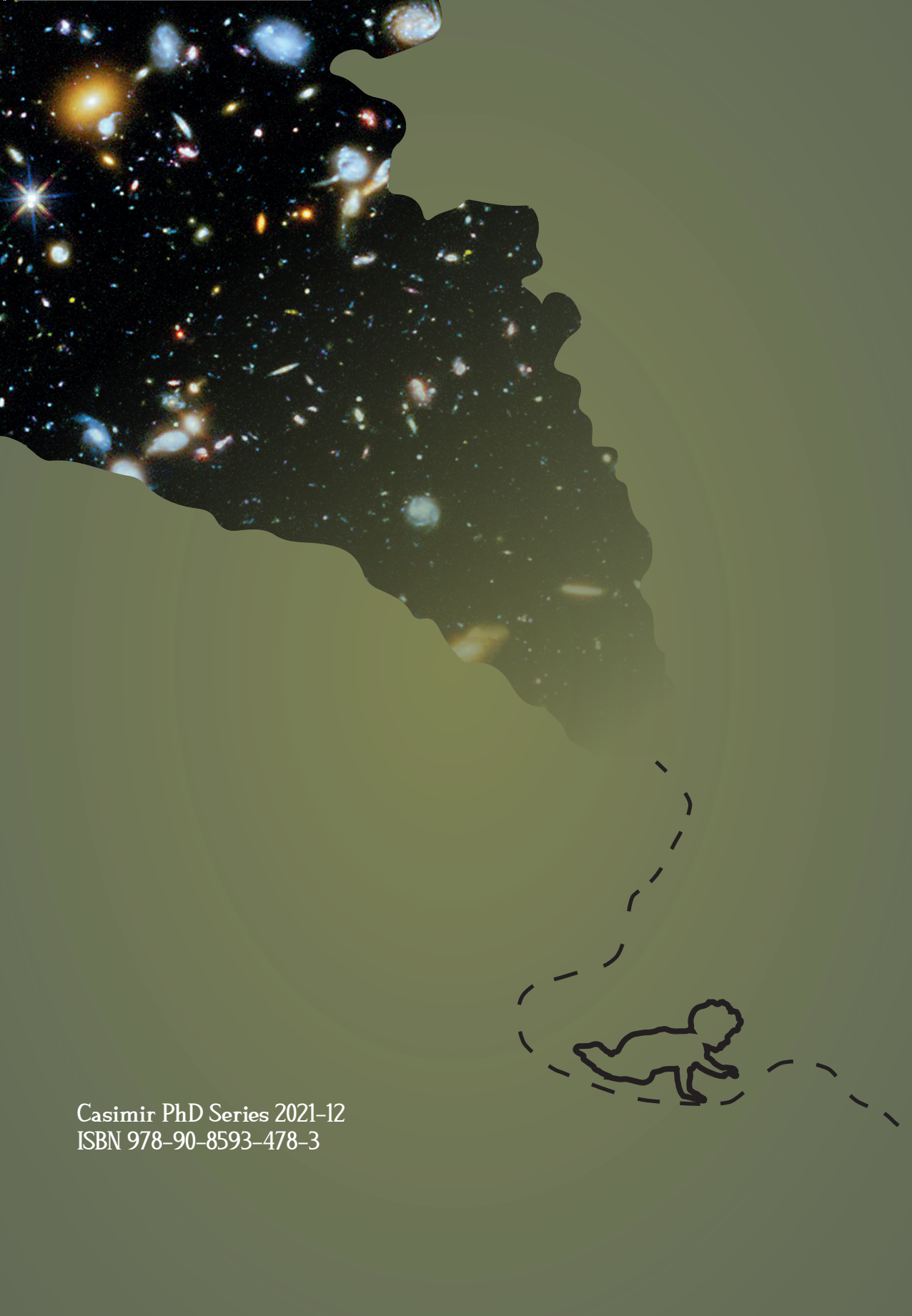

Casimir PhD Series 2021-12
ISBN 978-90-8593-478-3